



Digital Astronaut Project Biomechanical Models Biomechanical Modeling of Squat, Single-Leg Squat and Heel Raise Exercises on the Hybrid Ultimate Lifting Kit (HULK)

*William K. Thompson, Christopher A. Gallo, Lawton Crentsil, and Beth E. Lewandowski
Glenn Research Center, Cleveland, Ohio*

*Brad T. Humphreys
Zin Technologies, Inc., Middleburg Heights, Ohio*

*John K. DeWitt and Renita S. Fincke
Science, Technology and Engineering Group, Wyle Inc., Houston, Texas*

*Lealem Mulugeta
Universities Space Research Association, Houston, Texas*

NASA STI Program . . . in Profile

Since its founding, NASA has been dedicated to the advancement of aeronautics and space science. The NASA Scientific and Technical Information (STI) Program plays a key part in helping NASA maintain this important role.

The NASA STI Program operates under the auspices of the Agency Chief Information Officer. It collects, organizes, provides for archiving, and disseminates NASA's STI. The NASA STI Program provides access to the NASA Technical Report Server—Registered (NTRS Reg) and NASA Technical Report Server—Public (NTRS) thus providing one of the largest collections of aeronautical and space science STI in the world. Results are published in both non-NASA channels and by NASA in the NASA STI Report Series, which includes the following report types:

- **TECHNICAL PUBLICATION.** Reports of completed research or a major significant phase of research that present the results of NASA programs and include extensive data or theoretical analysis. Includes compilations of significant scientific and technical data and information deemed to be of continuing reference value. NASA counter-part of peer-reviewed formal professional papers, but has less stringent limitations on manuscript length and extent of graphic presentations.
- **TECHNICAL MEMORANDUM.** Scientific and technical findings that are preliminary or of specialized interest, e.g., “quick-release” reports, working papers, and bibliographies that contain minimal annotation. Does not contain extensive analysis.
- **CONTRACTOR REPORT.** Scientific and technical findings by NASA-sponsored contractors and grantees.
- **CONFERENCE PUBLICATION.** Collected papers from scientific and technical conferences, symposia, seminars, or other meetings sponsored or co-sponsored by NASA.
- **SPECIAL PUBLICATION.** Scientific, technical, or historical information from NASA programs, projects, and missions, often concerned with subjects having substantial public interest.
- **TECHNICAL TRANSLATION.** English-language translations of foreign scientific and technical material pertinent to NASA's mission.

For more information about the NASA STI program, see the following:

- Access the NASA STI program home page at <http://www.sti.nasa.gov>
- E-mail your question to help@sti.nasa.gov
- Fax your question to the NASA STI Information Desk at 757-864-6500
- Telephone the NASA STI Information Desk at 757-864-9658
- Write to:
NASA STI Program
Mail Stop 148
NASA Langley Research Center
Hampton, VA 23681-2199



Digital Astronaut Project Biomechanical Models Biomechanical Modeling of Squat, Single-Leg Squat and Heel Raise Exercises on the Hybrid Ultimate Lifting Kit (HULK)

*William K. Thompson, Christopher A. Gallo, Lawton Crentsil, and Beth E. Lewandowski
Glenn Research Center, Cleveland, Ohio*

*Brad T. Humphreys
Zin Technologies, Inc., Middleburg Heights, Ohio*

*John K. DeWitt and Renita S. Fincke
Science, Technology and Engineering Group, Wyle Inc., Houston, Texas*

*Lealem Mulugeta
Universities Space Research Association, Houston, Texas*

National Aeronautics and
Space Administration

Glenn Research Center
Cleveland, Ohio 44135

Acknowledgments

The authors wish to thank Justin Funk, Nathan Funk, Christopher Sheehan, and Gail Perusek for their assistance in this research.

This report contains preliminary findings,
subject to revision as analysis proceeds.

Trade names and trademarks are used in this report for identification
only. Their usage does not constitute an official endorsement,
either expressed or implied, by the National Aeronautics and
Space Administration.

Level of Review: This material has been technically reviewed by technical management.

Available from

NASA STI Program
Mail Stop 148
NASA Langley Research Center
Hampton, VA 23681-2199

National Technical Information Service
5285 Port Royal Road
Springfield, VA 22161
703-605-6000

This report is available in electronic form at <http://www.sti.nasa.gov/> and <http://ntrs.nasa.gov/>

Contents

Introduction and Mission	1
Specific Aims	2
Support of the HHC Path to Risk Reduction	2
Background	2
Exercises	2
Computational Modeling of Resistance Exercise	3
Harness Loading	3
Methods	4
Hulk Exercise Device	4
Exercise Protocols	4
Data Collection and Processing	7
Simulation of Bar Versus Harness Loading	7
OpenSim Exercise Models	8
Modifications to the Arnold Model	11
Analyses Performed and Statistical Methods	12
Results	12
Squat Exercise	12
Joint Kinematics for Parallel and Deep Squats	12
Kinematic Joint Angles for Deep and Parallel Squats	13
Average and Peak Resultant Joint Forces for Deep and Parallel Squats	16
Average and Peak Joint Moments for Deep and Parallel Squats	21
Average and Peak Muscle Forces by Muscle Group for Deep and Parallel Squats	26
Average and Peak Residual Forces and Moments for Deep and Parallel Squats	34
Average and Peak Reserve Moments for Deep and Parallel Squats	38
Single-Leg Squat Exercise	43
Joint Kinematics for Single-Leg Squat	43
Joint Moments for Single-Leg Squat	45
Resultant Joint Forces for Single-Leg Squat	48
Muscle Forces by Muscle Group for Single-Leg Squat	50
Residual Forces and Moments for the Single-Leg Squat	55
Reserve Moments for the Single-Leg Squat	57
Heel Raise Exercise	59
Joint Kinematics for Heel Raise	59
Joint Moments for Heel Raise	61
Resultant Joint Forces for Heel Raise	63
Muscle Group Forces for Heel Raise	65
Residual Forces and Moments for Heel Raise	66
Reserve Moments for Heel Raise	68
Summary of All Exercises	69
Discussion	71
Significance of Results	71
Validation of Results With Previous Exercise Studies	71
Squat	71
Single-Leg Squat	72
Heel Raise	72
Harness Loading Versus Bar Loading	73
Comparison with ARED Squat Integrated Muscle Model (ASM-im)	73
Comparison of Squat Versus Single-Leg Squat	74
Verification and Validation of the Models	75

Interpretation and Limitations	76
Future Work	76
Conclusions	77
Appendix A.—Acronyms	79
Appendix B.—Model Parameters and Configurations	81
Appendix C.—Measured External Force Data	83
C.1 Squat Exercise	83
C.2 Single-Leg Squat Exercise	89
C.3 Heel Raise Exercise	90
Appendix D.—Marker Set Used For Data Collection	91
Appendix E.—Procedure For Producing External Force Files From Device Load and Ground Reaction Force Data	93
References	97

List of Tables

Table 1.—Subject data used to develop the subject-specific exercise models	5
Table 2.—Summary of the exercise data collected	6
Table 3.—Major muscle groups and their constituent muscle actuators in OpenSim	10
Table 4.—Kinematic joint angle ranges for parallel and deep squats	12
Table 5.—Kinematic joint angle ranges for single-leg squat	43
Table 6.—Kinematic joint angle ranges in degrees for heel raise	60
Table 7.—(a) Peak resultant joint forces expressed as a multiple of BW, (b) Joint moment expressed as a multiple of BW-m, (c) muscle forces expressed as a multiple of BW for key joints for all exercises under all loading conditions	70
Table 8.—Comparison of peak values of key outcomes (joint angles, joint torques, resultant joint forces and muscle group forces) between the ARED squat model, ASM-im, and the HULK squat model	74
Table 9.—Credibility assessment for HULK biomechanical models using methods outlined in NASA-STD-2009	75

List of Figures

Figure 1.—HULK device configured in dual-tether (a) and single-tether (b) operation. Both dual- tether and single tether operation are intended to connect to various accessories, including the bar, shown at left, or a body harness (not shown)	4
Figure 2.—Subject performing (a) parallel and (b) deep squats on the HULK device. During parallel squats the thighs are approximately parallel to the floor at the bottom of the movement. During deep squats the subject descends to maximum depth	5
Figure 3.—Subject performing single-leg squats on the HULK device with the right leg as the target limb	5
Figure 4.—Subject performing heel raise exercise on the HULK device	6
Figure 5.—Harness loading on the Exxentric kBox 3 flywheel device (left) closely matches the harness loading scheme under consideration for this study. On HULK, the subject would straddle a single loading tether as shown in the rowing exercise depicted (right), but wearing a harness similar to the one shown on the left	7
Figure 6.—Distribution of harness loading on the upper back (30 percent) and lower back (70 percent) as indicated by the green arrows. Markers at the arrow tails indicate the points of application of the load	8
Figure 7.—Detailed view of the wrapping surfaces of the Arnold lower limb model in the (a) upper leg and a close-up of the (b) knee joint	9

Figure 8.—The OpenSim workflow used in the current study.....	10
Figure 9.—Quadriceps path at the knee in the unmodified (a) and modified (b) Arnold models at maximal knee flexion angle near 140°. The patellar wrapping surface (highlighted) was augmented in diameter and relocated anteriorly to correct the physiologically impossible muscle paths depicted on the left.....	11
Figure 10.—Kinematic joint angle histories during deep squats (left of each pairing) and parallel squats (right of each pairing) for the joints listed in Table 4.....	13
Figure 11.—Resultant joint forces in Newtons for deep and parallel squats under all loading conditions for the (a) hip and knee (patellofemoral and tibiofemoral) joints, (b) ankle and subtalar joints, and (c) lumbar joint with bar and harness loading separated.....	16
Figure 12.—Joint moments in Newton-meters for deep and parallel squats under all loading conditions for the (a) hip extension, hip abduction and knee extensor joints, (b) ankle plantar flexor and subtalar invertor, and (c) lumbar extension joint.....	21
Figure 13.—Muscle forces for deep and parallel squats under all loading conditions for the (a) hip extensor, hip flexor and hip adductor groups, (b) hip abductor, hip internal rotator and hip external rotator groups, (c) knee extensor, knee flexor and ankle dorsiflexor groups, and (d) ankle plantar flexor, subtalar evertor and subtalar invertor groups.....	26
Figure 14.—Average and peak residual forces in (a) Newtons for deep and parallel squats under all loading conditions for the FX, FY, FZ residual forces, and (b) Newton-meters for deep and parallel squats under all loading conditions for the MX, MY, MZ residual moments.....	34
Figure 15.—Reserve actuator moments in Newton-meters for deep and parallel squats under all loading conditions for the (a) hip flexion, hip adduction and hip rotation joint articulations and (b) knee flexion, ankle dorsiflexor and lumbar extension joint articulations.....	38
Figure 16.—Average reserve moments as a percentage of total joint moment for (a) deep squat and (b) parallel squat.....	42
Figure 17.—Joint kinematics trajectories for single-leg squat: (a) hip flexion, (b) hip adduction, (c) hip internal rotation, (d) knee flexion, (e) ankle dorsiflexion, (f) subtalar inversion, (g) MTP flexion, and (h) lumbar extension.....	43
Figure 18.—Peak and average joint moments in Newton-meters for single-leg squat under all loading conditions for the following joint articulations: (a) hip extension, (b) hip abduction, (c) hip internal rotation, (d) knee extension, (e) ankle plantar flexion, (f) ankle subtalar inversion, and (g) lumbar extension.....	45
Figure 19.—Resultant joint forces in Newtons for single-leg squat under all loading conditions for the following joints: (a) hip, (b) patellofemoral, (c) knee, (d) ankle, (e) subtalar, and (f) lumbar.....	48
Figure 20.—Average and peak muscle forces in Newtons by muscle group for single-leg squat under all loading conditions for the following groups: (a) hip extensors, (b) hip flexors, (c) hip adductors, (d) hip abductors, (e) hip internal rotators, (f) hip external rotators, (g) knee extensors, (h) knee flexors, (i) dorsiflexors, (j) plantar flexors, (k) subtalar invertors, (l) subtalar evertors, and (m) lumbar extensors.....	50
Figure 21.—Average and peak residual forces in Newtons and moments in Newton-meters for single-leg squat under all loading conditions for the following residual forces: (a) FX, (b) FY, (c) FZ; and residual moments: (d) MX, (e), MY, (f) MZ.....	55
Figure 22.—Average and peak reserve actuator moments for single-leg squat under all loading conditions for the following joint articulations: (a) hip flexion, (b) hip adduction, (c) hip rotation, (d) knee flexion, (e) ankle dorsiflexion, (f) subtalar inversion (g) lumbar extension.....	57
Figure 23.—Average reserve moments as a percentage of total joint moment for single-leg squat.....	59
Figure 24.—Joint kinematics trajectories for heel raise: (a) ankle dorsiflexion, (b) subtalar inversion, (c) MTP flexion and (d) lumbar extension.....	60

Figure 25.—Peak and average joint moments in Newton-meters for heel raise under all loading conditions for the following joint articulations: (a) ankle angle, (b) subtalar angle, (c) MTP angle and (d) lumbar extension.	61
Figure 26.—Resultant joint forces in Newtons for heel raise under all loading conditions for the following joints: (a) ankle, (b) subtalar, (c) MTP and (d) lumbar.....	63
Figure 27.—Average and peak muscle forces by muscle group for heel raise under all loading conditions for the following groups: (a) plantar flexors, (b) subtalar inverters, and (c) lumbar extensors.....	65
Figure 28.—Average and peak residual forces in Newton and moments in Newton-meters for heel raise under all loading conditions for the following residual forces: (a) FX, (b) FY, (c) FZ, and residual moments: (d) MX, (e), MY, (f) MZ.....	66
Figure 29.—Average and peak reserve actuator moments for heel raise under all loading conditions for the following joint articulations: (a) ankle plantar flexion, (b) subtalar inversion, (c) MTP extension, and (d) lumbar extension.	68
Figure 30.—Average reserve moments as a percentage of total joint moment for heel raise.....	69
Figure 31.—External force data as measured during deep and parallel squats. Average and peak (a) ground reaction forces in the normal (Y) direction, (b) resultant ground reaction forces in the shear direction, and (c) cable tension forces on the bar reported by the HULK device.	83
Figure 32.—External force data as measured during single-leg squats. Average and peak ground reaction forces in the normal (Y) and shear directions for the SLS and average and peak cable tension forces on the bar reported by the HULK device.	89
Figure 33.—External force data as measured during heel raises. Average and peak ground reaction forces in the normal (Y) and shear directions for the SLS and average and peak cable tension forces on the bar reported by the HULK device.	90
Figure 34.—Modified plug-in gait marker set used for motion capture data collection.....	91

Digital Astronaut Project Biomechanical Models Biomechanical Modeling of Squat, Single-Leg Squat and Heel Raise Exercises on the Hybrid Ultimate Lifting Kit (HULK)

William K. Thompson, Christopher A. Gallo, Lawton Crentsil,* and Beth E. Lewandowski
National Aeronautics and Space Administration
Glenn Research Center
Cleveland, Ohio 44135

Brad T. Humphreys
Zin Technologies, Inc.
Middleburg Heights, Ohio 44130

John K. DeWitt and Renita S. Fincke
Science, Technology and Engineering Group
Wyle Inc.
Houston, Texas 77058

Lealem Mulugeta
Universities Space Research Association
Houston, Texas 77058

Introduction and Mission

The NASA Digital Astronaut Project (DAP) implements well-validated computational models to predict and assess spaceflight health and performance risks, and to enhance countermeasure development. The DAP Musculoskeletal Modeling effort is developing computational models to inform exercise countermeasure development and to predict physical performance capabilities after a length of time in space. For example, integrated exercise device-biomechanical models can determine localized loading, which will be used as input to muscle and bone adaptation models to estimate the effectiveness of the exercise countermeasure. In addition, simulations of mission tasks can be used to estimate the astronaut's ability to perform the task after exposure to microgravity and after using various exercise countermeasures. The software package OpenSim (Stanford University, Palo Alto, CA) (Ref. 1) is being used to create the DAP biomechanical models and its built-in muscle model is the starting point for the DAP muscle model.

During Exploration missions, such as those to asteroids and Mars, astronauts will be exposed to reduced gravity for extended periods. Therefore, the crew must have access to exercise countermeasures that can maintain their musculoskeletal and aerobic health. Exploration vehicles may have very limited volume and power available to accommodate such capabilities, even more so than the International Space Station (ISS). The exercise devices flown on Exploration missions must be designed to provide sufficient load during the performance of various resistance and aerobic/anaerobic exercises while meeting potential additional requirements of limited mass, volume and power. Given that it is not practical to manufacture and test (ground, analog and/or flight) all candidate devices, nor is it always possible to obtain data such as localized muscle and bone loading empirically, computational modeling can estimate the localized loading during various exercise modalities performed on a given device to help formulate exercise prescriptions and other operational considerations. With this in mind, NASA's Digital Astronaut Project (DAP) is supporting the Advanced Exercise Concepts (AEC) Project, Exercise Physiology and Countermeasures (ExPC) laboratory and NSBRI-funded researchers by developing and implementing well-validated computational models of

* NASA Lewis' Educational and Research Collaborative Internship (LERCIP)

exercises with advanced exercise device concepts. This report focuses specifically on lower-body resistance exercises performed with the Hybrid Ultimate Lifting Kit (HULK) device as a deliverable to the AEC Project.

Specific Aims

This report documents the results of biomechanical modeling and analysis with two specific aims:

1. Estimate localized loading by joint (torque and force) and muscle groups (force) for the squat, heel raise and single-leg squat exercises on the HULK.
2. Compare localized loading when the subject exercises using a metal bar vs. a body harness, assuming similar kinematics between these two cases. (Data for harness loading have not yet been collected).

Support of the HHC Path to Risk Reduction

The DAP biomechanical modeling efforts help to reduce overall mission risk by addressing gaps (Ref. 2) in the Bone and Muscle disciplines within the Human Health and Countermeasures (HHC) Element.

Muscle

Gap M7: Can the current in-flight performance be maintained with reduced exercise volume?

Gap M8: What is the minimum exercise regimen needed to maintain fitness levels for tasks?

Gap M9: What is the minimum set of exercise hardware needed to maintain those (M8) fitness levels?

Bone

Gap Fracture 2: We need to characterize the loads applied to bone for standard in-mission activities.

Gap Fracture 3: We need a validated method to estimate the risk of fracture by evaluating the ratio of applied loads to bone fracture loads for expected mechanically-loaded activities during a mission.

DAP biomechanical models quantify the expected localized load stimulus at specific joints or within specific muscle groups for a given exercise on a particular exercise device performed in a specific manner. This informs the gaps listed above with quantitative information that is difficult or impractical to gather empirically.

Background

Exercises

The squat is renowned as the classic lower body resistance training exercise, working not only most of the lower limb musculature, but the hips and core as well (Ref. 3). For NASA, the lumbar spine, hip, knee and ankle joints are of particular interest in terms of loading stimulus seen by the adjacent bones and the muscles that articulate these joints, where high localized loss of both bone and muscle occur (Ref. 4). The single-leg squat is a related exercise with far less published data in the literature. Its primary interest to the NASA community lies in its potential to exercise the lower musculature using lower external loads and with a smaller overall device footprint, possibly making it more desirable for use in a spacecraft. Previous studies (e.g., Ref. 5) have shown that the single-leg version of the squat emphasizes hip extension and de-emphasizes knee extension versus the traditional squat. This implies that the single-leg squat and traditional squat are different exercises and will produce different outcomes in training programs or as

exercise countermeasures for spaceflight. The heel raise is a localized movement of the distal lower limbs that works primarily the plantar flexors, subtalar inverters/everters and the toe extensors (Refs. 6, 7, 8, and 9). The heel-raise exercise is of particular interest to NASA because of the lack of space-based research that has effectively minimized loss of musculature in the distal lower limbs during longer exposures to microgravity (Ref. 10).

Computational Modeling of Resistance Exercise

Computational simulation results for lower-body resistance training exercises, using OpenSim or equivalent tools, appear throughout the literature. One group reports using OpenSim to study a microgravity countermeasure combining artificial gravity, exercise and vibration during the performance of single- and two-legged squats; they conclude, based on simulation results, that the countermeasure performance may surpass that of currently deployed equipment (Ref. 11). Another group modeled hip muscle force during squatting movements in OpenSim for direct comparison to EMG measurements. They found good general correlation between loads and EMG activity, and they estimated hip muscle force loads well below 25 percent maximal for unweighted squats (Ref. 12). Still another group used OpenSim to study force depression and force enhancement induced by active muscle shortening and lengthening, respectively, to represent muscle history effects. Based on results from body weight and lightly-loaded squats and heel raises, they conclude that their modifications give a more accurate description of underlying forces and activations for the lower limb musculature (Ref. 13).

The study reported herein is unique in its use of computational simulation to investigate a variety of exercises at higher intensities (at or near the subject's three-repetition maximum) and over the fullest range of motion to maximal squatting depth and heel raise trajectory. In this realm the literature is sparse, and the present study is breaking new ground in the study of complex human motion on a novel device, and in the context of microgravity countermeasures.

Harness Loading

Changing the loading configuration of the HULK device from two-point loading to single-point loading, may result in changes in body posture and to the location of the center of mass of the system. These changes could play a significant role in the joint torques and muscle forces that are produced. For example when comparing a narrow stance squat and a wide stance squat, gluteus maximus activity is greater in a wide stance compared with a narrow stance squat (Ref. 14) and hip extension moments are greater in the medium and wide stance squats than in narrow stance squats (Ref. 15). No significant difference in quadriceps and hamstring activity is observed between narrow stance and wide stance squats (Refs. 14 and 16), however more tibiofemoral compressive force is generated during wide stance squat than narrow stance squat (Ref. 16) and knee extensor moments are greater in the medium and wide stance squats than in narrow stance squats (Ref. 15). The narrow stance squat produces more gastrocnemius activity than the wide stance squat (Ref. 16) and ankle plantar flexion moment is produced during narrow stance squats, whereas ankle dorsiflexor moment is produced during medium and wide stance squats (Ref. 15). The restriction of the knees so they do not move forward of the toes during a squat results in an increase in hip torque and a decrease in knee torque (Ref. 17). Front squats result in lower knee compressive forces and knee extensor moments than back squats, with no significant differences in quadriceps and hamstring activity (Ref. 18). Similarly, counterbalance squats decrease knee joint moment and quadriceps activity, while increasing hip joint moment and gluteus maximus activity, compared to a regular squat (Ref. 19).

Chiu et al. compared the sagittal plane joint kinetics during front squat and single-leg squat exercises, performed with free weights and with a flywheel resistance device (Ref. 20). In both exercises, the net joint impulse, the average net joint moment and the average net joint power at the knee joint were lower when using the flywheel device, then when using free weights, with slight to significant increases in these measurements at the hip and ankle joints (Ref. 20). Performing squat and single-leg squat exercises on devices such as the flywheel device in this study, where there is a single point of loading, centrally located anterior to the subject, could result in less of a hypertrophic effect within the knee extensor muscles.

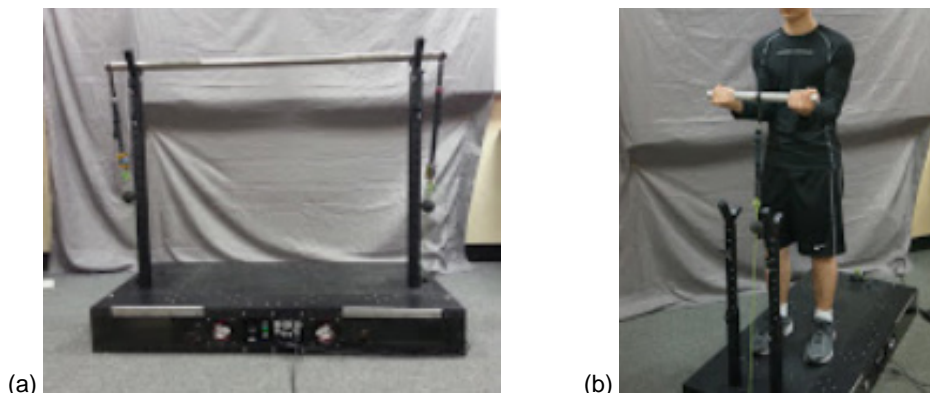


Figure 1.—HULK device configured in dual-tether (a) and single-tether (b) operation. Both dual-tether and single tether operation are intended to connect to various accessories, including the bar, shown at left, or a body harness (not shown).

Methods

Hulk Exercise Device

The HULK is a compact exercise device intended to fit within the confines of NASA’s next generation launch vehicle, the Multi-Purpose Crew Vehicle (MPCV). Given that the volume inside MPCV is limited, the device must be small enough to fit, yet allow the astronauts to perform necessary exercises with sufficient intensity to generate an appropriate loading stimulus. The HULK is shown in Figure 1 which represents the second design iteration resulting in a more compact and improved exercise package over the previous concept. The base is approximately 4 ft long, 2 ft wide and 6 in. tall. Two removable supports can be installed on each end to rest a 45.25 in. long bar on when not exercising. The test subject holds onto the bar which is connected to the resistance apparatus located underneath the top platform through two cables on each end. Resistance is created by pneumatic cylinders and pulleys. Cable tension force data are obtained through wireless load cells attached in line with the cables during the exercise motion. It is possible to replace the dual-tethered bar with a single tethered harness using one tether of the HULK, as shown in Figure 1.

Exercise Protocols

The male subject was a regular resistance trainee with anthropometry within the astronaut population as shown in Table 1.

After providing informed consent, the subject performed three exercises: squat (SQ), single-leg squat (SLS) and heel raise (HR), both with the device and at body weight (BW), except for SLS, where a BW trial was unintentionally omitted. Furthermore, the subject performed the squats to parallel (SQP), i.e., thighs parallel to the floor, and deep squats (SQD) as shown in Figure 2. The anterior/posterior bar position was located above the heels and the knees were vertically aligned with the toes at the bottom of the movement. A NASA IRB approved these exercise protocols.

The subject performed SLS using the right leg as the primary load bearing leg (Figure 3). The subject performed heel raises over the full ankle range of motion possible (Figure 4). Table 2 summarizes the load lifted and repetitions performed for each exercise.

The load settings on the device were set based on the subject’s perception of light (L), medium (M), and heavy (H) compared to his perceived one-repetition maximum (1 RM).

TABLE 1.—SUBJECT DATA USED TO DEVELOP THE SUBJECT-SPECIFIC EXERCISE MODELS

Subject	
Gender	Male
Height, cm	183 (90 th percentile)
Mass, kg.....	76 (75 th percentile)

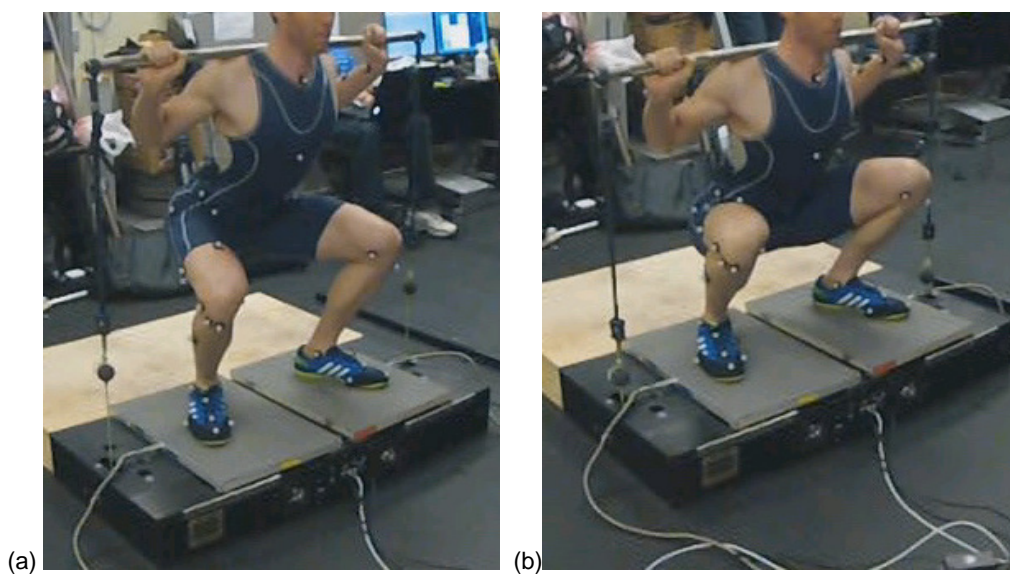


Figure 2.—Subject performing (a) parallel and (b) deep squats on the HULK device. During parallel squats the thighs are approximately parallel to the floor at the bottom of the movement. During deep squats the subject descends to maximum depth.



Figure 3.—Subject performing single-leg squats on the HULK device with the right leg as the target limb.

TABLE 2.—SUMMARY OF THE EXERCISE DATA COLLECTED

Exercise	Load, lb/kg		Repetitions
Deep Squat (SQD)	BW	Yes	3
	Light	125/57	3
	Medium	155/70	3
	Heavy	185/84	3
Parallel Squat (SQP)	BW	Yes	3
	Light	125/57	3
	Medium	155/70	3
	Heavy	185/84	3
Single-Leg Squat (SLS)	BW	No Trial	0
	Light	No Trial	0
	Medium	60/27	3
	Heavy	100/45	3
Heel Raise (HR)	BW	Yes	4
	Light	No Trial	0
	Medium	150/68	4
	Heavy	225/102	4



Figure 4.—Subject performing heel raise exercise on the HULK device.

Data Collection and Processing

Data collection occurred in May 2014 at NASA Johnson Space Center (JSC). HULK records the applied load using load cells (Omega Inc., Miniature Series, LC-300) and bar displacement using encoders (US Digital, E5 Series) at 200 Hz. Bilateral ground reaction forces (GRF) were measured at 1,000 Hz using two 40- by 60-cm quartz crystal piezoelectric force plates (Model 9261, Kistler Instruments AG). GRF data were down-sampled and device data up-sampled to 250 Hz in Matlab to match the motion capture (mocap) data. For the heel raise exercise, the subject stood on metal platforms placed on each force platform to allow for full ankle range of motion as shown in Figure 4.

Mocap data were collected with the Smart-D 12 camera system at 250 Hz (BTS Bioengineering, Milan, IT). Three-dimensional position data were collected of spherical reflective markers approximately 10 mm in diameter and placed at key anatomical sites on the subject (see Appendix D for specific marker locations). Prior to data collection the cameras were calibrated with an activity volume encompassing the subject and device according to the manufacturer's specifications and procedures. Calibration error was on the order of 0.1 mm. Mocap and GRF data were collected simultaneously with a single computer workstation.

After data collection, motion capture data were processed using BTS Smart Track software, which removed erroneous marker trajectories and any false light reflections in the room that mimicked markers.

Manual modification of the OpenSim files containing external loads was necessary by appending the device loading data synchronized with the GRF data. Appendix E describes the process by which the device load and GRF data were manually synced, subsampled, interpolated and resolved into their respective (x,y,z) coordinates using a combination of Mathworks Matlab and Microsoft Excel.

Simulation of Bar Versus Harness Loading

Specific Aim 2 of this study seeks to quantify the effects of harness loading vs. bar loading. In an effort to conserve volume, a single-tethered harness loading configuration, extending from the core of the body to the exercise device, is being considered over the two-point bar loading configuration illustrated in Figure 2. A commercially available equivalent of this type of harness loading is shown in Figure 5.



Figure 5.—Harness loading on the Exxentric kBox 3 flywheel device (left) closely matches the harness loading scheme under consideration for this study. On HULK, the subject would straddle a single loading tether as shown in the rowing exercise depicted (right), but wearing a harness similar to the one shown on the left.

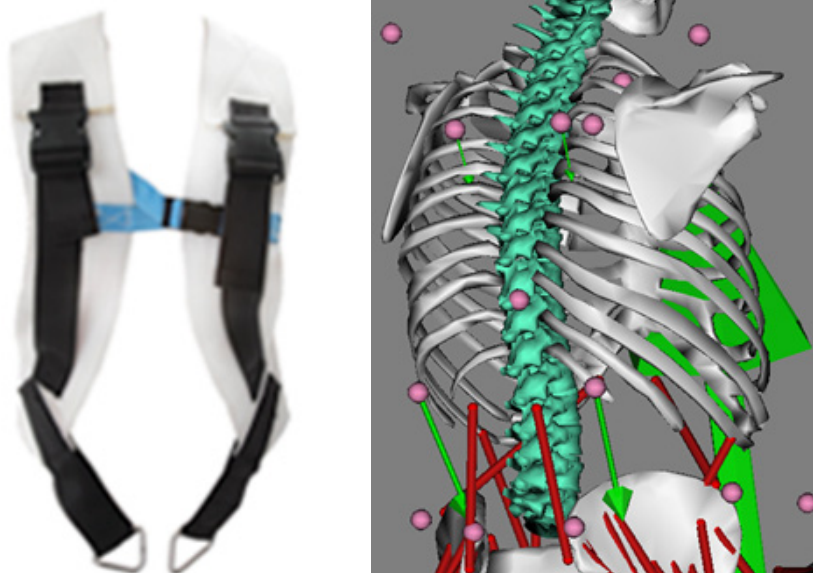


Figure 6.—Distribution of harness loading on the upper back (30 percent) and lower back (70 percent) as indicated by the green arrows. Markers at the arrow tails indicate the points of application of the load.

It is desirable to know the effect of loading configuration on the joint torques, resultant joint forces and muscle forces produced during the exercises. To simulate the harness loading, the measured bar load was distributed between the upper back (70 percent) and lower back (30 percent) across total of four points of load application to the biomechanical model, as shown in Figure 6. The authors estimated these proportions from simple trials of cable-based equivalents of the exercises under study while wearing a harness.

Although kinematic and kinetic data exists for the bar loading configuration, as explained above, data has not been collected to date on the harness loading configuration. We accounted for the lack of kinematic and kinetic data for the harness loading configuration and made the following simplifying assumptions for this preliminary modeling effort:

1. The kinematics of the exercise (i.e., joint angle histories) and the measured GRF and device loads are all essentially the same between the bar-loaded versus harness-loaded cases.
2. The proportional split between loading on the upper (70 percent) and lower back (30 percent) is both accurate and unchanging throughout the range of motion.
3. All loads are directed at all times in the same direction as the cable tether attached to the harness.

OpenSim Exercise Models

There are individual OpenSim models for each exercise. All OpenSim models are based on a modified version of the Arnold lower-limb model (Ref. 21) that is publicly available from the OpenSim website (Ref. 22). The modified Arnold lower limb model contains 21 body segments (no arms) and 96 lower limb muscles. This model uses wrapping surfaces extensively in the lower limbs in order to accommodate more severe knee flexion angles.

Muscles in OpenSim are modeled as line elements between two-points. Wrap surfaces allow for the muscle elements to conformably follow anatomical surfaces. The wrap surfaces allow the muscles to follow a path that is a realistic approximation to the movement of the human body. Without a wrap surface, a muscle could move through a bone or move at a sharp angle, resulting in a discontinuity or an incorrect muscle joint moment arm. The modeling of the knee joint benefited from the wrap surfaces the most, with knee force being reduced by more than half when the wrap surfaces were active in the model. Figure 7 shows the model both with and without wrap surfaces.

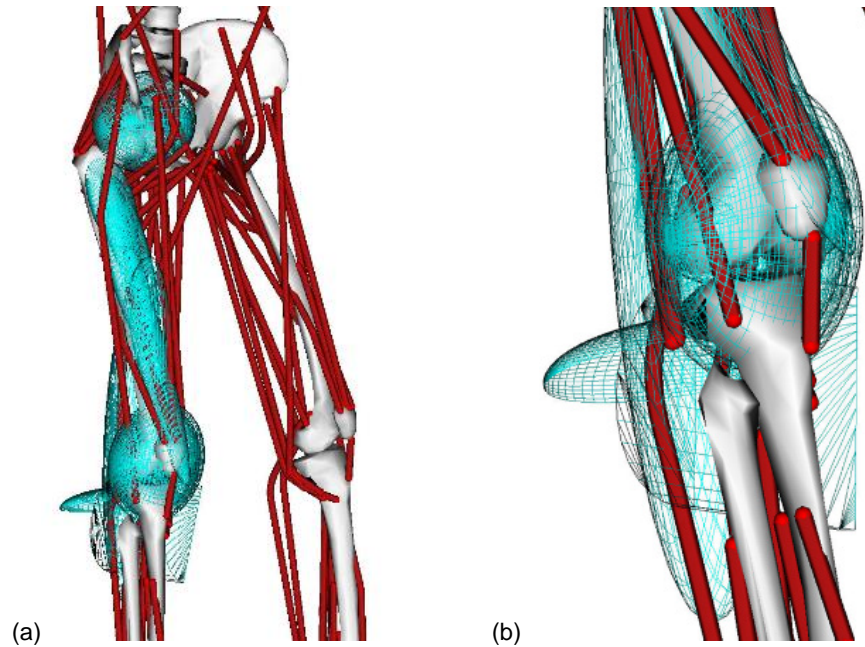


Figure 7.—Detailed view of the wrapping surfaces of the Arnold lower limb model in the (a) upper leg and a close-up of the (b) knee joint

The muscle model in the modified Arnold lower limb model was updated to the Millard muscle model (Ref. 23) which performs better at the extremes of the range of motion (Ref. 23). The maximum isometric strength parameters were increased to reflect the conditioning of the subject and to ensure the model was strong enough for the heavy loads during kinetic analyses. The final muscle parameters selected for the models are listed in Appendix B.

An added bar object attached to the torso of the model using a custom joint that permitted three directions of bar rotation but no bar translations relative to the torso. The spatial location of the joint was the midpoint of the coordinates of the two markers at either end of the bar. This point varies slightly with each set of each exercise, and this variation is reflected in the models.

The modeling process followed the standard OpenSim workflow as shown in Figure 8.

The modified Arnold lower limb model was first scaled to the subject's anthropometrics using marker position data from a static mocap trial in which the subject assumes a neutral posture and remains still. Methods used for scaling followed the procedure outlined in the OpenSim User's Guide (Ref. 22). The subject's mass also guided the calculation of the new mass distributions from the original Arnold model.

Data files containing marker positions produce the inverse kinematics (IK) solutions for joint angle histories. IK was an iterative process, whereby the marker placements and weightings were adjusted until the root mean square (RMS) and maximum marker position errors are within the OpenSim best practices guidelines of 2 and 4 cm, respectively.

Low-pass filtering of the kinematic and GRF data occurred in OpenSim using a 3rd-order low-pass IIR Butterworth digital filter with a cutoff frequency of 6 Hz.

The models also require compensatory residual forces and moments applied at the hip and torque reserves applied at all joints in order to fully execute the movements during static optimization. Residuals are non-physical forces that account for inconsistencies between experimental GRFs and joint accelerations estimated from experimental motion capture data. A model design goal is to reduce these residuals and reserves to a negligible level compared with the muscle forces and muscle-generated moments. However, in practice residuals can never be reduced to zero, because experimental data are always imperfect. Residual values are included in the results, and they are a key input to the model self-verification process.

Muscles are grouped by the joint articulation they actuate. Table 3 shows the names of the muscle groups that appear in later sections of the report and their constituent muscles for the right leg only. An exception is the lumbar joint, which is actuated by symmetric muscles on both sides of the body.

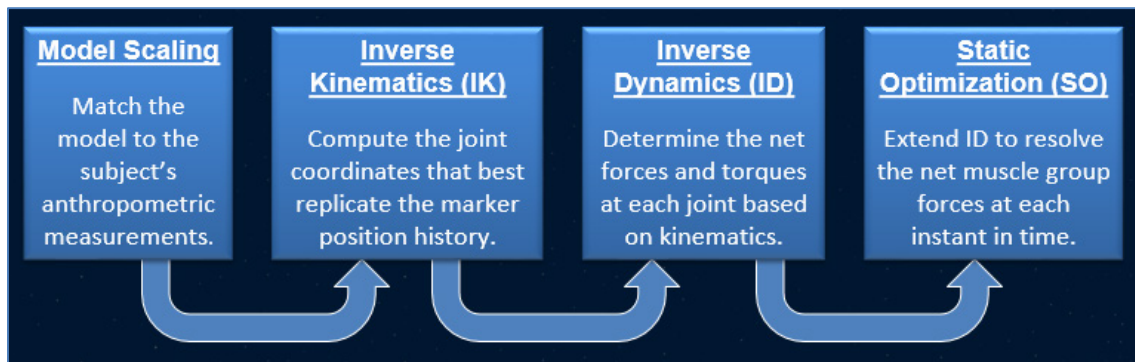


Figure 8.—The OpenSim workflow used in the current study.

TABLE 3.—MAJOR MUSCLE GROUPS AND THEIR CONSTITUENT MUSCLE ACTUATORS IN OpenSim

Hip Adductors	Hip Flexors	Hip Internal Rotators	Knee Flexors	Ankle Dorsiflexors	Subtalar Inverters	Lumbar Flexors
addbrev_r	addbrev_r	glmed1_r	bfnh_r	edl_r	edl_r	intobl_r
addlong_r	addlong_r	glmed2_r	bfnh_l	ehl_r	perbrev_r	intobl_l
addmagDist_r	gmin1_r	glmed3_r	gaslat_r	pertert_r	perlong_r	extobl_r
addmagIsch_r	grac_r	gmin1_r	gasmed_r	tibant_r	pertert_r	extobl_l
addmagMid_r	iliacus_r	iliacus_r	grac_r			
addmagProx_r	pect_r	psoas_r	sart_r			
bfnh_r	psoas_r	tfl_r	semimem_r			
grac_r	recfem_r		semiten_r			
pect_r	sart_r					
semimem_r	tfl_r					
semiten_r						
Hip Abductors	Hip Extensors	Hip External Rotators	Knee Extensors	Ankle Plantar Flexors	Subtalar Everters	Lumbar Extensors
gmax1_r	addlong_r	gem_r	patlig_r	fdl_r	eni_r	ercspn_r
glmed1_r	addmagDist_r	gmin3_r	recfem_r	fhl_r	fdl_r	ercspn_l
glmed2_r	addmagIsch_r	piri_r	vasint_r	gaslat_r	fhl_r	
glmed3_r	addmagMid_r	quadfem_r	vaslat_r	gasmed_r	tibant_r	
gmin1_r	addmagProx_r		vasmed_r	perbrev_r	tibpost_r	
gmin2_r	bfnh_r			perlong_r		
gmin3_r	gmax1_r			soleus_r		
piri_r	gmax2_r			tibpost_r		
sart_r	gmax3_r					
tfl_r	glmed1_r					
	glmed2_r					
	glmed3_r					
	gmin3_r					
	semimem_r					
	semiten_r					

For all joint articulations, a positive value indicates motion in the direction specified by the name (e.g., knee flexion), whereas a negative value indicates motion in the opposite direction (e.g., knee extension). Joints are generally not abbreviated for clarity, with the exception of the metatarsophalangeal (MTP) joint.

Modifications to the Arnold Model

The Arnold lower limb model (Ref. 21) used for the squat analysis was originally developed for gait and running motions. The squat motions in this study exhibited knee flexion angles exceeding 140° under near-maximal loading, a phenomenon not seen in gait and running. The base model was not designed for this extreme motion, and some of the muscles assumed an unnatural path as a result. The model includes wrap surfaces placed at the knee that are geometric shapes (e.g., sphere, cylinder, oval) to help guide the muscles to follow the correct path. Each wrap surface is linked to the specific muscles that are intended to wrap around them.

As shown in Figure 9, under maximal knee flexion, the quadriceps muscles in the unmodified Arnold lower limb model would flip from the anterior portion of the wrap surface at the knee to the opposite posterior side.

The anterior thigh muscles (rectus femoris and vastus intermedius, vastus lateralis and vastus medialis) are all knee extensors. The cylindrical wrap surface that guided these muscles required a change in diameter from 5 to 6 cm and slight translation anteriorly towards the patella. This resulted in the muscles following the wrap surface properly at the knee throughout the range of motion for the entire test during squat and single-leg squat exercises. Additional path points were also added; one near the posterior end of each of the four muscles and another proximal to that. These new wrap points prevented the muscle from extending into the femur or into the patella.

The biceps femoris long head and short head muscles in the posterior side of the thigh and the gastrocnemius lateral and medial muscles in the calf also required the location and size of their wrap surfaces to be slightly adjusted.

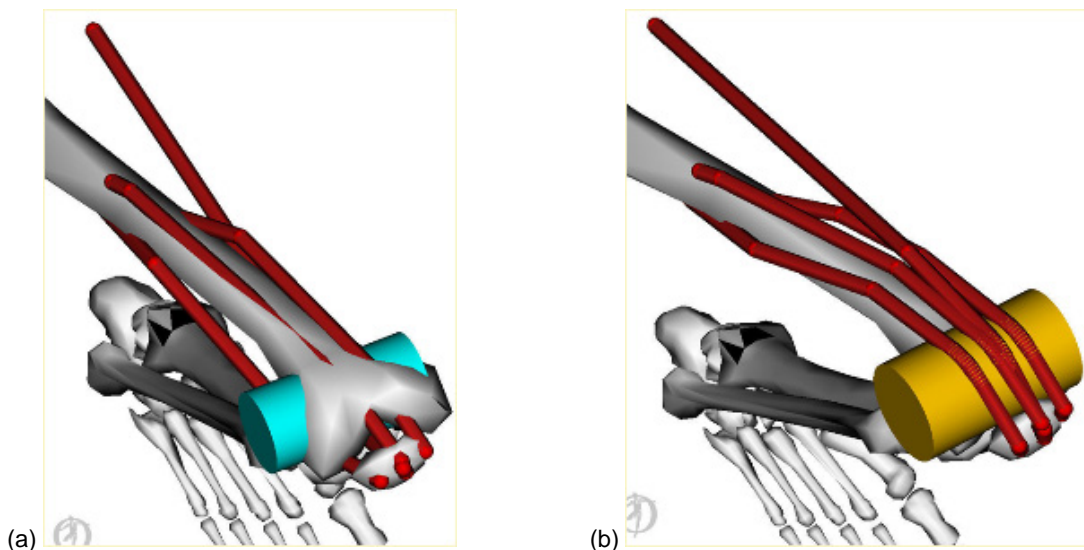


Figure 9.—Quadriceps path at the knee in the unmodified (a) and modified (b) Arnold models at maximal knee flexion angle near 140° . The patellar wrapping surface (highlighted) was augmented in diameter and relocated anteriorly to correct the physiologically impossible muscle paths depicted on the left.

Analyses Performed and Statistical Methods

The key outcomes of interest from the modeling process are joint angle ranges, joint moments, resultant joint forces, muscle tension forces by muscle group and residual/reserve forces. For all key outcomes, time histories, peak and averaged values were computed. Since there are multiple reps for each exercise (see Table 2), peak and average results appear as mean values with bars indicating the standard error (SE). Pairwise comparisons (e.g., parallel vs. deep squats) employed Student’s t-test for hypothesis testing to determine any statistically significant differences ($p < 0.05$) in mean values.

For static optimization (SO) analyses, the polynomial exponent was 4, precision was 12 and muscle force-length-velocity relationship was disabled. Further analyses performed using the SO results included muscle moments, muscle moment arms, muscle forces and activations, and resultant joint forces. Joint reaction analysis calculates the joint forces and moments transferred between consecutive bodies as a result of all loads acting on the model. These forces and moments correspond to the internal loads carried by the joint structure (Ref. 22). Resultant joint force refers to the magnitude of the joint reaction force.

Results

Squat Exercise

Joint Kinematics for Parallel and Deep Squats

Table 4 summarizes the joint angle ranges for the major lower body joints during both parallel and deep squats for the right leg. Left leg results are similar and are omitted. The subject is right-side dominant.

Figure 10 shows the motion histories of these joints over the course of each set. Figure 11 to Figure 13 show the joint moments, resultant joint forces and muscle tension forces, respectively. Figure 14 shows the model’s residual forces and moments during the squat movement, and Figure 15 shows the reserve actuator moments. Figure 16 shows the reserve joint moments expressed as a percentage of the total joint moments as determined from ID.

Technical problems during the third rep of the D185 (heavy deep squat) exercise resulted in a loss of data. Results for the first two reps are shown.

TABLE 4.—KINEMATIC JOINT ANGLE RANGES FOR PARALLEL AND DEEP SQUATS

Joint articulation during squats	Parallel squat		Deep squat	
	Angle at top of movement, °	Angle at bottom of movement, °	Angle at top of movement, °	Angle at bottom of movement, °
Hip flexion	16	116	14	129
Hip adduction	-4	-31	-5	-33
Hip internal rotation	-23	12	-22	30
Knee flexion	-2	128	-4	145
Ankle dorsiflexion	-7	34	-7	39
Subtalar inversion	-13	6	-13	17
MTP flexion	15	-11	18	-8
Lumbar extension	11	-11	12	-20

Kinematic Joint Angles for Deep and Parallel Squats

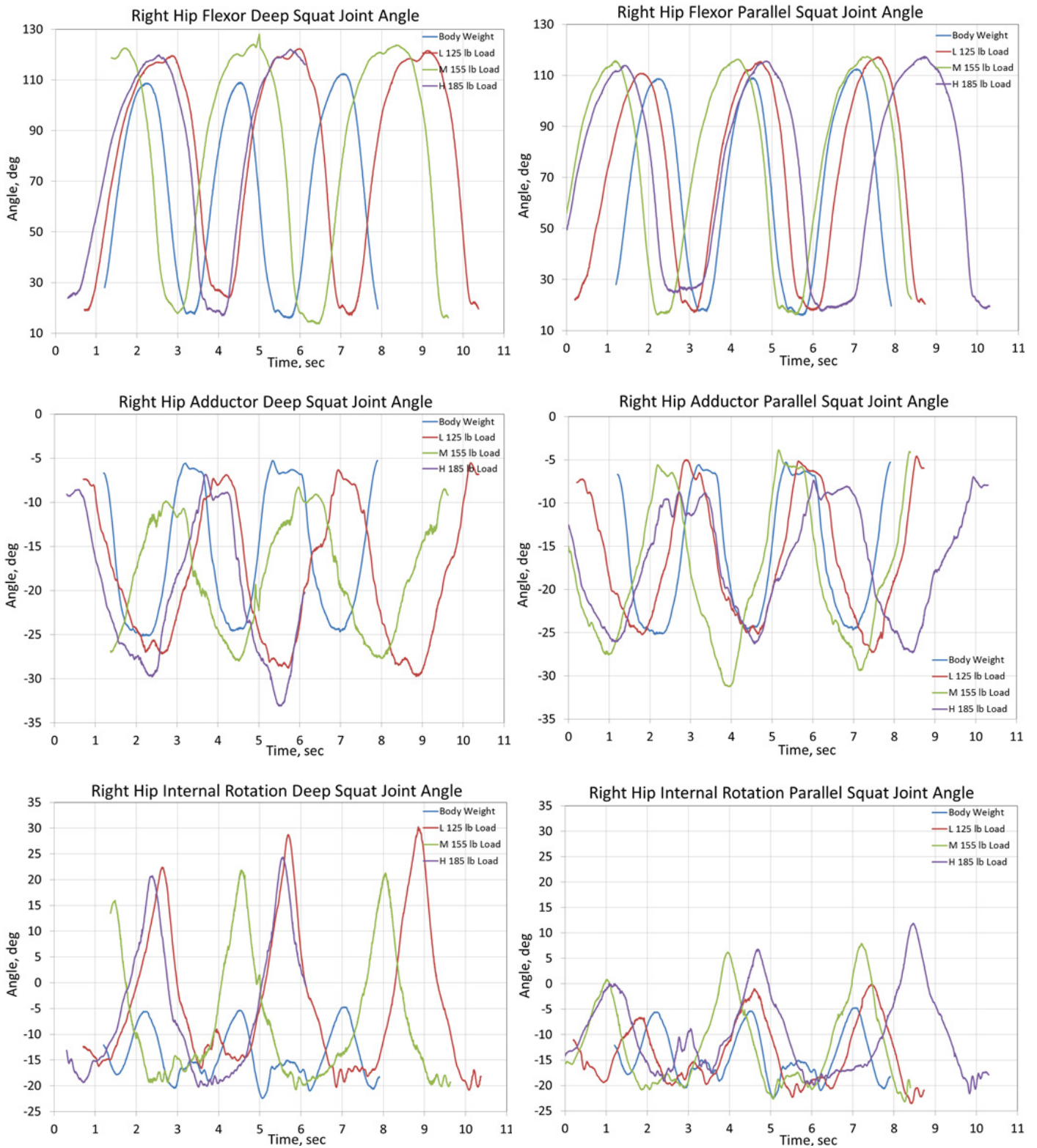


Figure 10.—Kinematic joint angle histories during deep squats (left of each pairing) and parallel squats (right of each pairing) for the joints listed in Table 4.

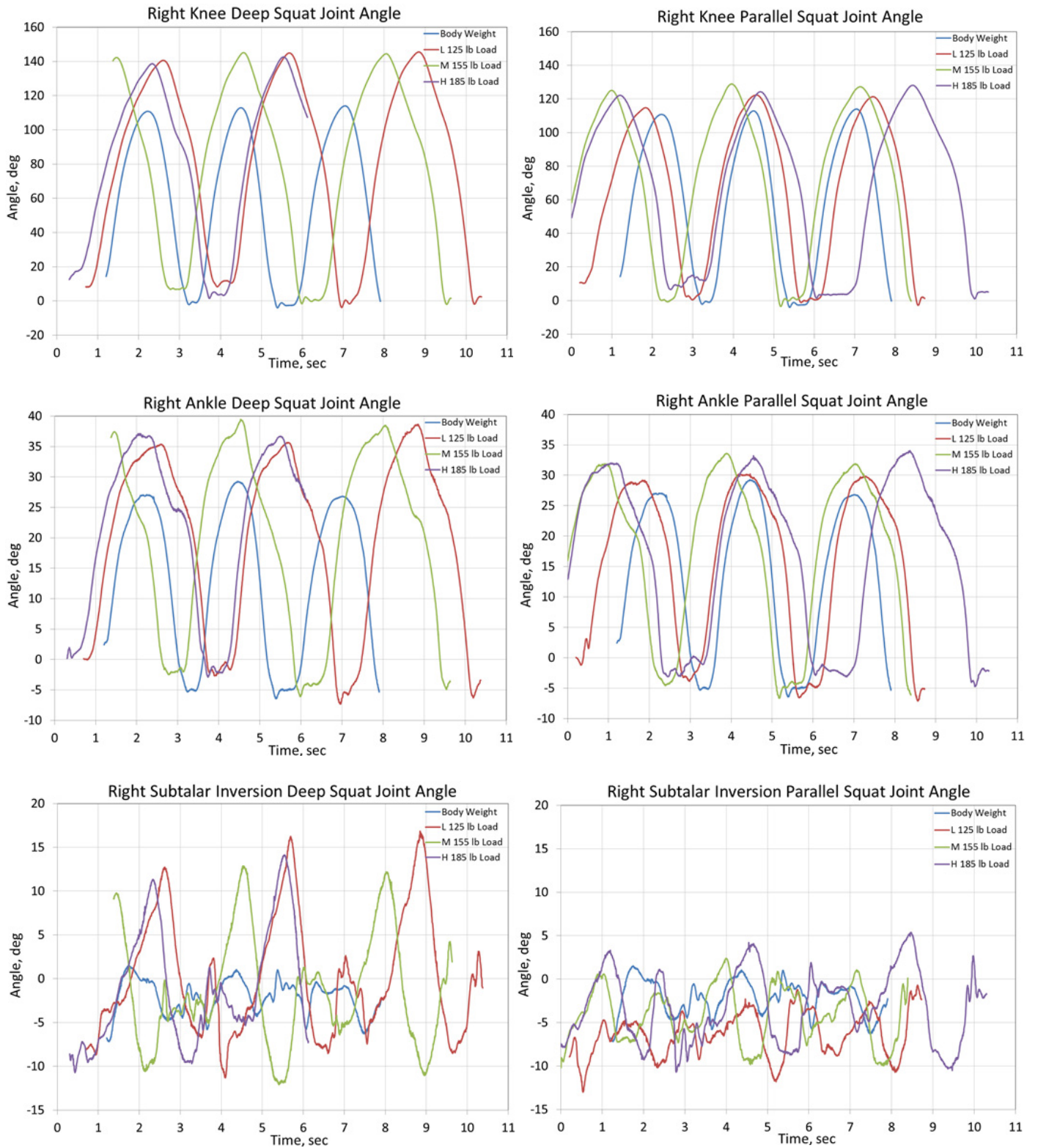


Figure 10.—Continued. Kinematic joint angle histories during deep squats (left of each pairing) and parallel squats (right of each pairing) for the joints listed in Table 4.

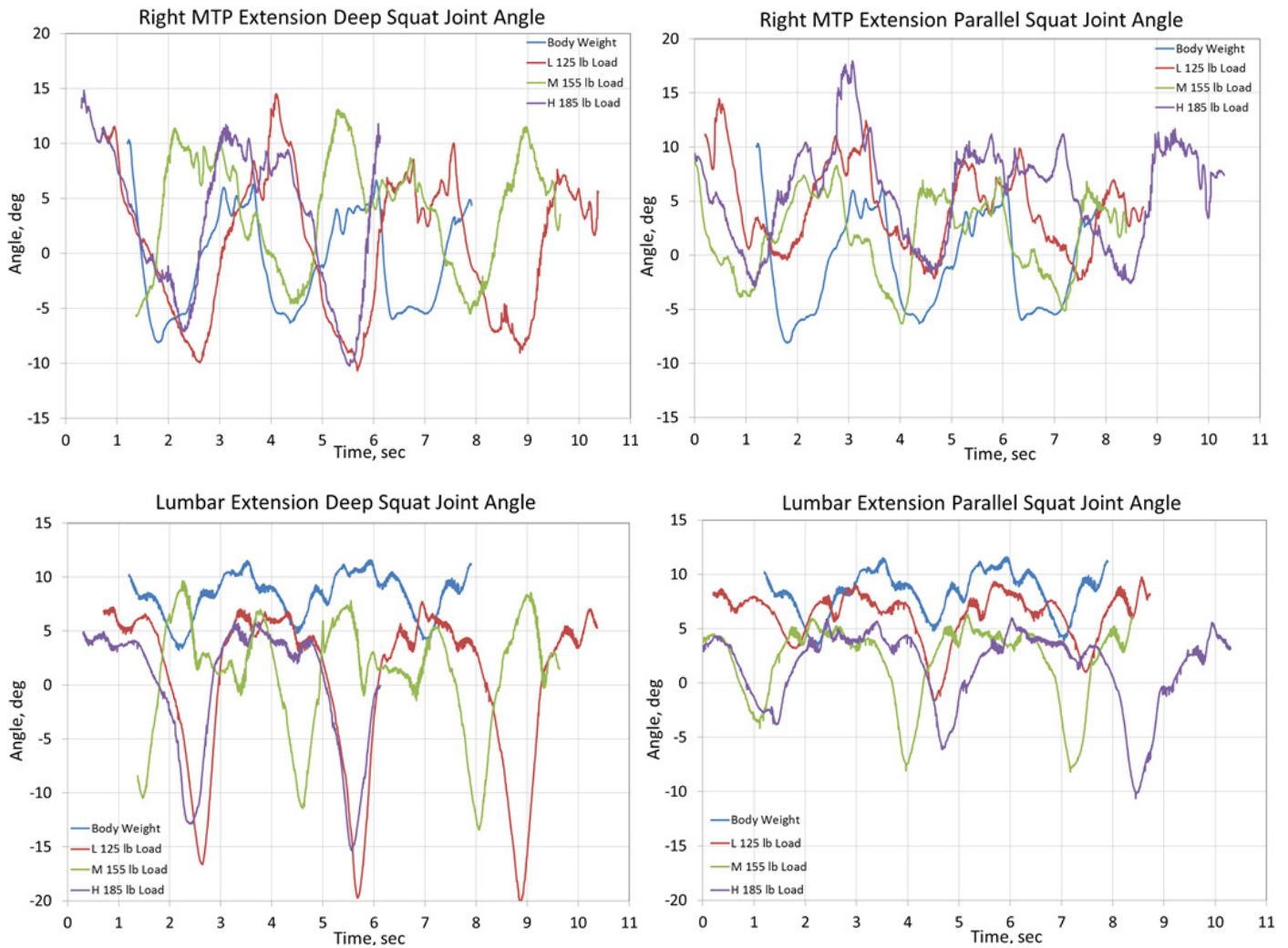


Figure 10.—Concluded. Kinematic joint angle histories during deep squats (left of each pairing) and parallel squats (right of each pairing) for the joints listed in Table 4.

Average and Peak Resultant Joint Forces for Deep and Parallel Squats

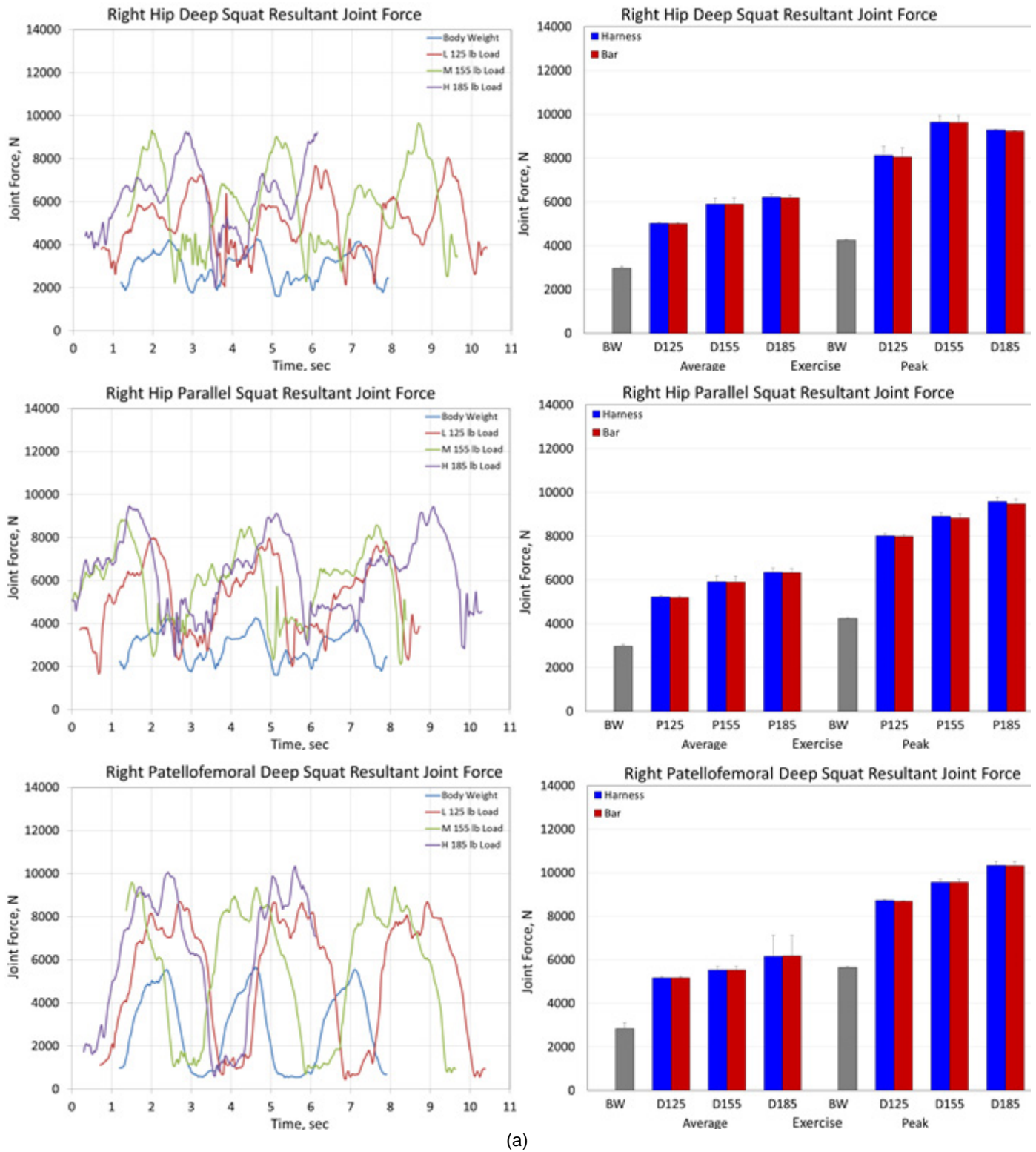


Figure 11.—Resultant joint forces in Newtons for deep and parallel squats under all loading conditions for the (a) hip and knee (patellofemoral and tibiofemoral) joints, (b) ankle and subtalar joints, and (c) lumbar joint with bar and harness loading separated.

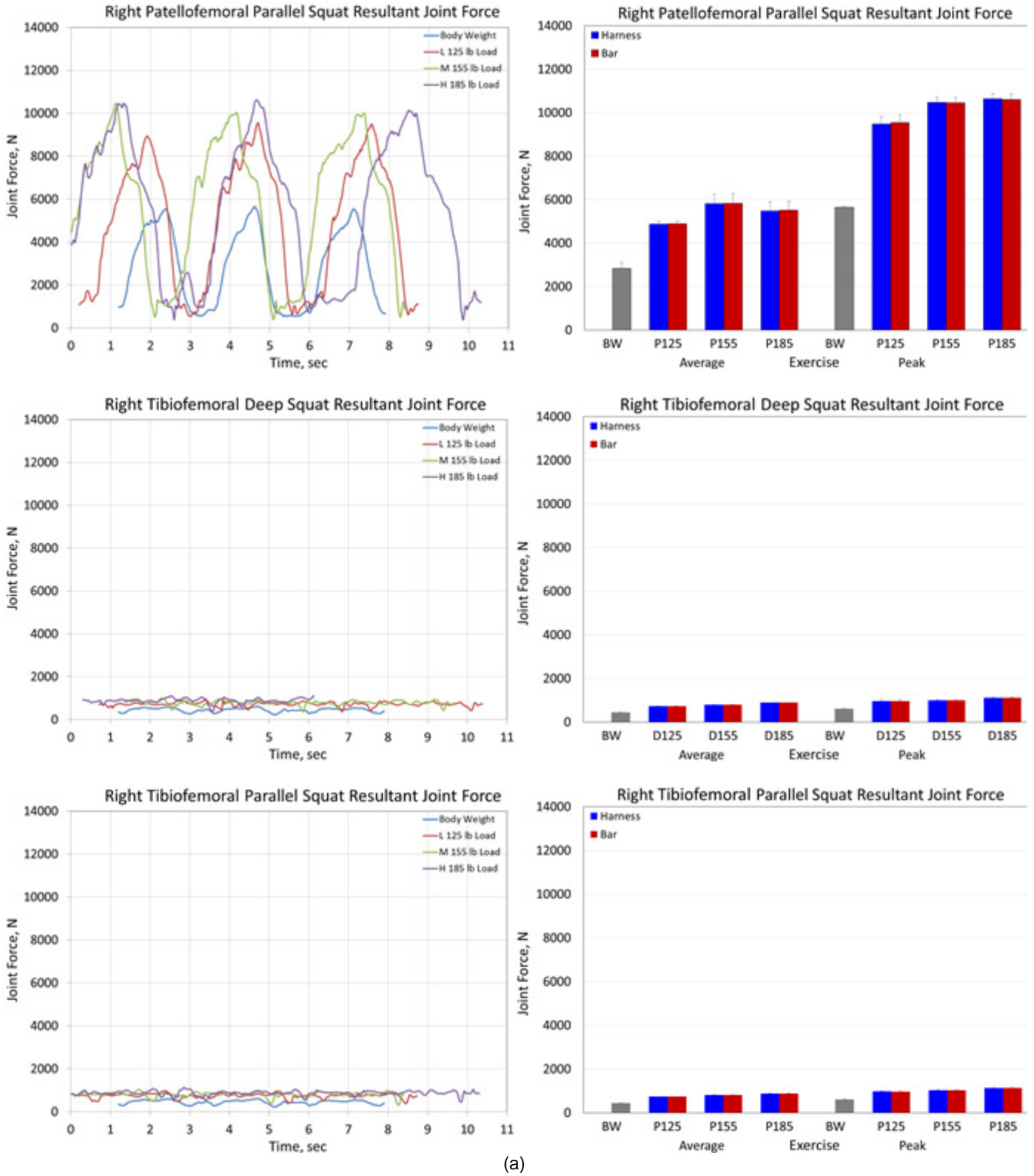
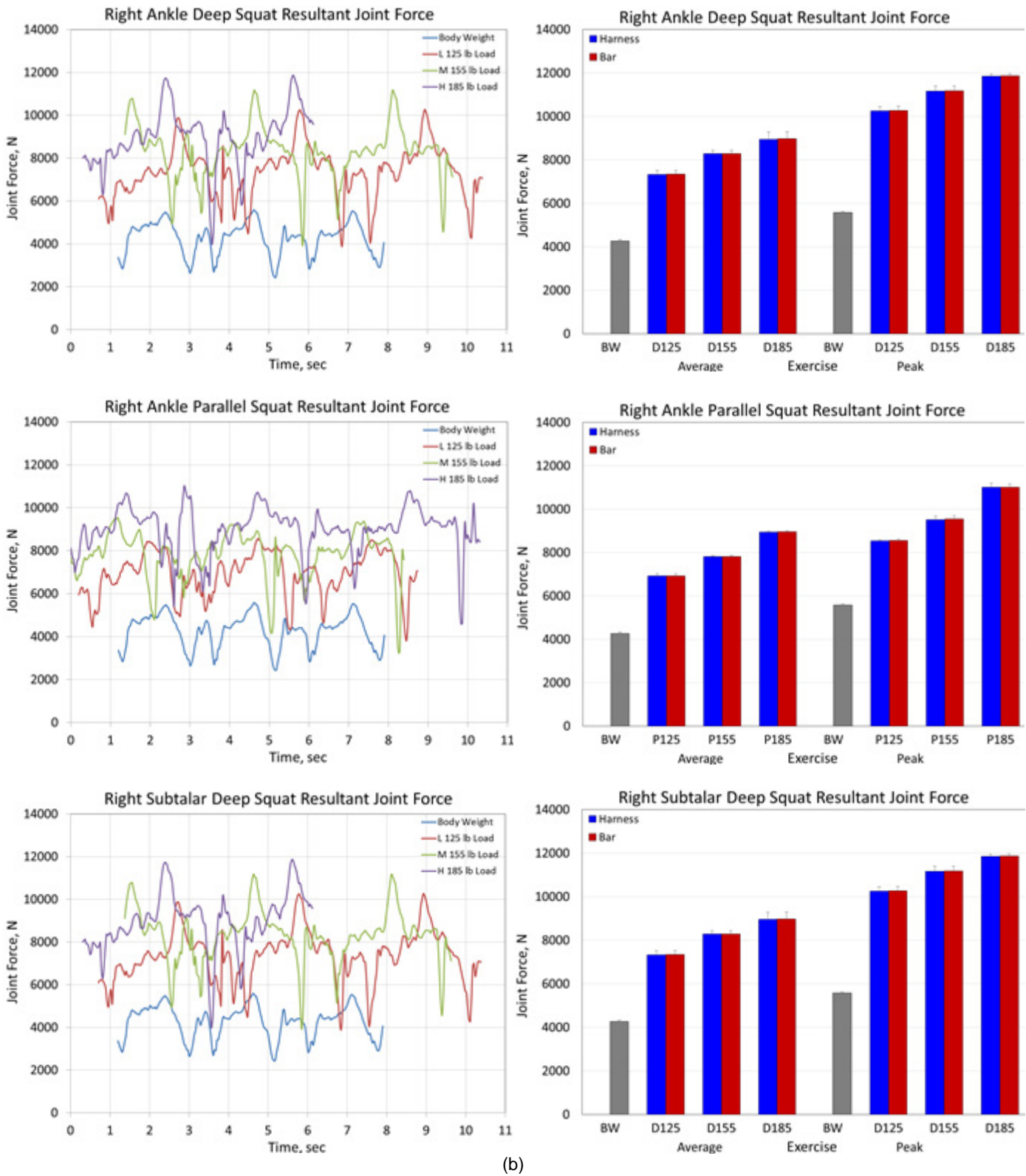


Figure 11.—Continued. Resultant joint forces in Newtons for deep and parallel squats under all loading conditions for the (a) hip and knee (patellofemoral and tibiofemoral) joints, (b) ankle and subtalar joints, and (c) lumbar joint with bar and harness loading separated.



(b)

Figure 11.—Continued. Resultant joint forces in Newtons for deep and parallel squats under all loading conditions for the (a) hip and knee (patellofemoral and tibiofemoral) joints, (b) ankle and subtalar joints, and (c) lumbar joint with bar and harness loading separated.

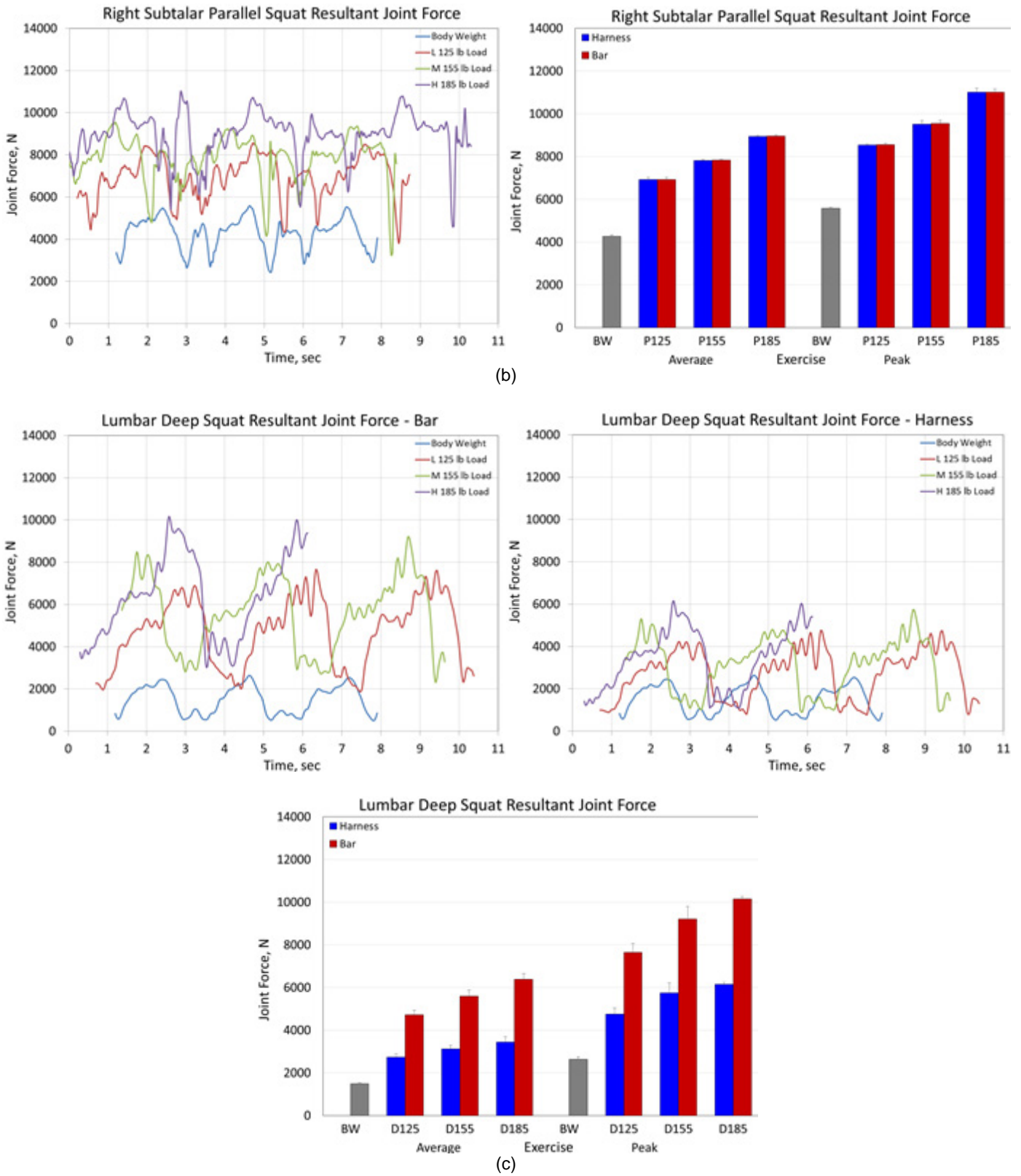


Figure 11.—Continued. Resultant joint forces in Newtons for deep and parallel squats under all loading conditions for the (a) hip and knee (patellofemoral and tibiofemoral) joints, (b) ankle and subtalar joints, and (c) lumbar joint with bar and harness loading separated.

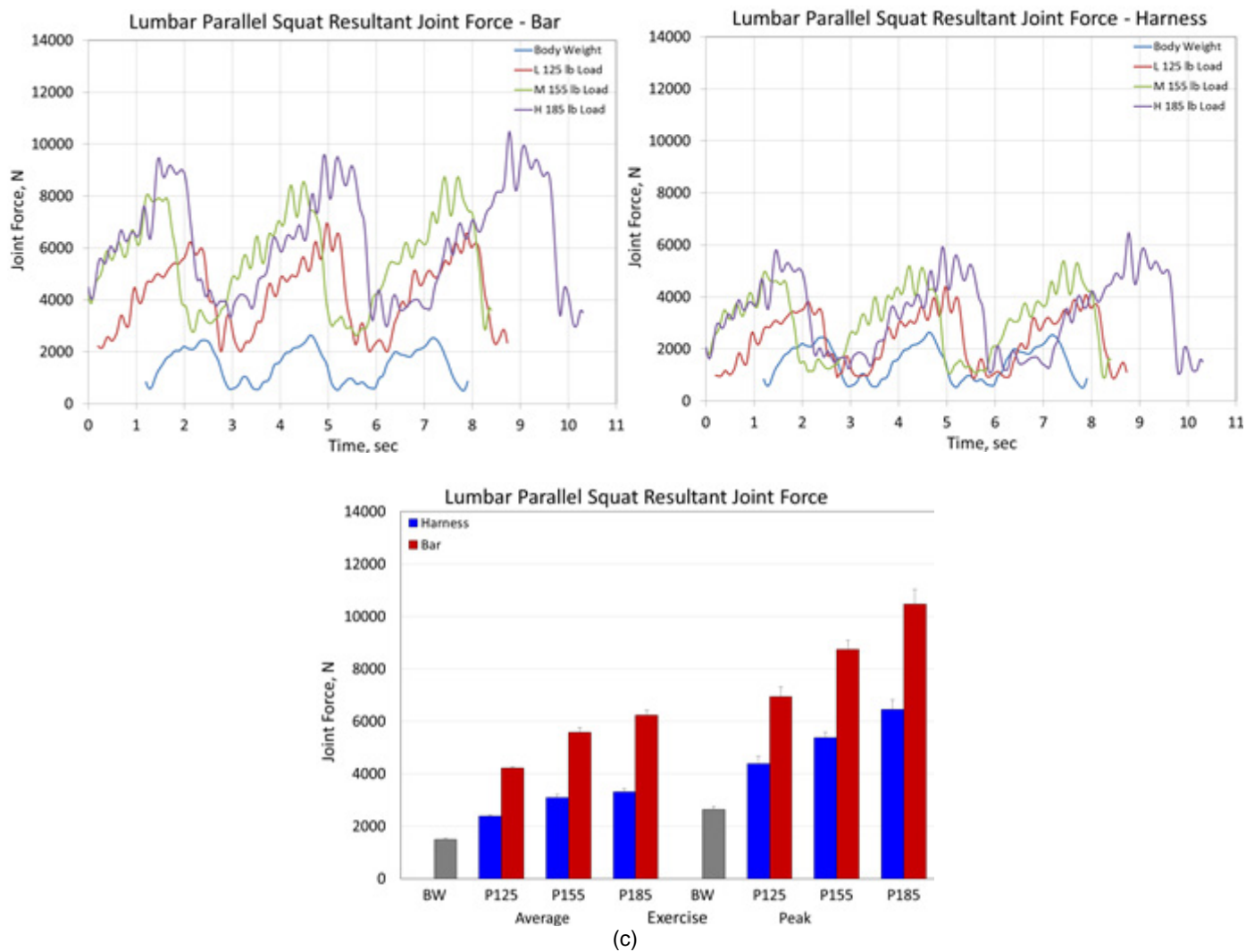


Figure 11.—Concluded. Resultant joint forces in Newtons for deep and parallel squats under all loading conditions for the (a) hip and knee (patellofemoral and tibiofemoral) joints, (b) ankle and subtalar joints, and (c) lumbar joint with bar and harness loading separated.

Average and Peak Joint Moments for Deep and Parallel Squats

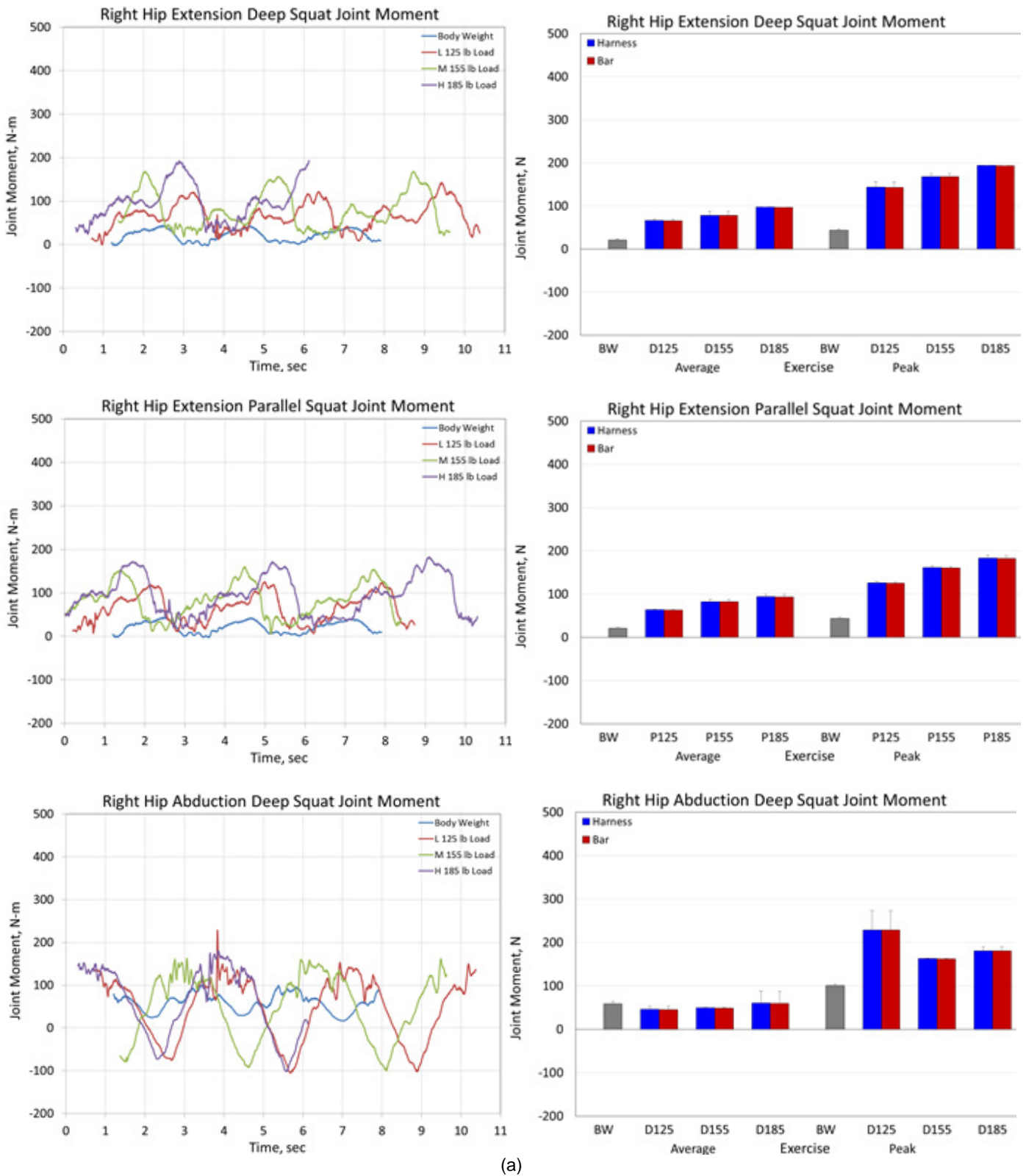


Figure 12.—Joint moments in Newton-meters for deep and parallel squats under all loading conditions for the (a) hip extension, hip abduction and knee extensor joints, (b) ankle plantar flexor and subtalar invertor, and (c) lumbar extension joint.

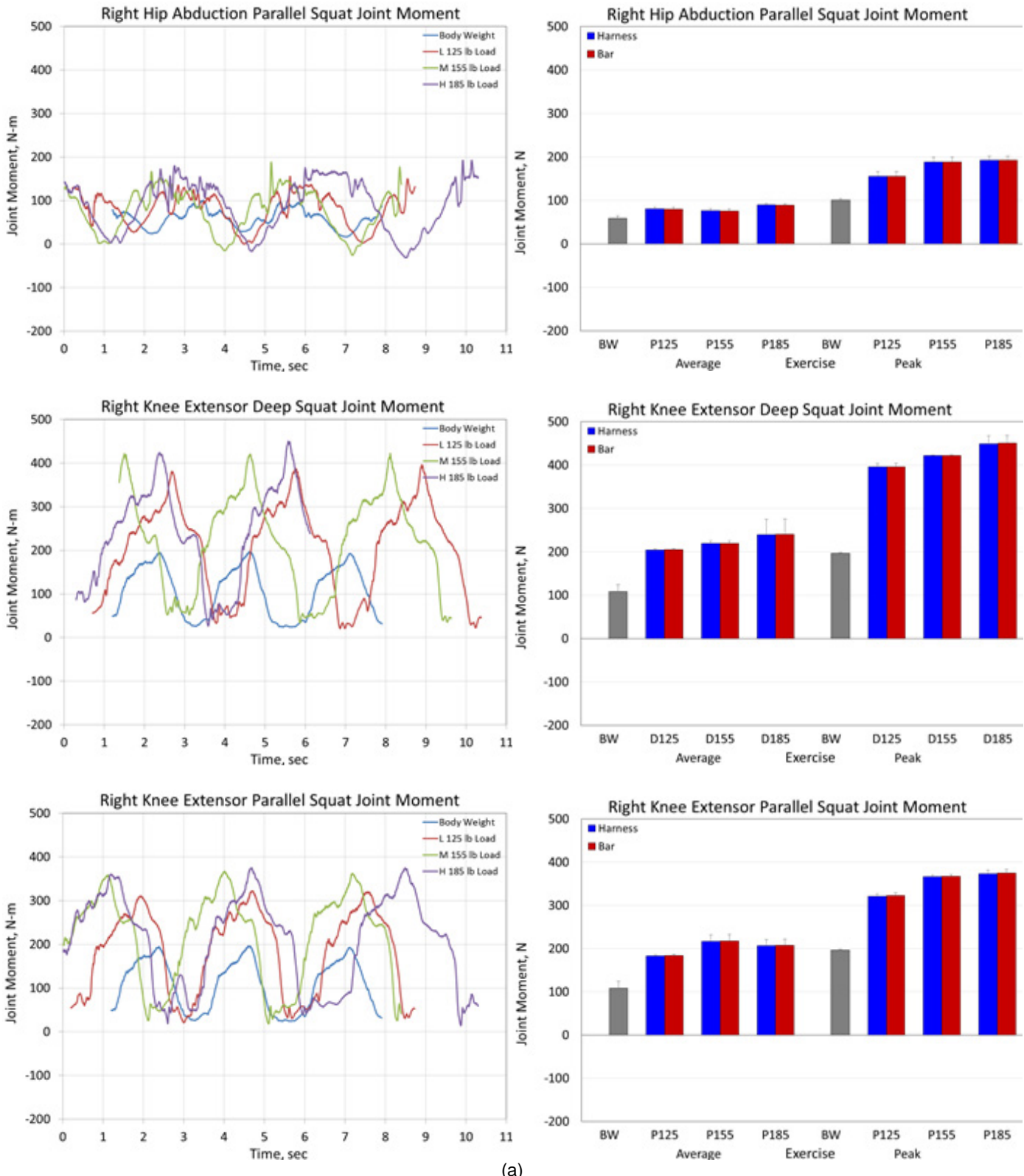
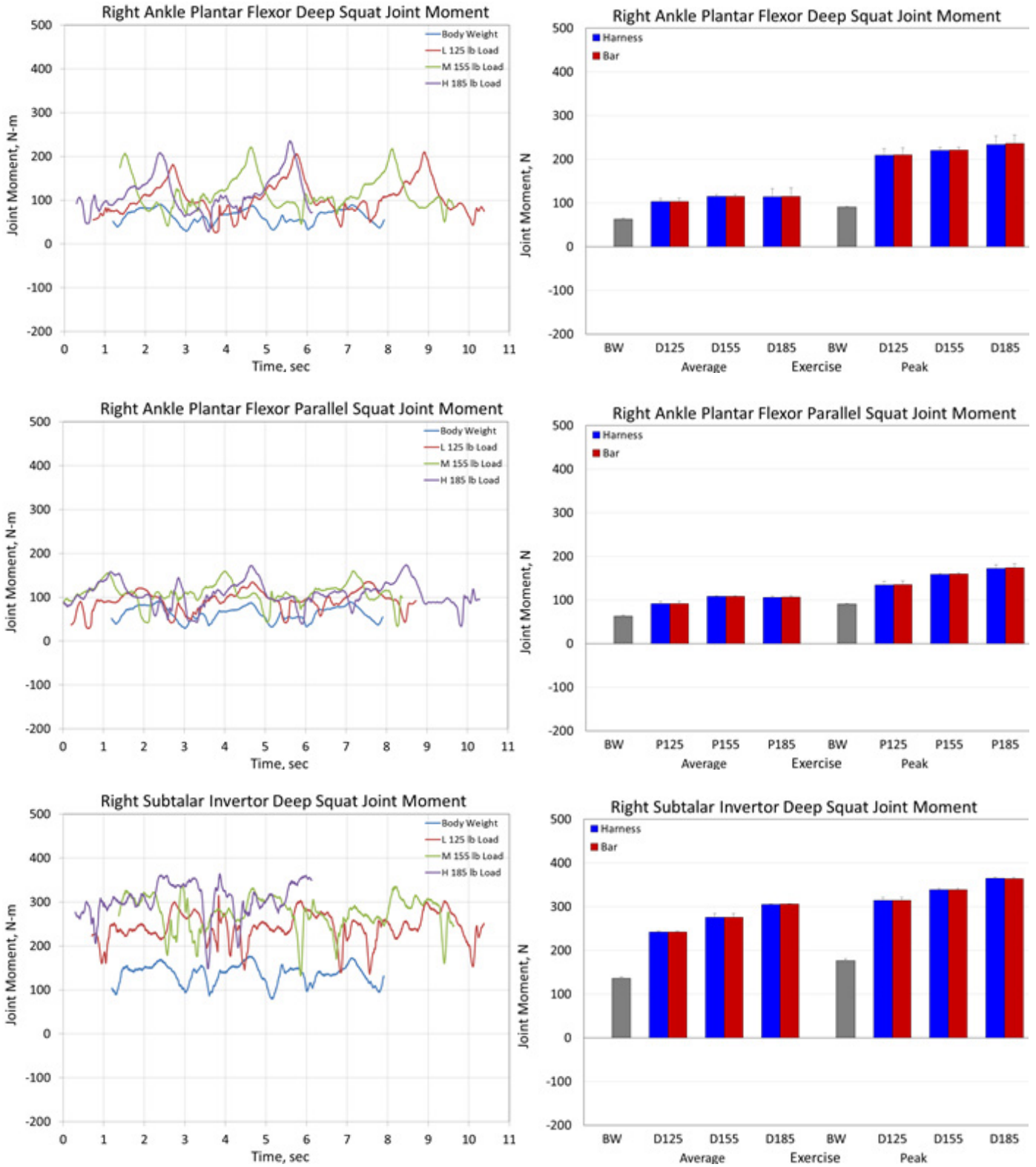


Figure 12.—Continued. Joint moments in Newton-meters for deep and parallel squats under all loading conditions for the (a) hip extension, hip abduction and knee extensor joints, (b) ankle plantar flexor and subtalar invertor, and (c) lumbar extension joint.



(b)

Figure 12.—Continued. Joint moments in Newton-meters for deep and parallel squats under all loading conditions for the (a) hip extension, hip abduction and knee extensor joints, (b) ankle plantar flexor and subtalar invertor, and (c) lumbar extension joint.

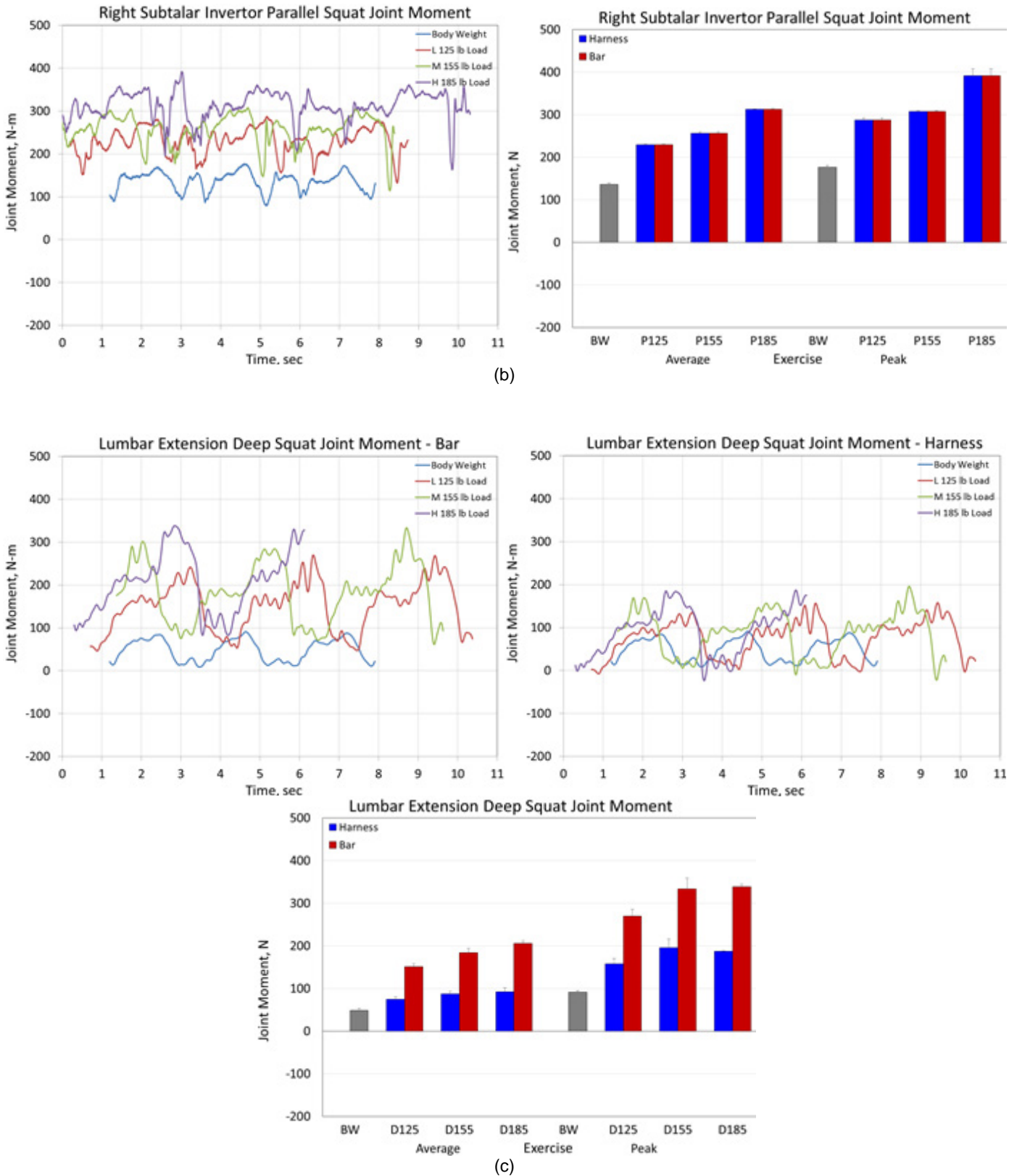


Figure 12.—Continued. Joint moments in Newton-meters for deep and parallel squats under all loading conditions for the (a) hip extension, hip abduction and knee extensor joints, (b) ankle plantar flexor and subtalar invertor, and (c) lumbar extension joint.

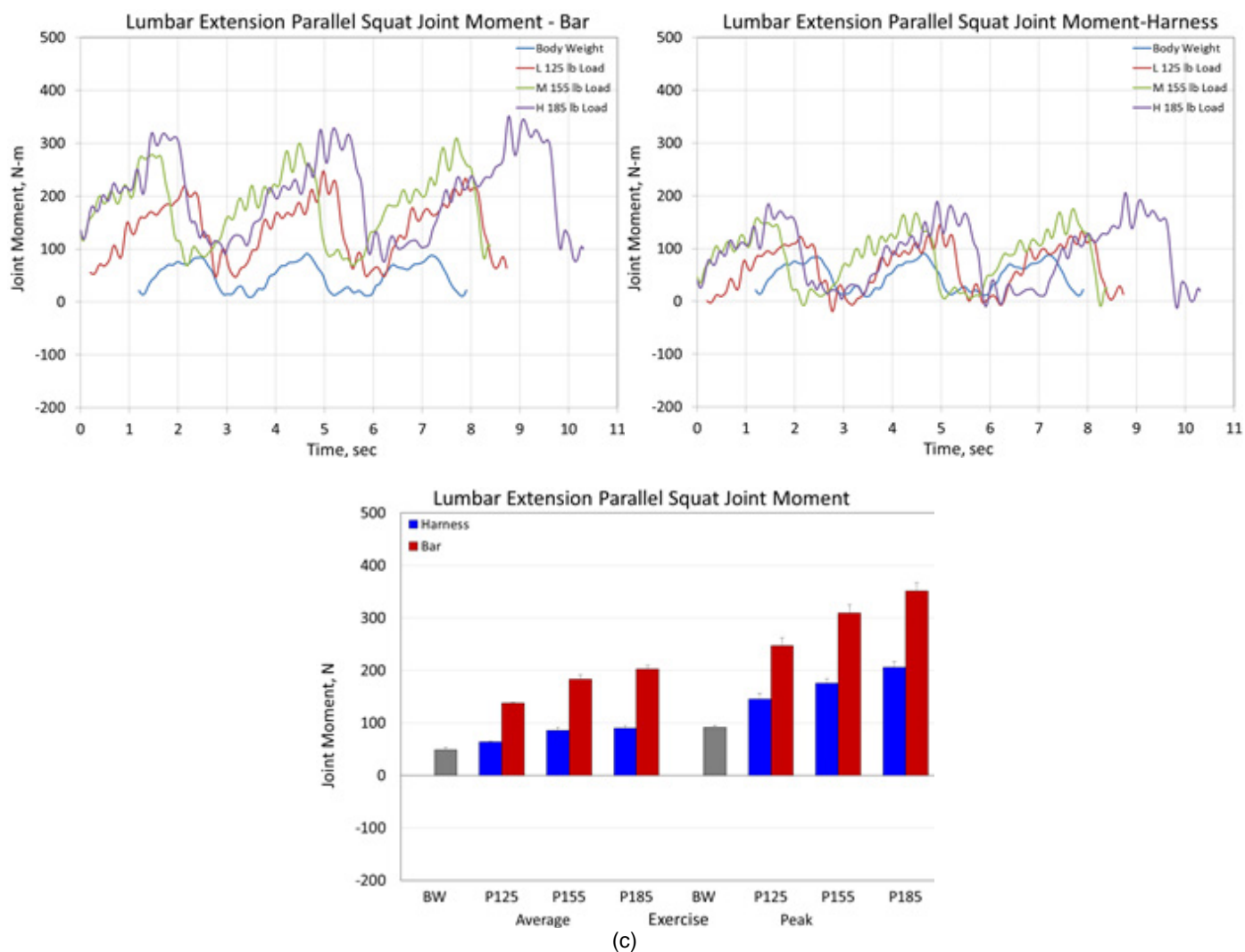


Figure 12.—Concluded. Joint moments in Newton-meters for deep and parallel squats under all loading conditions for the (a) hip extension, hip abduction and knee extensor joints, (b) ankle plantar flexor and subtalar invertor, and (c) lumbar extension joint.

Average and Peak Muscle Forces by Muscle Group for Deep and Parallel Squats

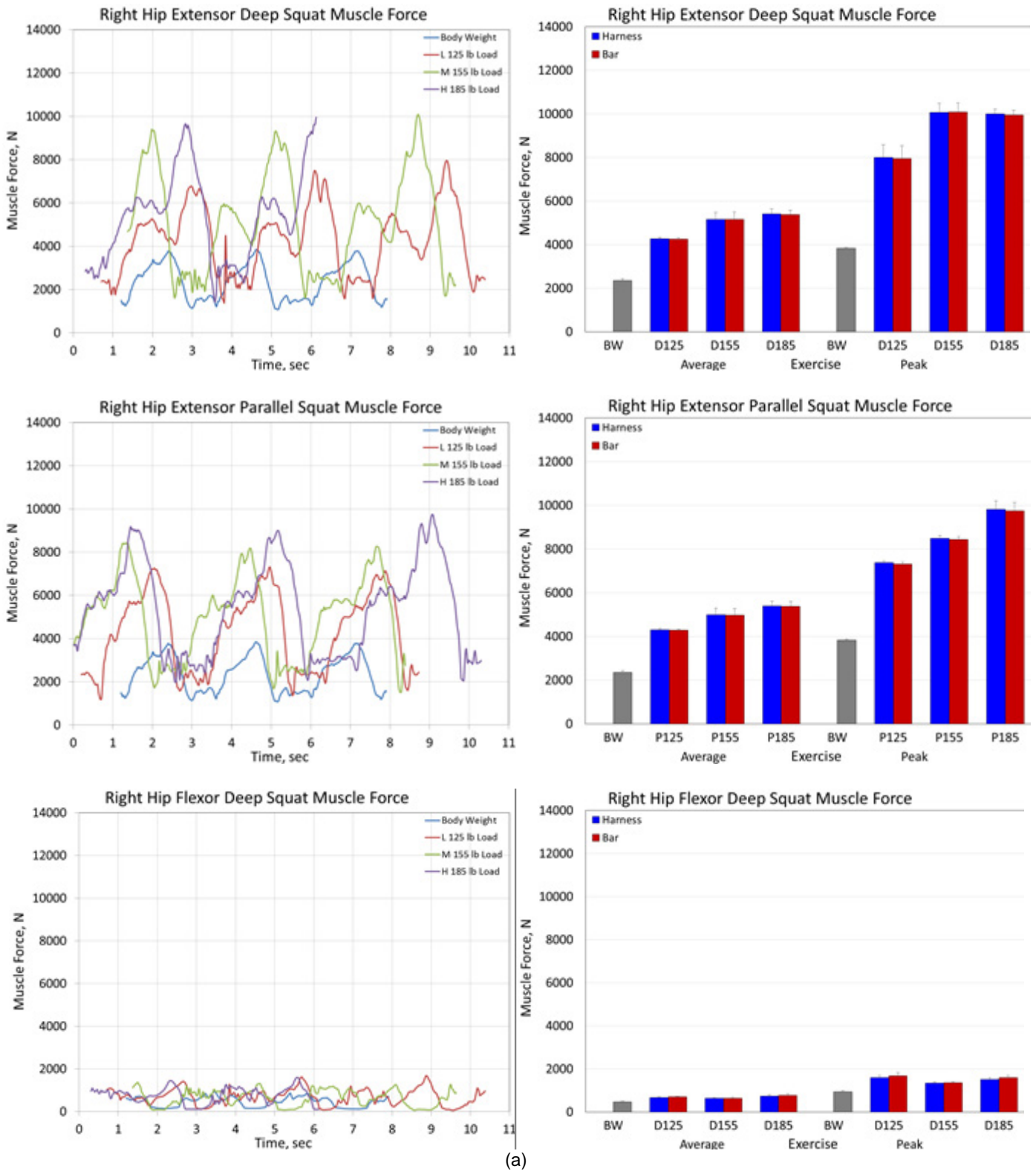
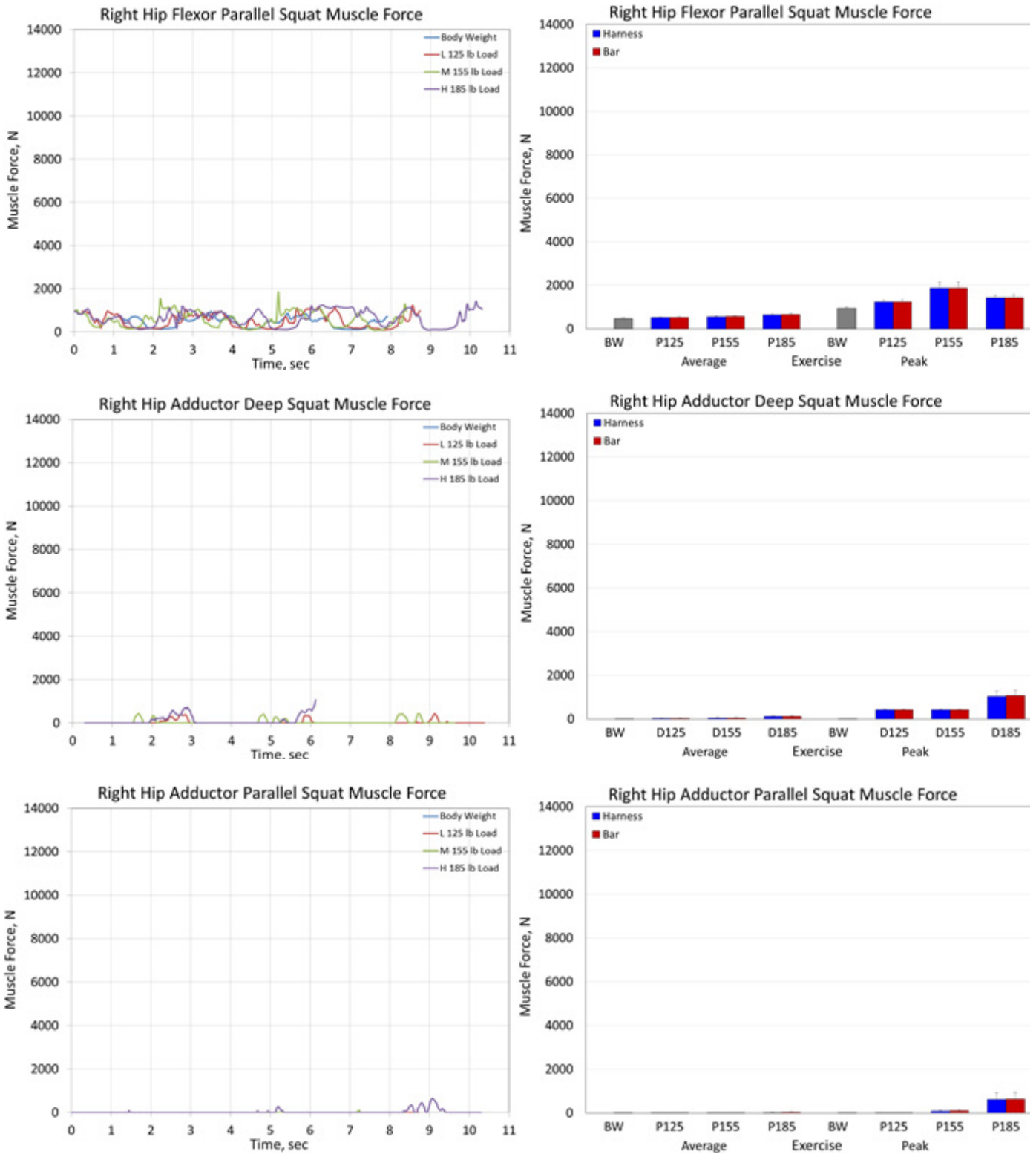
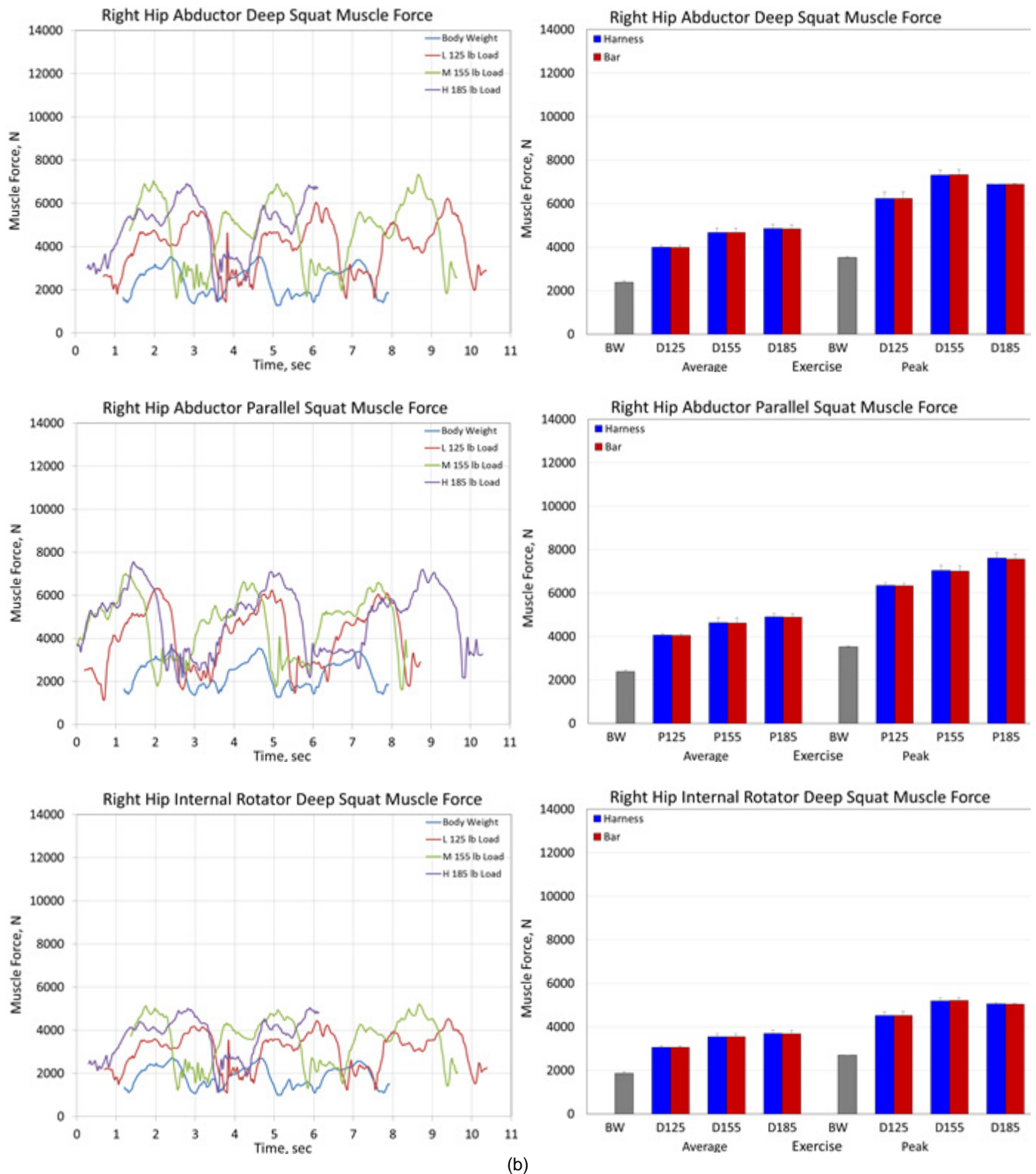


Figure 13.—Muscle forces for deep and parallel squats under all loading conditions for the (a) hip extensor, hip flexor and hip adductor groups, (b) hip abductor, hip internal rotator and hip external rotator groups, (c) knee extensor, knee flexor and ankle dorsiflexor groups, and (d) ankle plantar flexor, subtalar evertor and subtalar invertor groups.



(a)

Figure 13.—Continued. Muscle forces for deep and parallel squats under all loading conditions for the (a) hip extensor, hip flexor and hip adductor groups, (b) hip abductor, hip internal rotator and hip external rotator groups, (c) knee extensor, knee flexor and ankle dorsiflexor groups, and (d) ankle plantar flexor, subtalar evertor and subtalar invertor groups.



(b)

Figure 13.—Continued. Muscle forces for deep and parallel squats under all loading conditions for the (a) hip extensor, hip flexor and hip adductor groups, (b) hip abductor, hip internal rotator and hip external rotator groups, (c) knee extensor, knee flexor and ankle dorsiflexor groups, and (d) ankle plantar flexor, subtalar evtor and subtalar invertor groups.

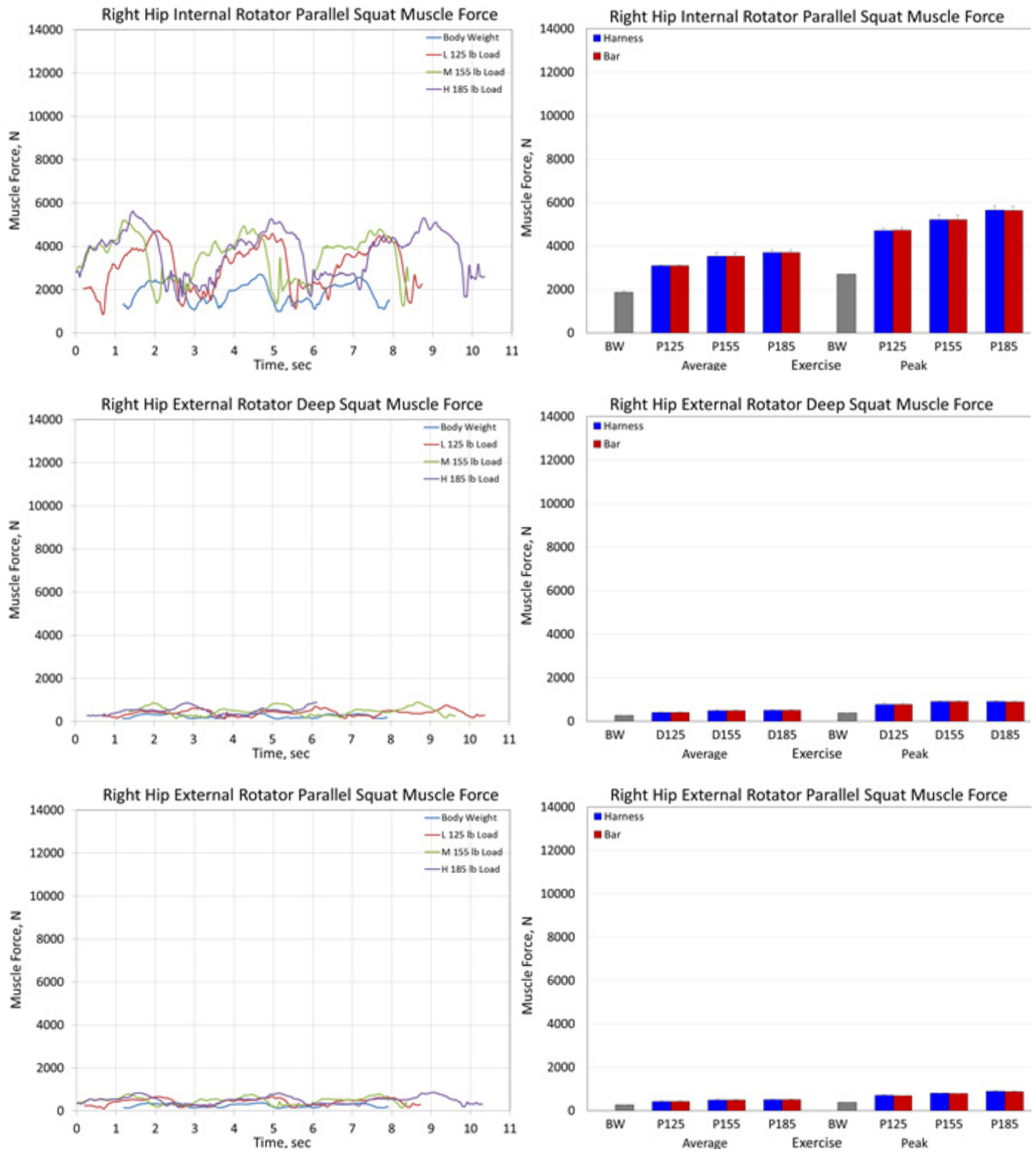
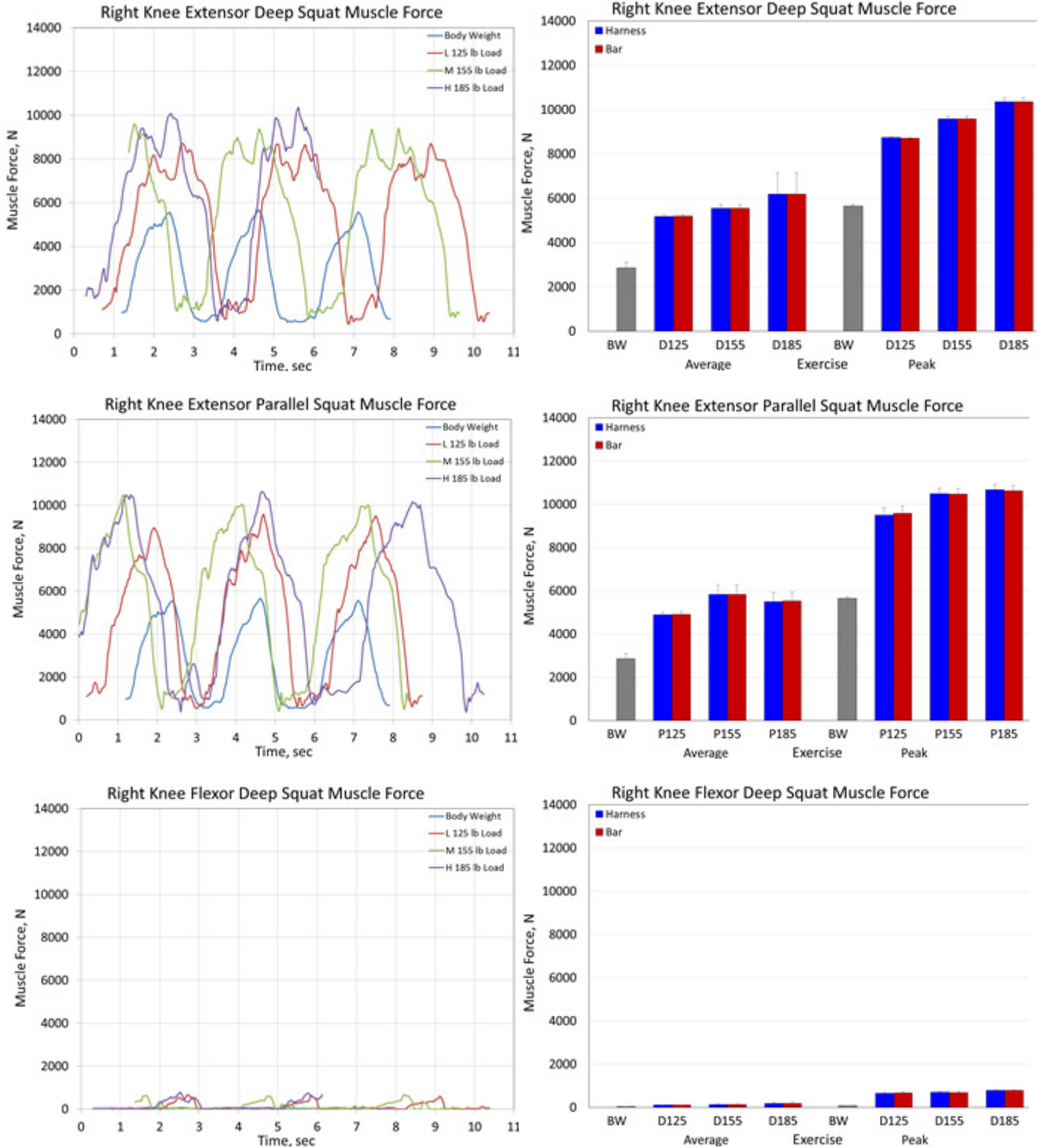
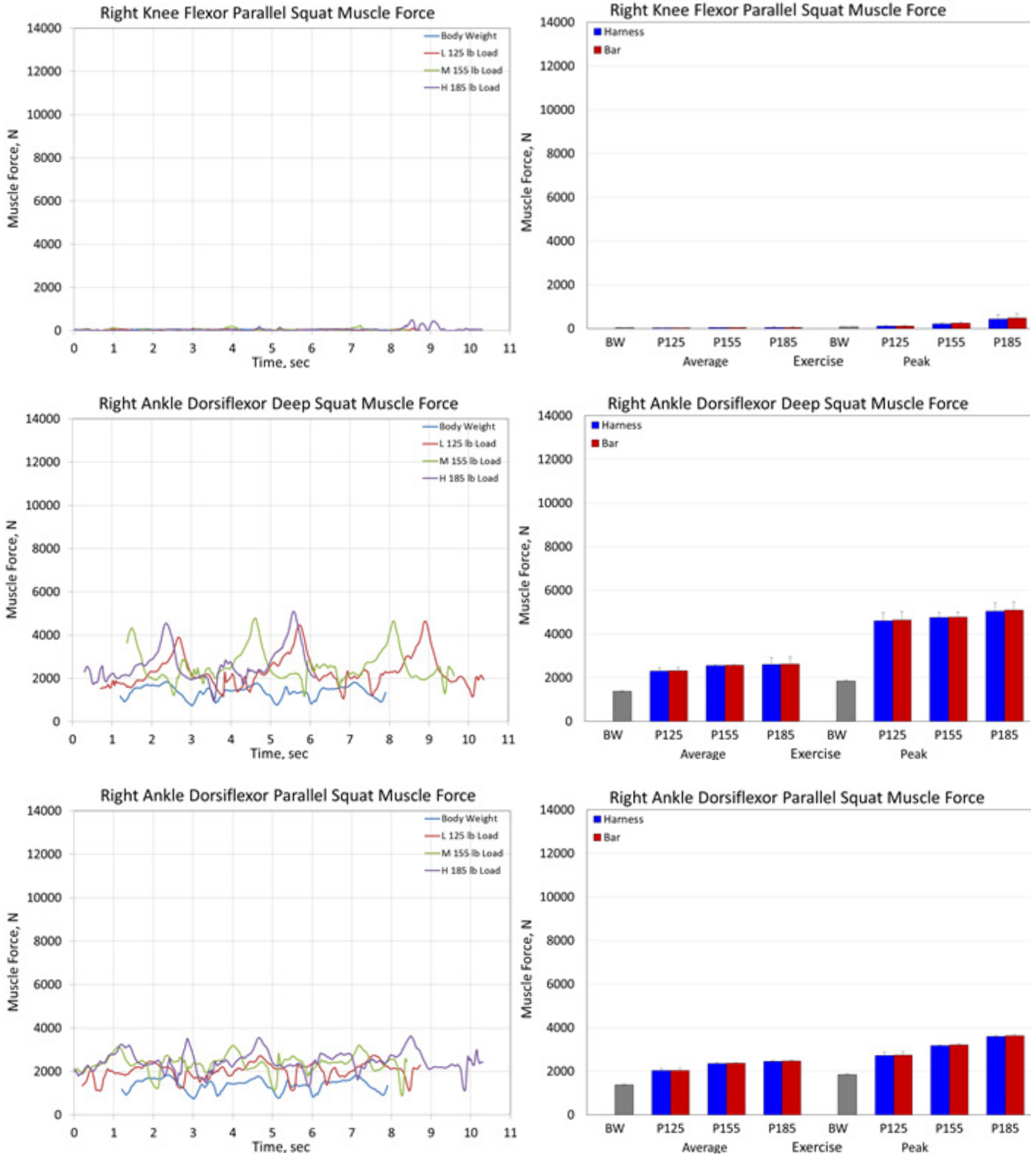


Figure 13.—Continued. Muscle forces for deep and parallel squats under all loading conditions for the (a) hip extensor, hip flexor and hip adductor groups, (b) hip abductor, hip internal rotator and hip external rotator groups, (c) knee extensor, knee flexor and ankle dorsiflexor groups, and (d) ankle plantar flexor, subtalar evertor and subtalar invertor groups.



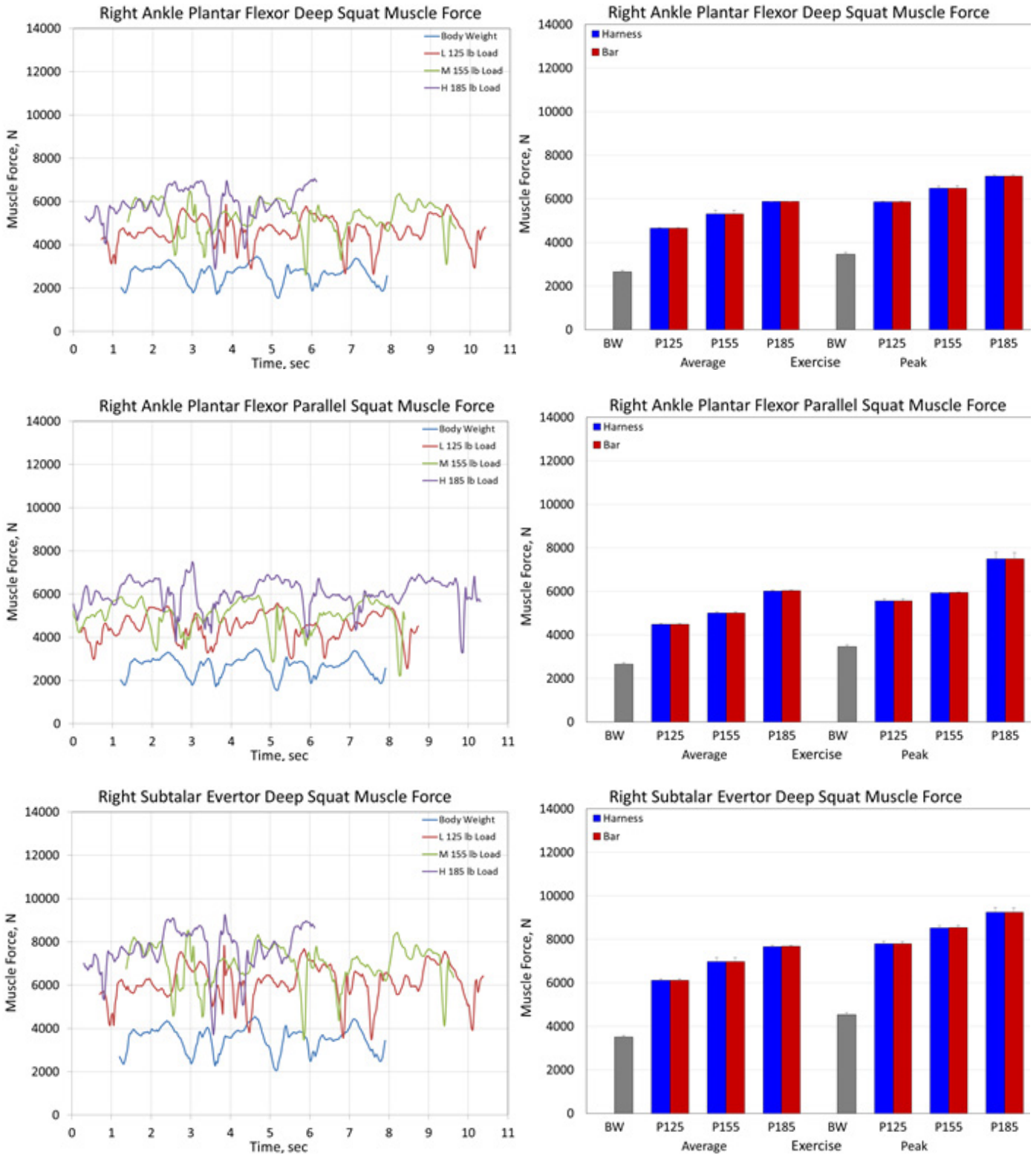
(c)

Figure 13.—Continued. Muscle forces for deep and parallel squats under all loading conditions for the (a) hip extensor, hip flexor and hip adductor groups, (b) hip abductor, hip internal rotator and hip external rotator groups, (c) knee extensor, knee flexor and ankle dorsiflexor groups, and (d) ankle plantar flexor, subtalar evertor and subtalar invertor groups.



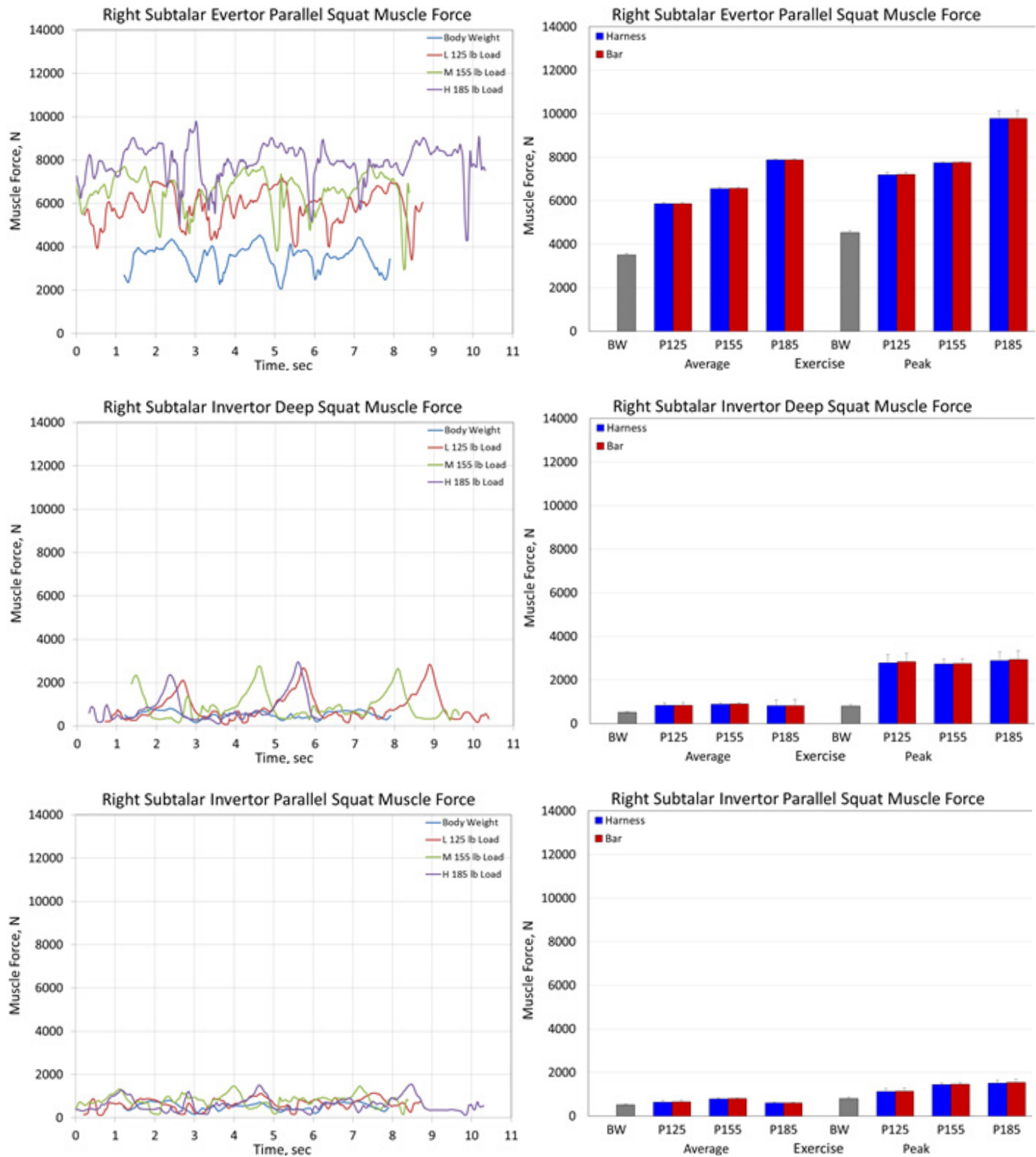
(c)

Figure 13.—Continued. Muscle forces for deep and parallel squats under all loading conditions for the (a) hip extensor, hip flexor and hip adductor groups, (b) hip abductor, hip internal rotator and hip external rotator groups, (c) knee extensor, knee flexor and ankle dorsiflexor groups, and (d) ankle plantar flexor, subtalar evertor and subtalar invertor groups.



(d)

Figure 13.—Continued. Muscle forces for deep and parallel squats under all loading conditions for the (a) hip extensor, hip flexor and hip adductor groups, (b) hip abductor, hip internal rotator and hip external rotator groups, (c) knee extensor, knee flexor and ankle dorsiflexor groups, and (d) ankle plantar flexor, subtalar evertor and subtalar invertor groups.



(d)

Figure 13.—Concluded. Muscle forces for deep and parallel squats under all loading conditions for the (a) hip extensor, hip flexor and hip adductor groups, (b) hip abductor, hip internal rotator and hip external rotator groups, (c) knee extensor, knee flexor and ankle dorsiflexor groups, and (d) ankle plantar flexor, subtalar evertor and subtalar invertor groups.

Average and Peak Residual Forces and Moments for Deep and Parallel Squats

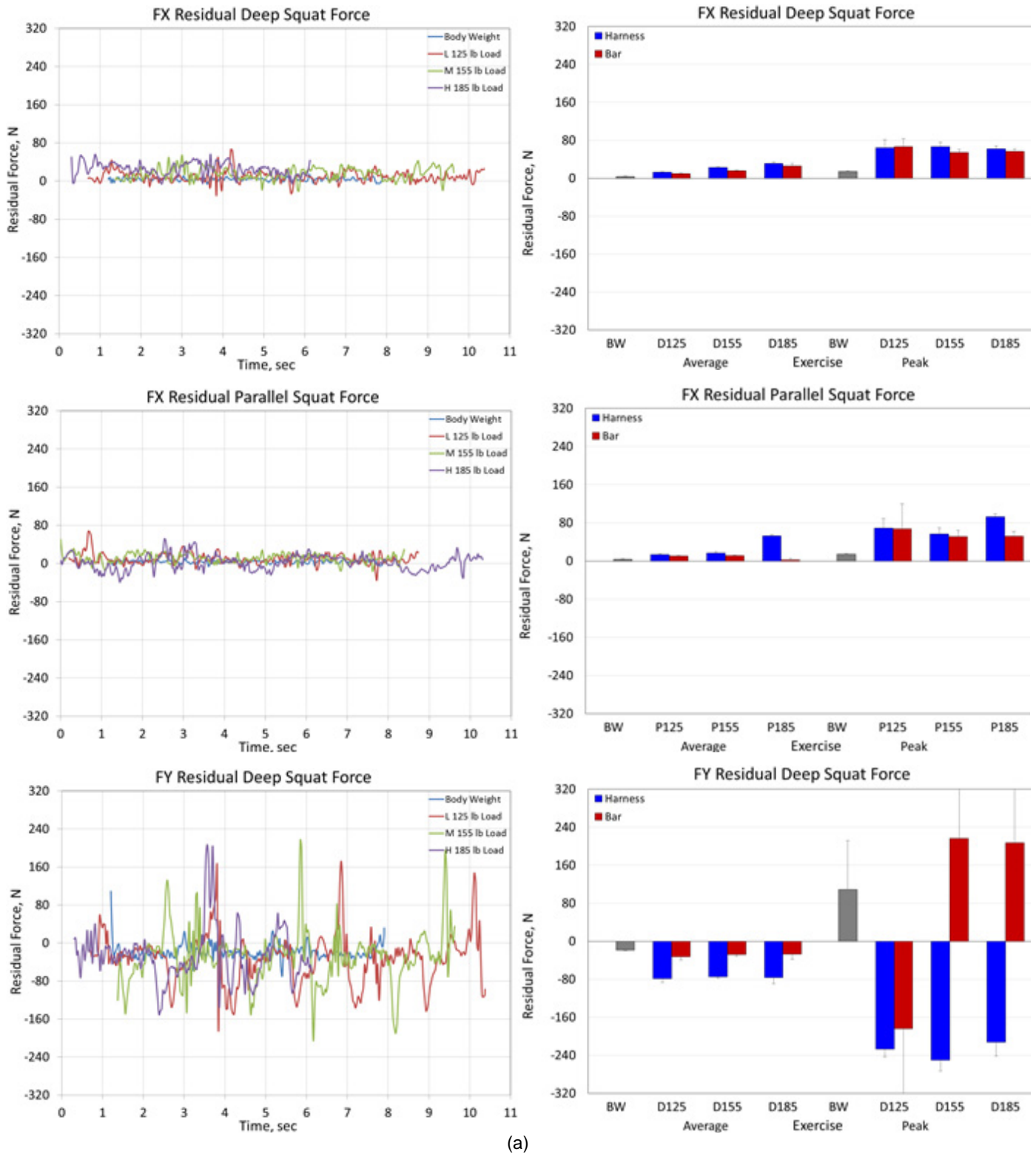
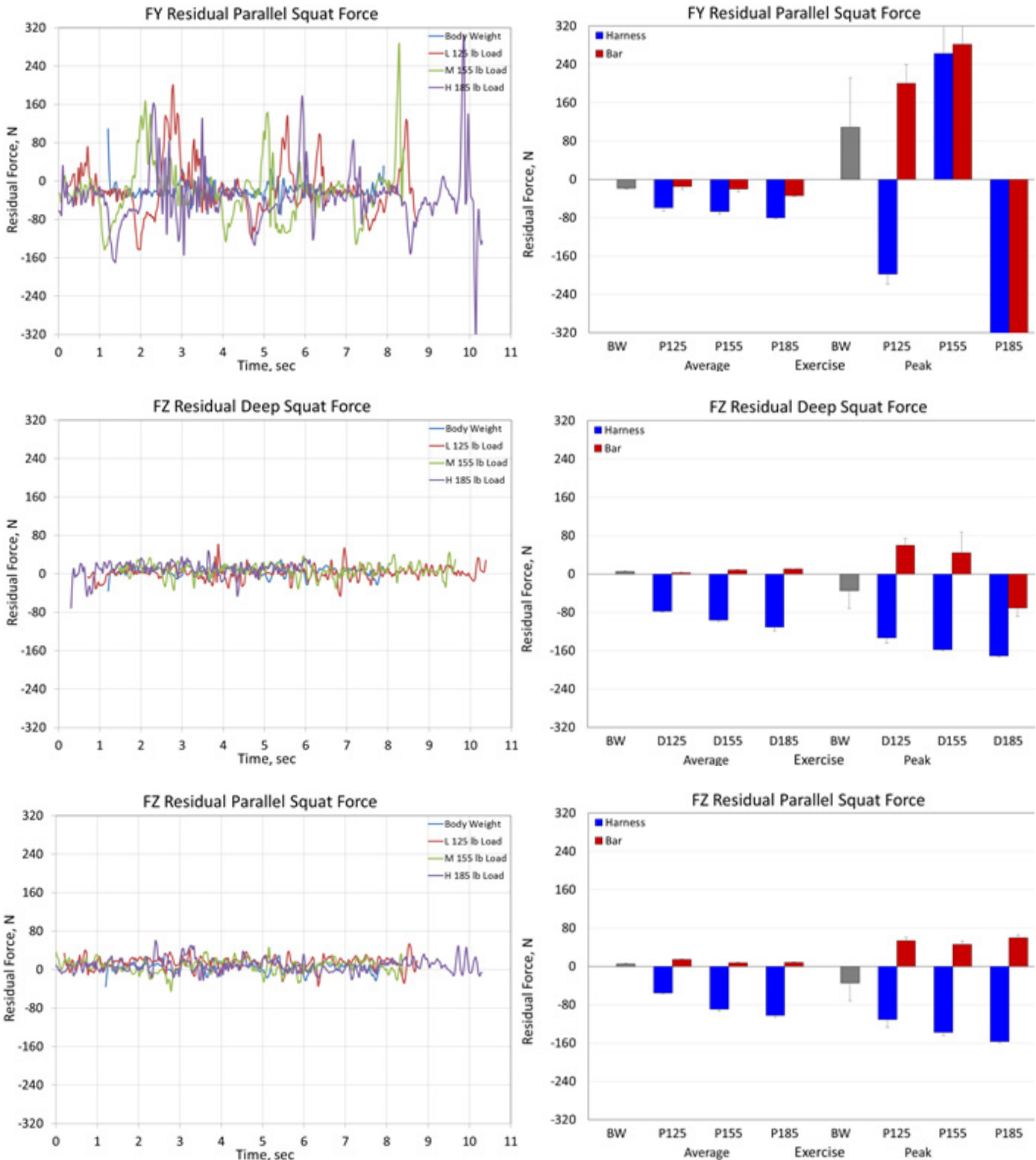


Figure 14.—Average and peak residual forces in (a) Newtons for deep and parallel squats under all loading conditions for the FX, FY, FZ residual forces, and (b) Newton-meters for deep and parallel squats under all loading conditions for the MX, MY, MZ residual moments.



(a)

Figure 14.—Continued. Average and peak residual forces in (a) Newtons for deep and parallel squats under all loading conditions for the FX, FY, FZ residual forces, and (b) Newton-meters for deep and parallel squats under all loading conditions for the MX, MY, MZ residual moments.

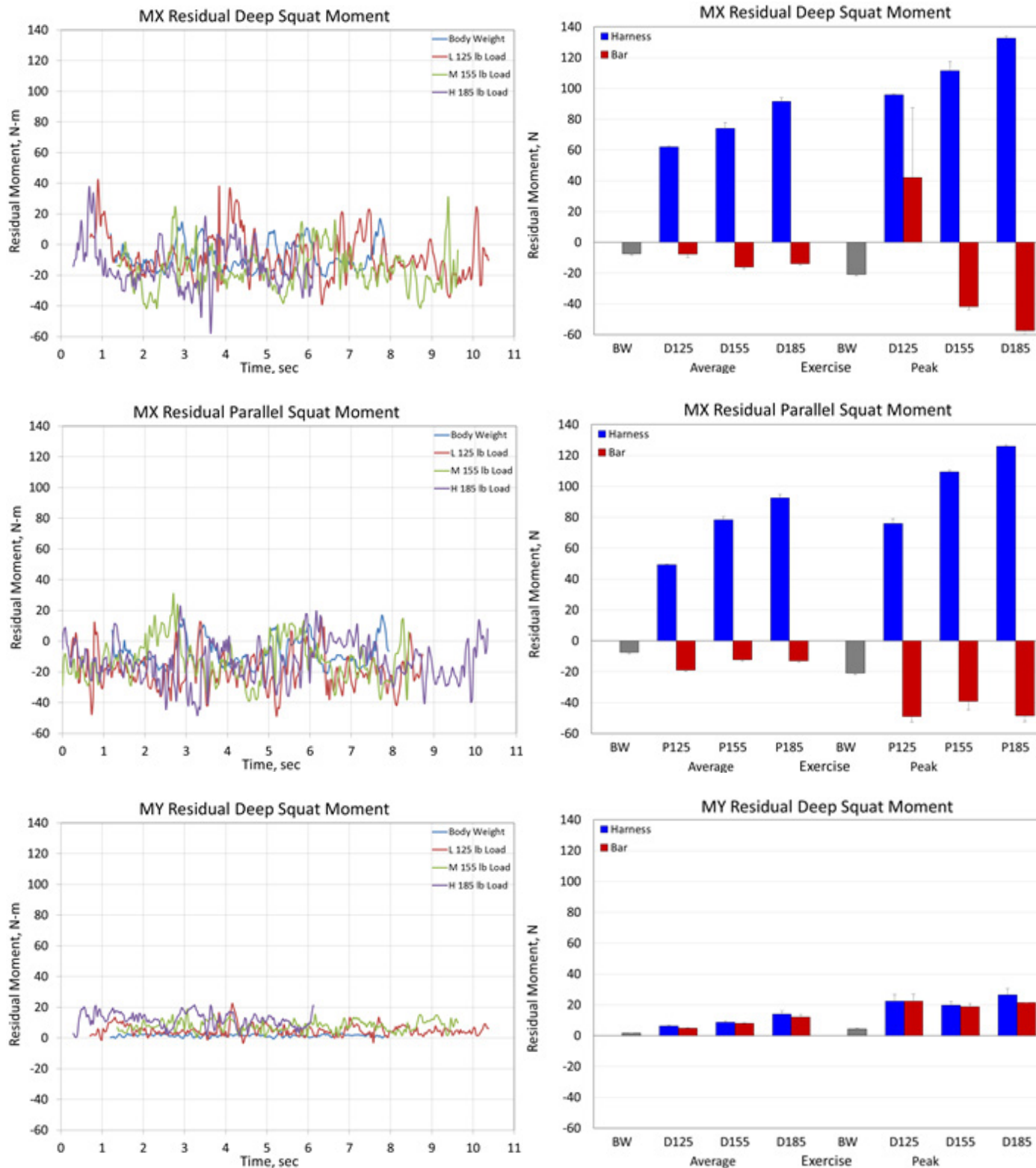


Figure 14.—Continued. Average and peak residual forces in (a) Newtons for deep and parallel squats under all loading conditions for the FX, FY, FZ residual forces, and (b) Newton-meters for deep and parallel squats under all loading conditions for the MX, MY, MZ residual moments.

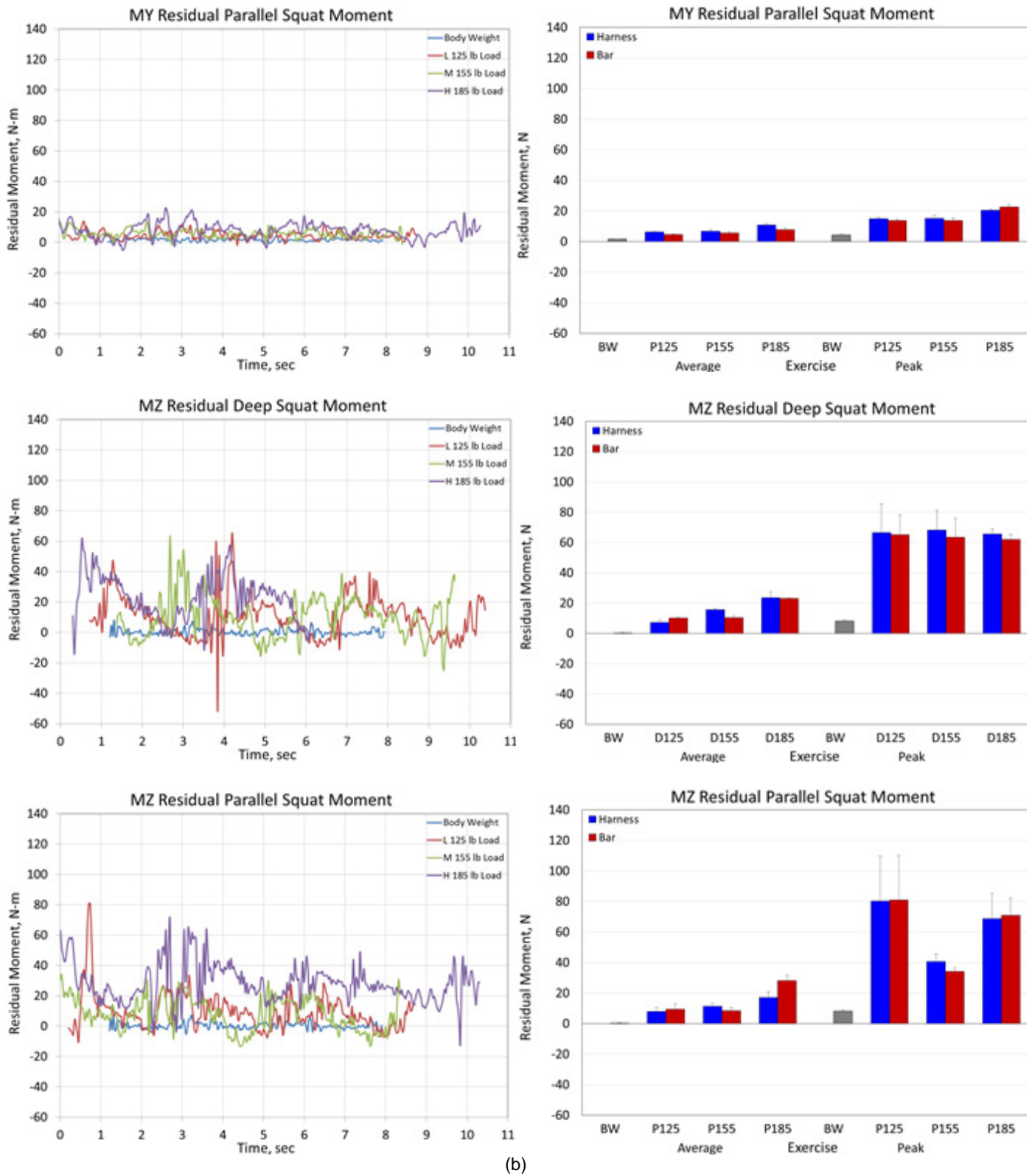
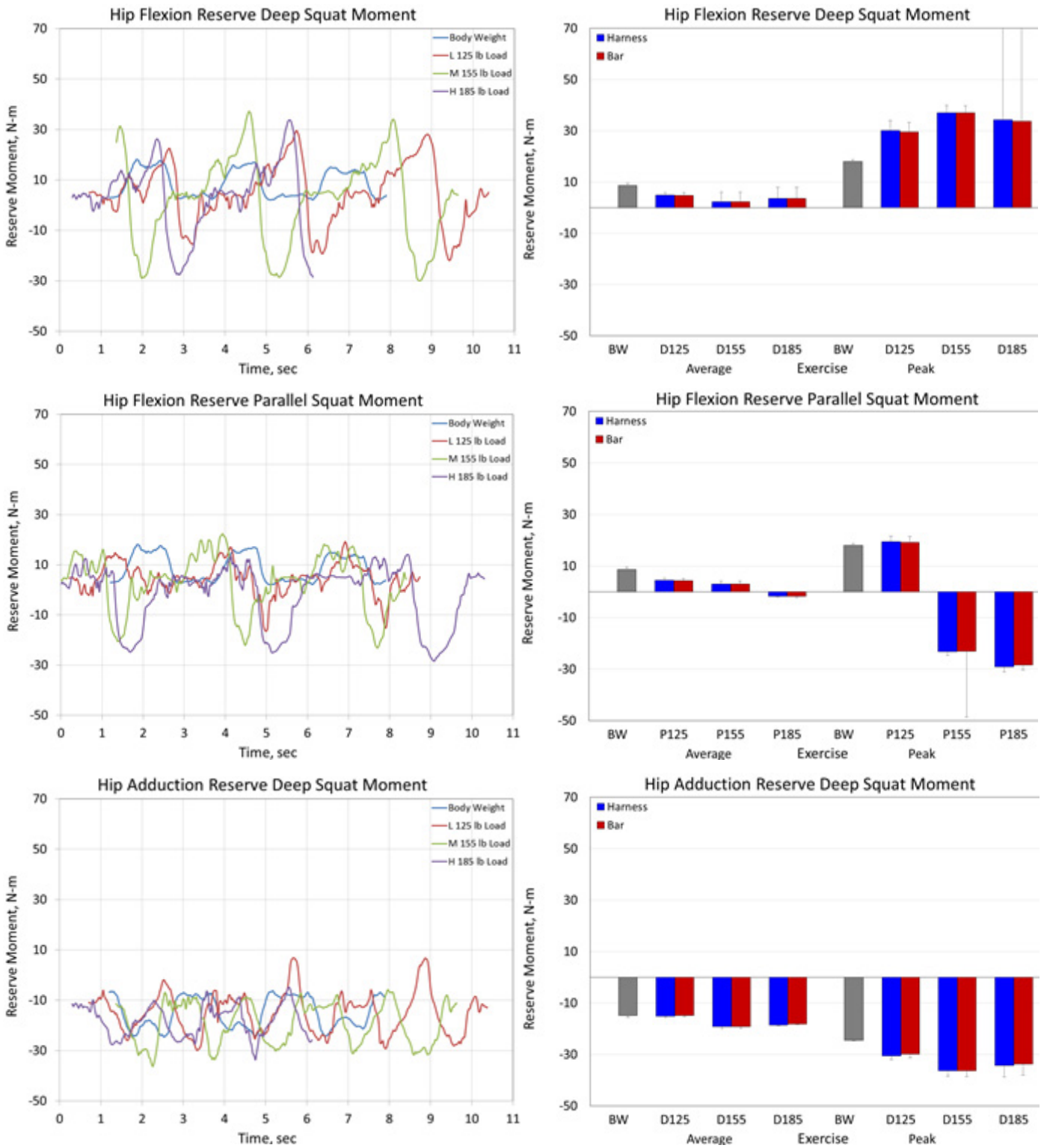


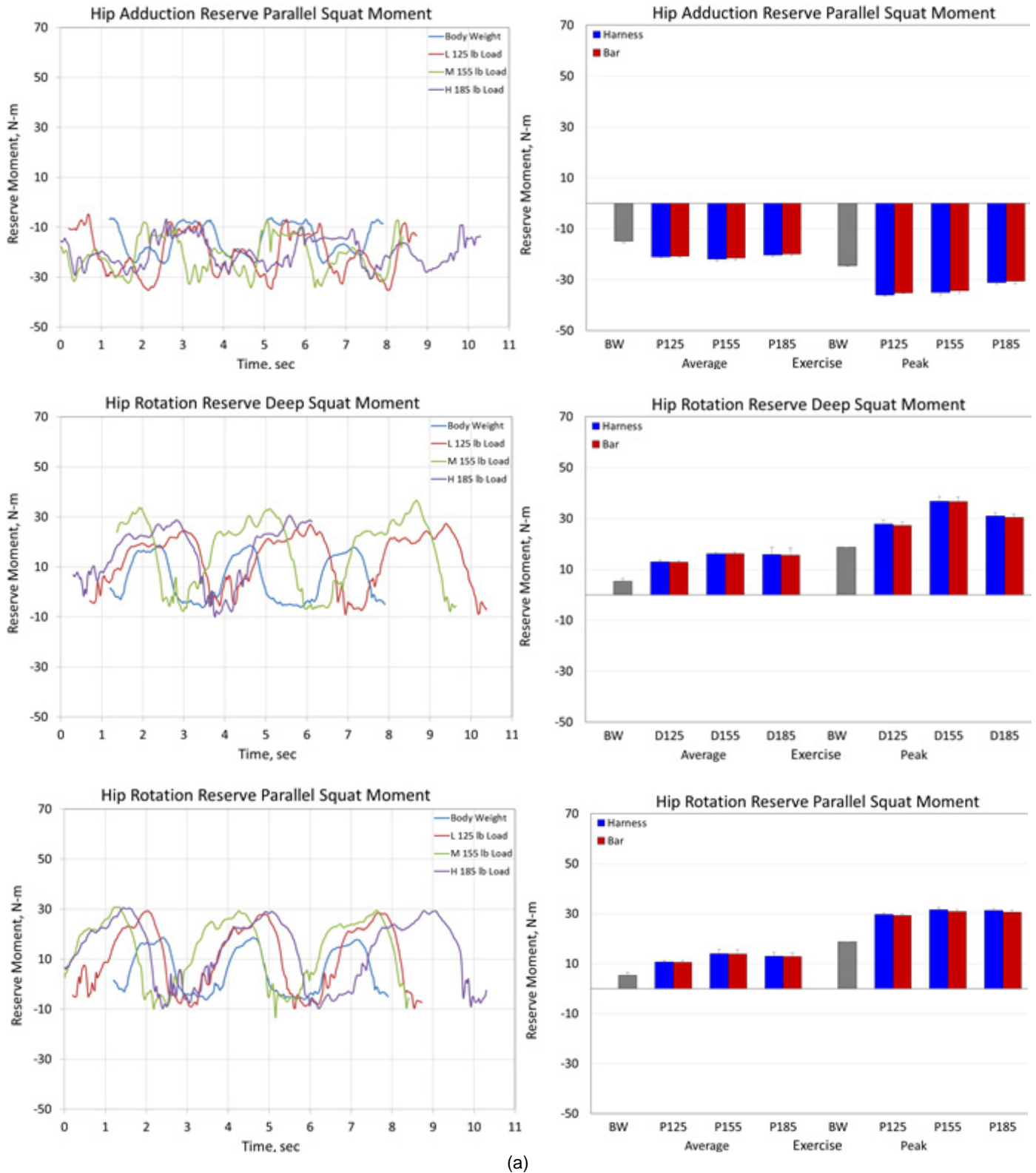
Figure 14.—Concluded. Average and peak residual forces in (a) Newtons for deep and parallel squats under all loading conditions for the FX, FY, FZ residual forces, and (b) Newton-meters for deep and parallel squats under all loading conditions for the MX, MY, MZ residual moments.

Average and Peak Reserve Moments for Deep and Parallel Squats



(a)

Figure 15.—Reserve actuator moments in Newton-meters for deep and parallel squats under all loading conditions for the (a) hip flexion, hip adduction and hip rotation joint articulations and (b) knee flexion, ankle dorsiflexor and lumbar extension joint articulations.



(a)

Figure 15.—Continued. Reserve actuator moments in Newton-meters for deep and parallel squats under all loading conditions for the (a) hip flexion, hip adduction and hip rotation joint articulations, and (b) knee flexion, ankle dorsiflexor and lumbar extension joint articulations.

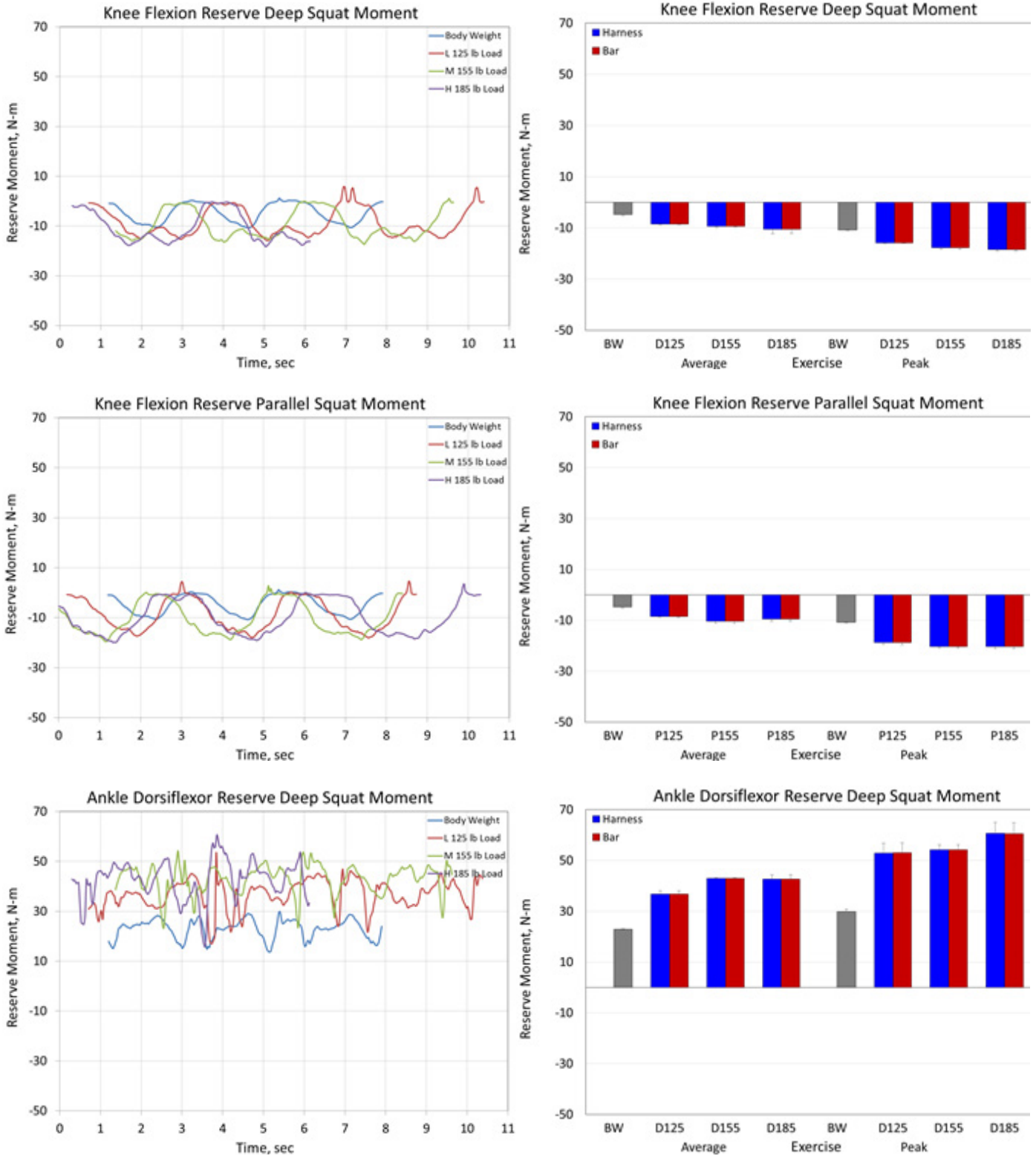
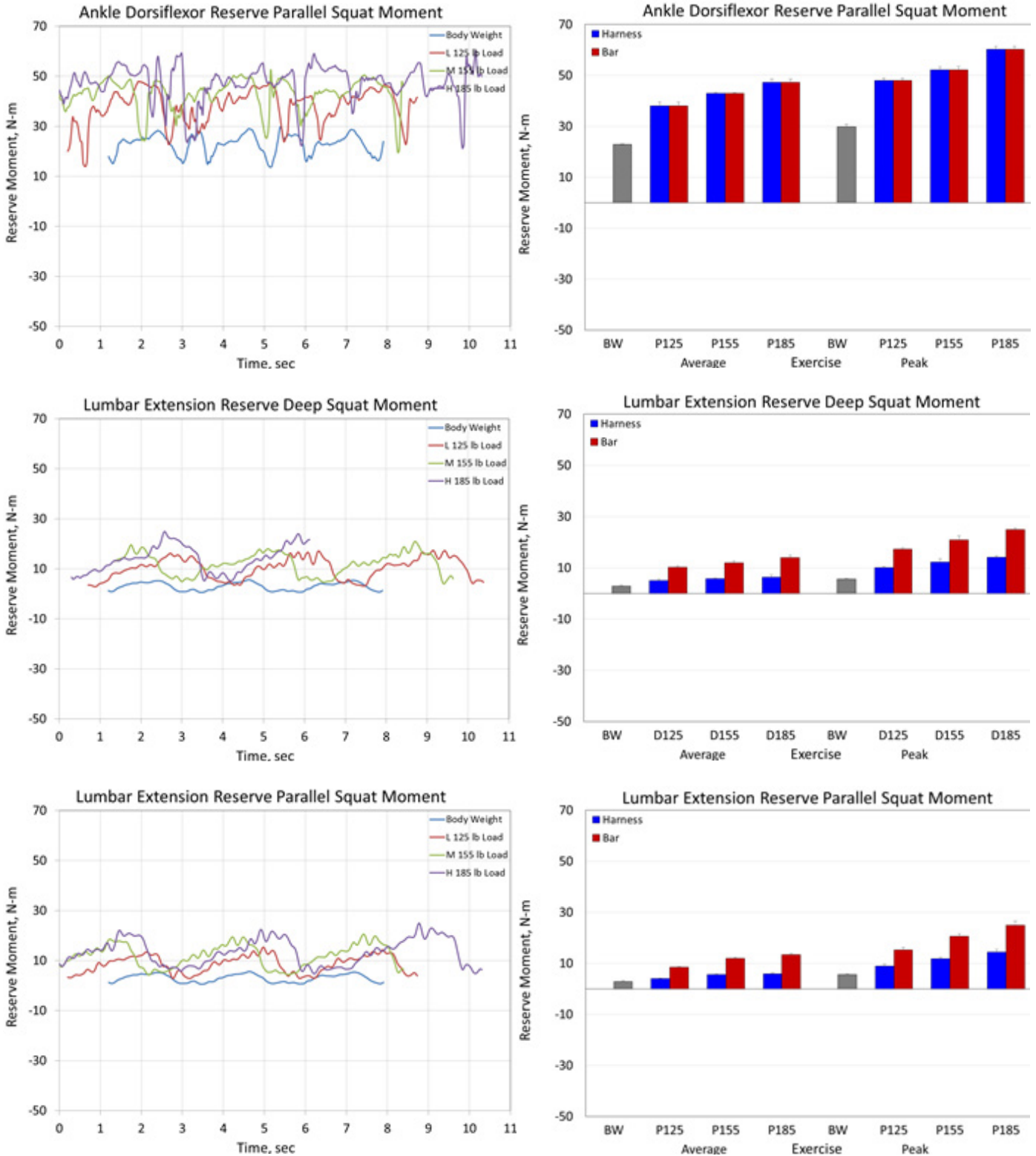


Figure 15.—Continued. Reserve actuator moments in Newton-meters for deep and parallel squats under all loading conditions for the (a) hip flexion, hip adduction and hip rotation joint articulations, and (b) knee flexion, ankle dorsiflexor and lumbar extension joint articulations.



(b)

Figure 15.—Concluded. Reserve actuator moments in Newton-meters for deep and parallel squats under all loading conditions for the (a) hip flexion, hip adduction and hip rotation joint articulations, and (b) knee flexion, ankle dorsiflexor and lumbar extension joint articulations.

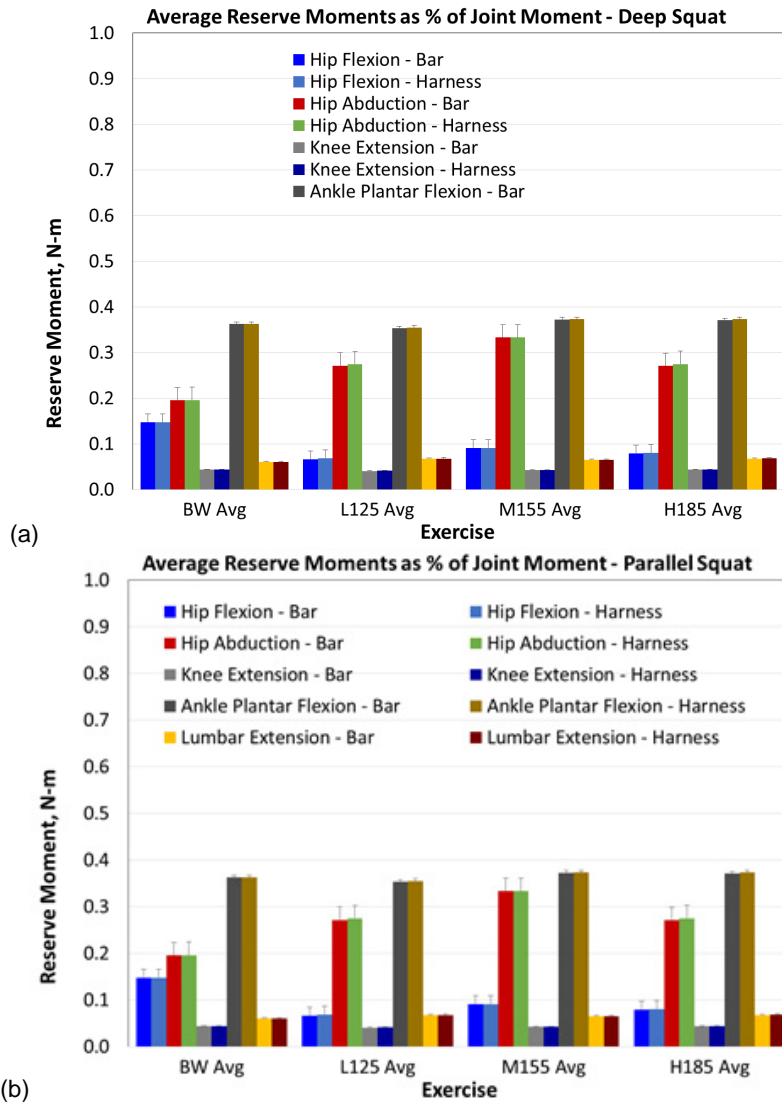


Figure 16.—Average reserve moments as a percentage of total joint moment for (a) deep squat and (b) parallel squat.

Single-Leg Squat Exercise

Joint Kinematics for Single-Leg Squat

Table 5 summarizes the joint angle ranges for the major lower body joints during the single-leg squat for the right leg. Figure 17 shows kinematic trajectories for the major joints on the right side of the body. Left leg (unloaded) results are omitted for brevity. Figure 18 to Figure 20 describe the kinetics of the model, i.e., joint moments, resultant joint forces and muscle tension forces, respectively. Figure 21 describes the model’s residual forces and moments during the squat movement, and Figure 22 describes the reserve actuator moments. Figure 23 shows the reserve joint moments expressed as a percentage of the total joint moments as determined from ID.

TABLE 5.—KINEMATIC JOINT ANGLE RANGES FOR SINGLE-LEG SQUAT

Joint articulation during single-leg squat	Angle at top of movement, °	Angle at bottom of movement, °
Hip flexion	3	37
Hip abduction	-1	7
Hip internal rotation	-4	-14
Knee flexion	10	122
Ankle dorsiflexion	-6	32
Subtalar inversion	-3	-22
MTP flexion	6	-9
Lumbar extension	13	1

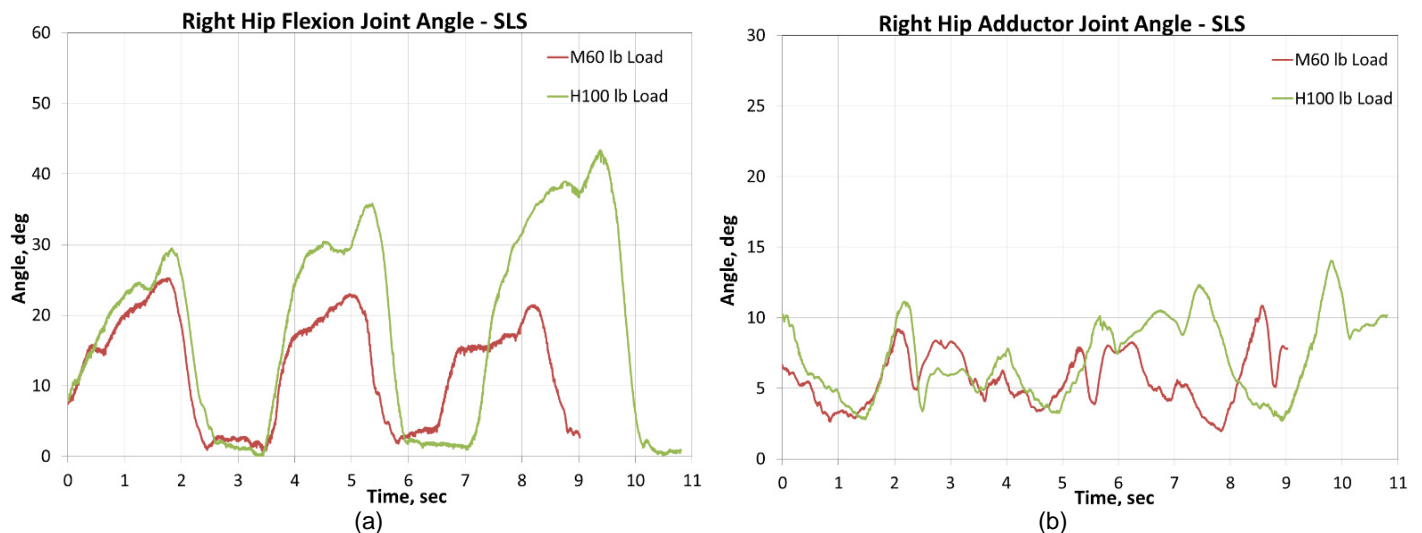


Figure 17.—Joint kinematics trajectories for single-leg squat: (a) hip flexion, (b) hip adduction, (c) hip internal rotation, (d) knee flexion, (e) ankle dorsiflexion, (f) subtalar inversion, (g) MTP flexion, and (h) lumbar extension.

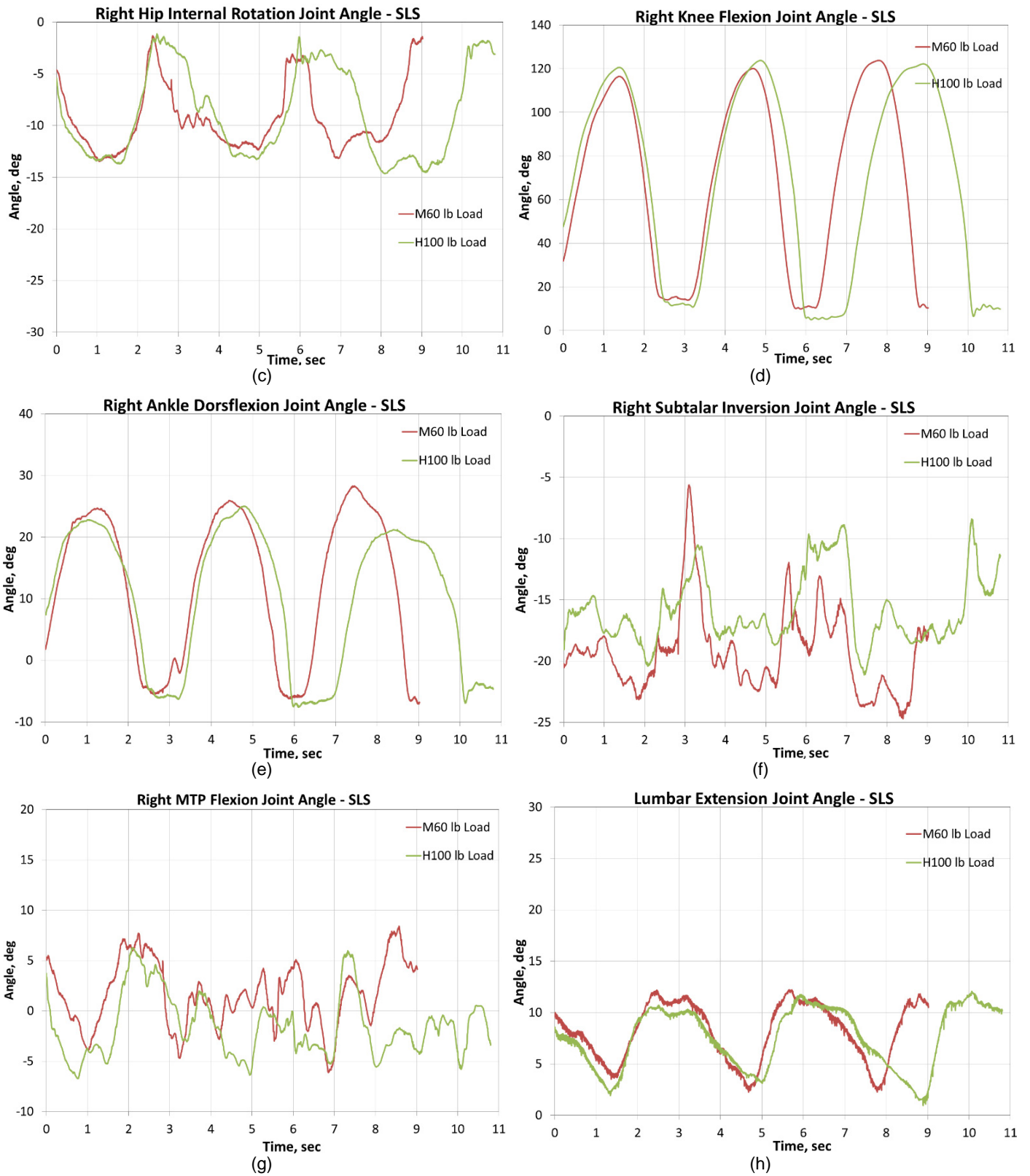


Figure 17.—Concluded. Joint kinematics trajectories for single-leg squat: (a) hip flexion, (b) hip adduction, (c) hip internal rotation, (d) knee flexion, (e) ankle dorsiflexion, (f) subtalar inversion, (g) MTP flexion and (h) lumbar extension.

Joint Moments for Single-Leg Squat

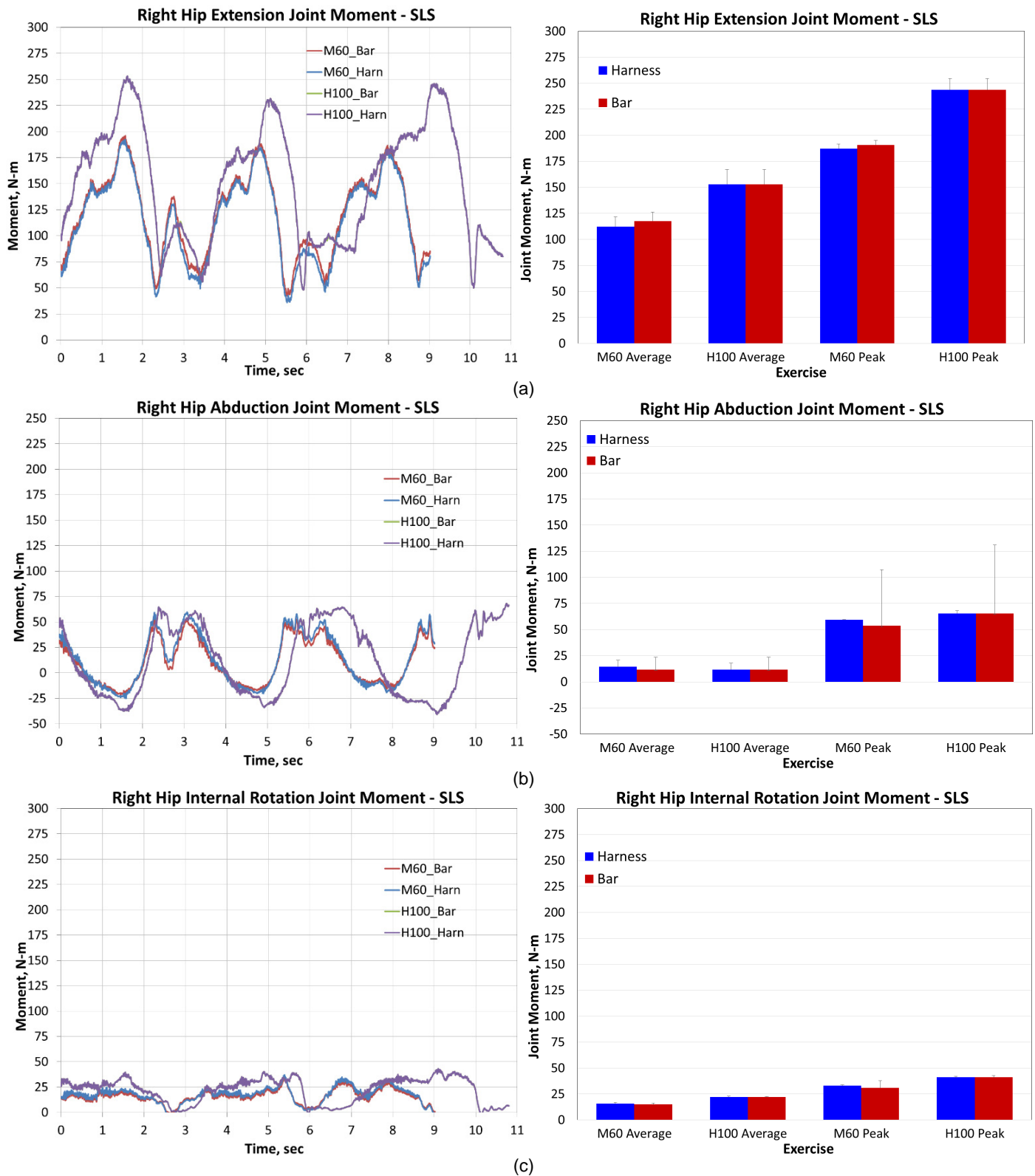
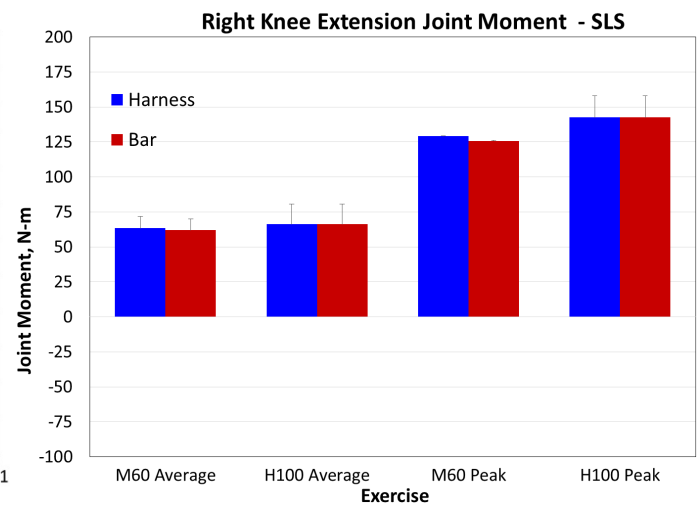
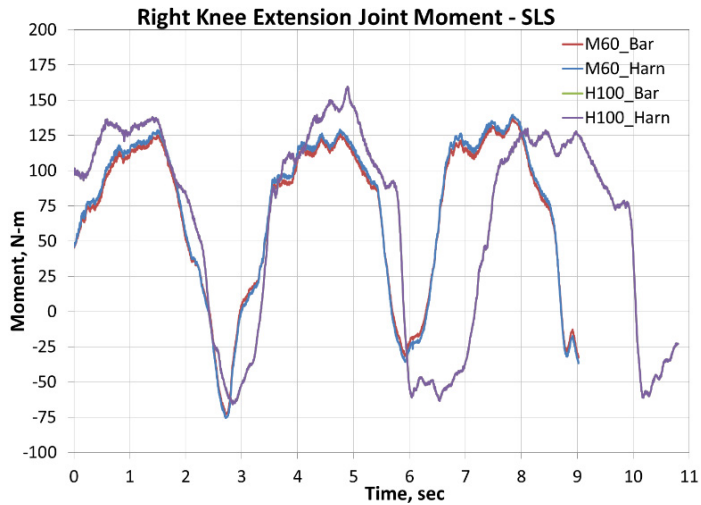
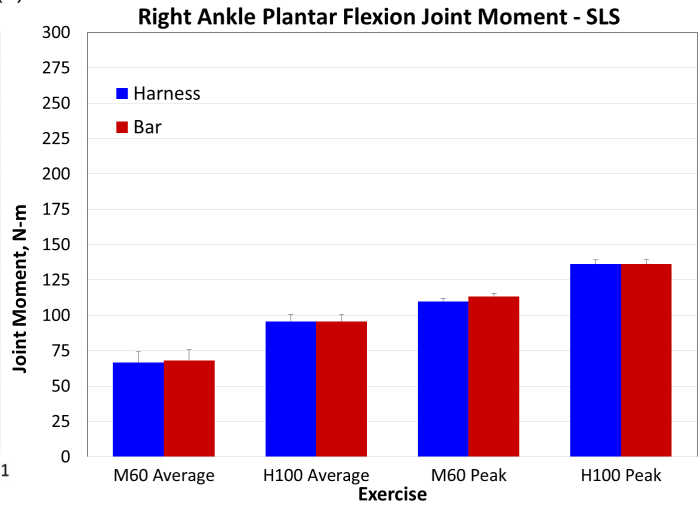
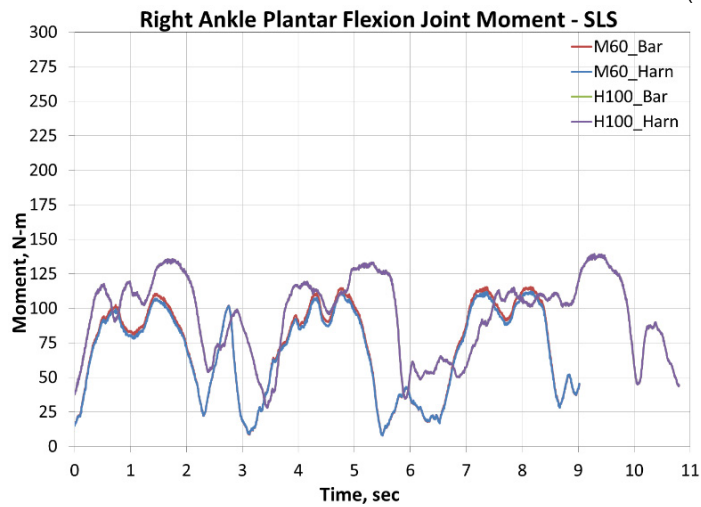


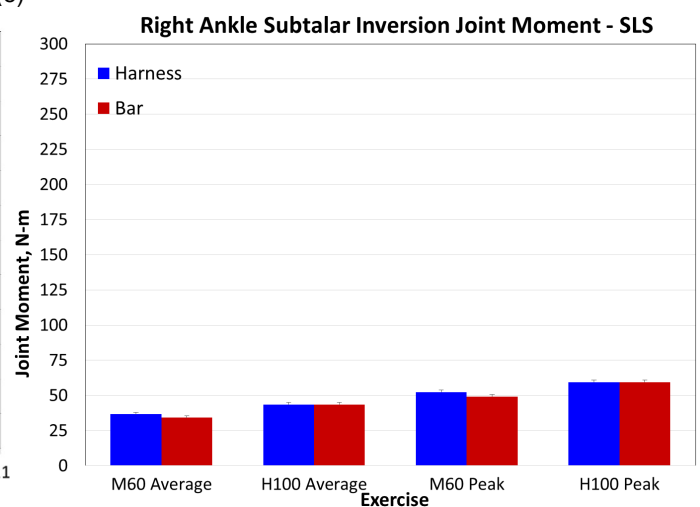
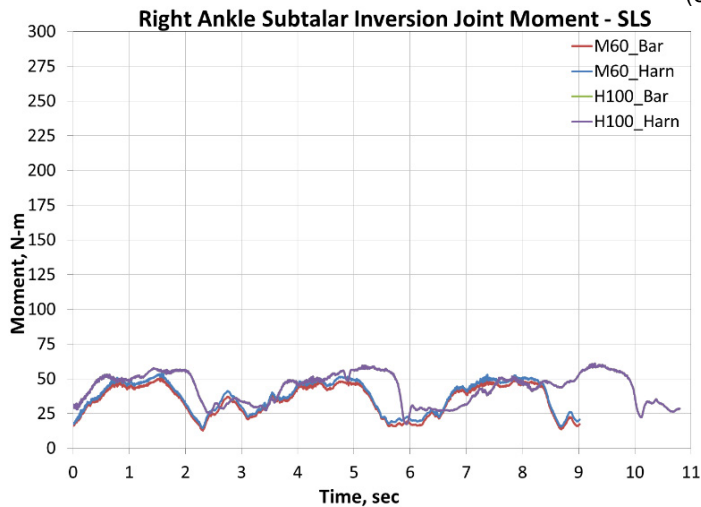
Figure 18.—Peak and average joint moments in Newton-meters for single-leg squat under all loading conditions for the following joint articulations: (a) hip extension, (b) hip abduction, (c) hip internal rotation, (d) knee extension, (e) ankle plantar flexion, (f) ankle subtalar inversion, and (g) lumbar extension.



(d)



(e)



(f)

Figure 18.—Continued. Peak and average joint moments in Newton-meters for single-leg squat under all loading conditions for the following joint articulations: (a) hip extension, (b) hip abduction, (c) hip internal rotation, (d) knee extension, (e) ankle plantar flexion, (f) ankle subtalar inversion, and (g) lumbar extension.

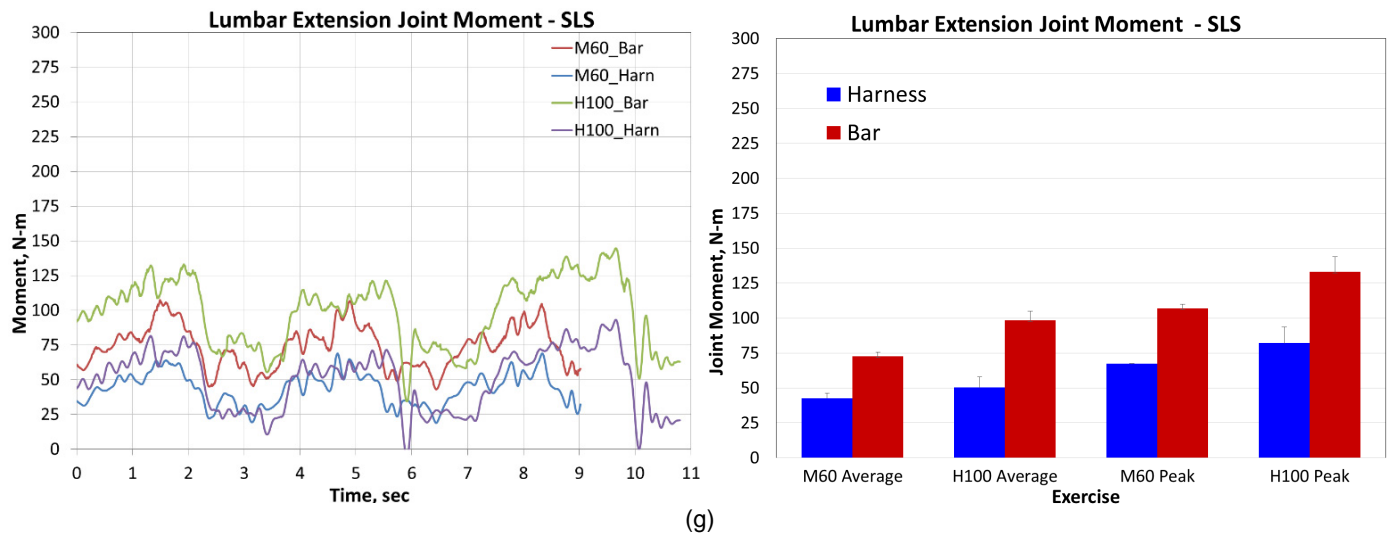


Figure 18.—Concluded. Peak and average joint moments in Newton-meters for single-leg squat under all loading conditions for the following joint articulations: (a) hip extension, (b) hip abduction, (c) hip internal rotation, (d) knee extension, (e) ankle plantar flexion, (f) ankle subtalar inversion, and (g) lumbar extension.

Resultant Joint Forces for Single-Leg Squat

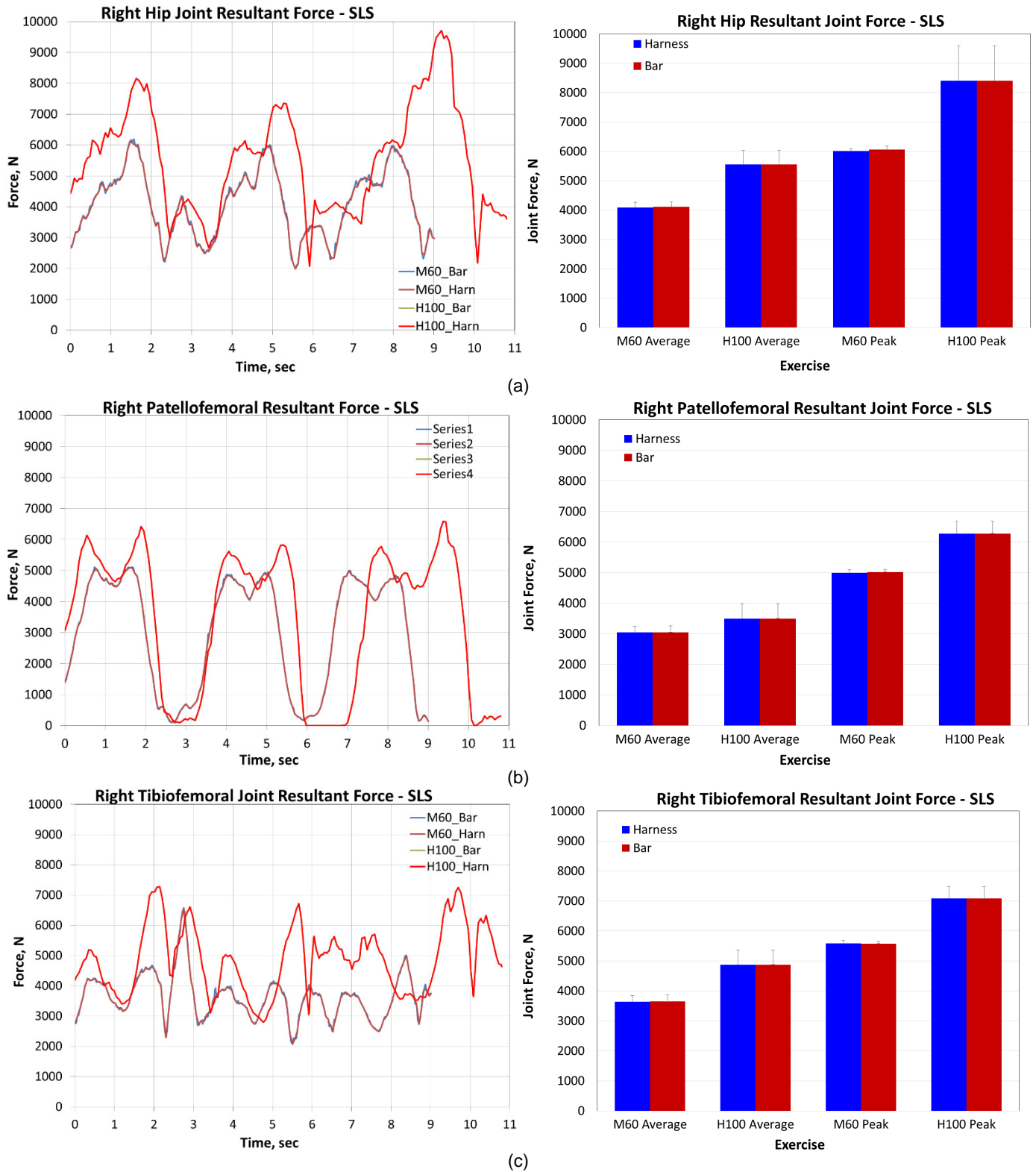
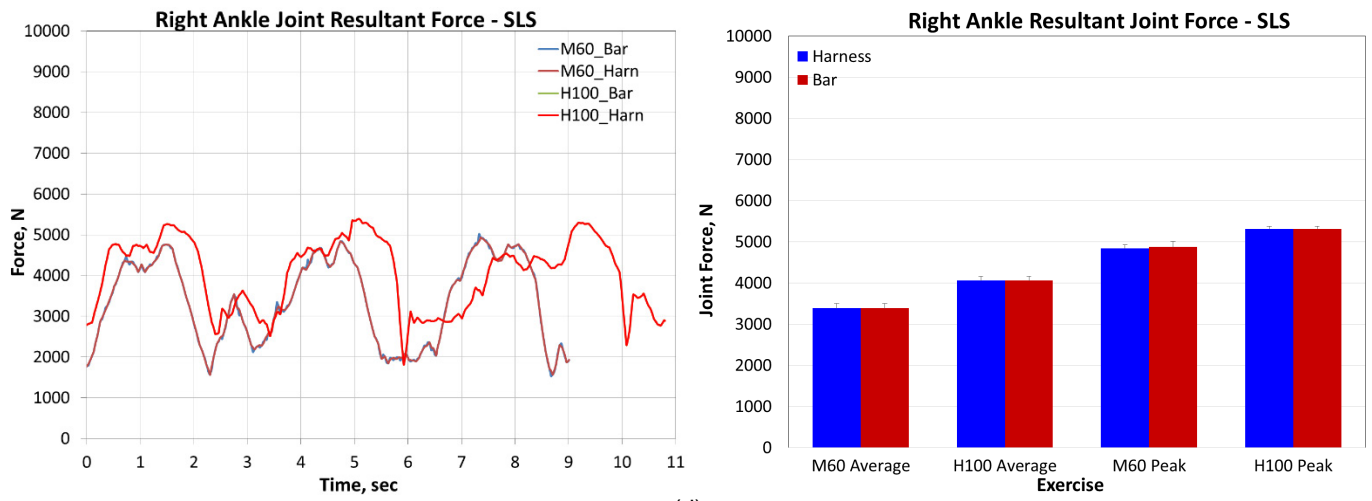
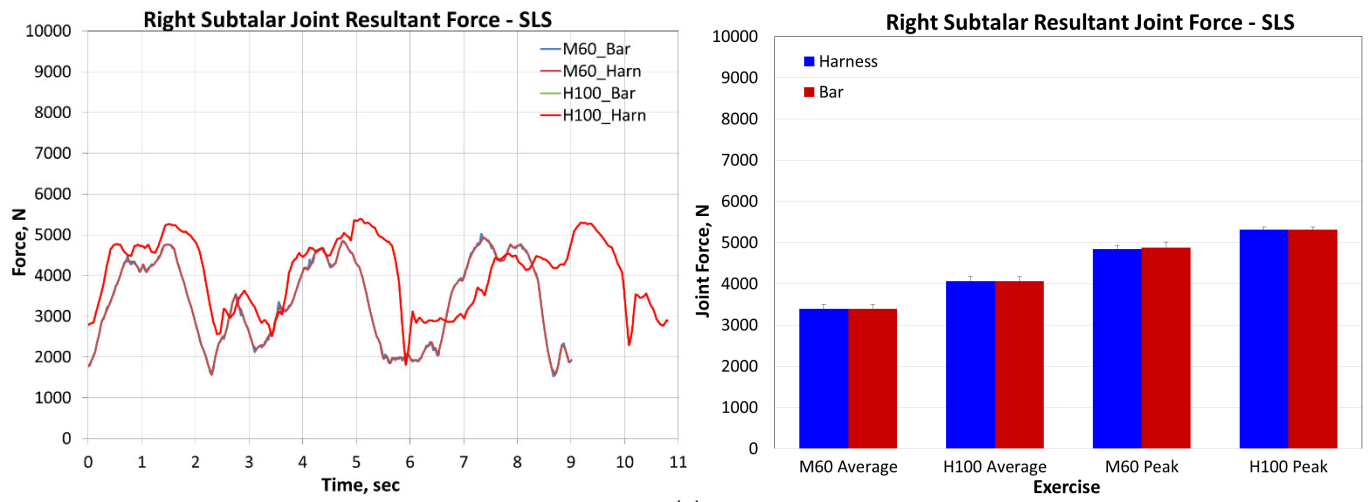


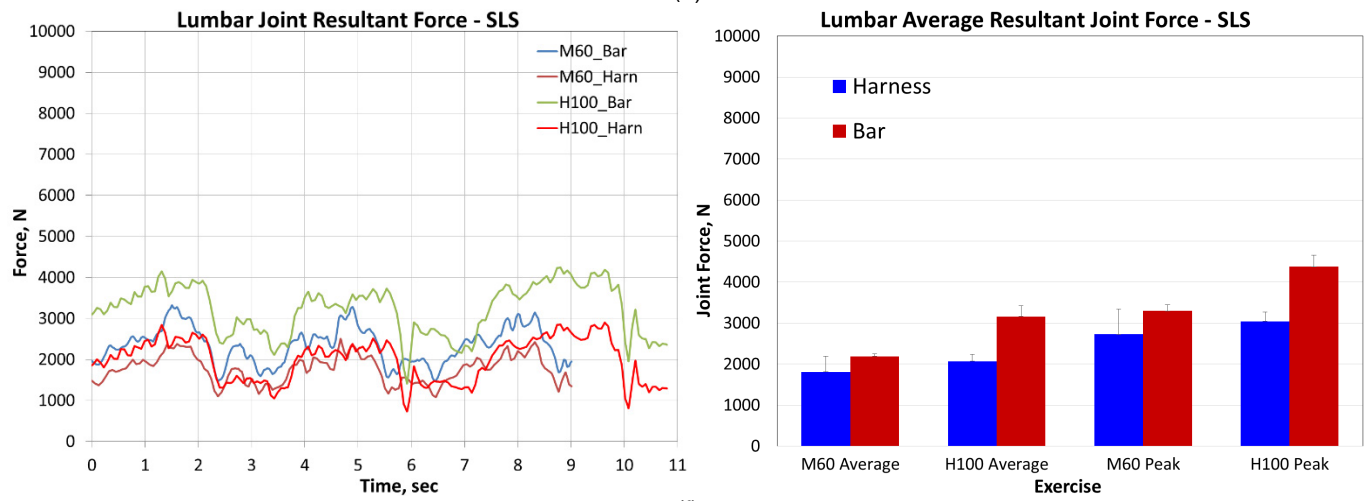
Figure 19.—Resultant joint forces in Newtons for single-leg squat under all loading conditions for the following joints: (a) hip, (b) patellofemoral, (c) knee, (d) ankle, (e) subtalar, and (f) lumbar.



(d)



(e)



(f)

Figure 19.—Concluded. Resultant joint forces in Newtons for single-leg squat under all loading conditions for the following joints: (a) hip, (b) patellofemoral, (c) knee, (d) ankle, (e) subtalar, and (f) lumbar.

Muscle Forces by Muscle Group for Single-Leg Squat

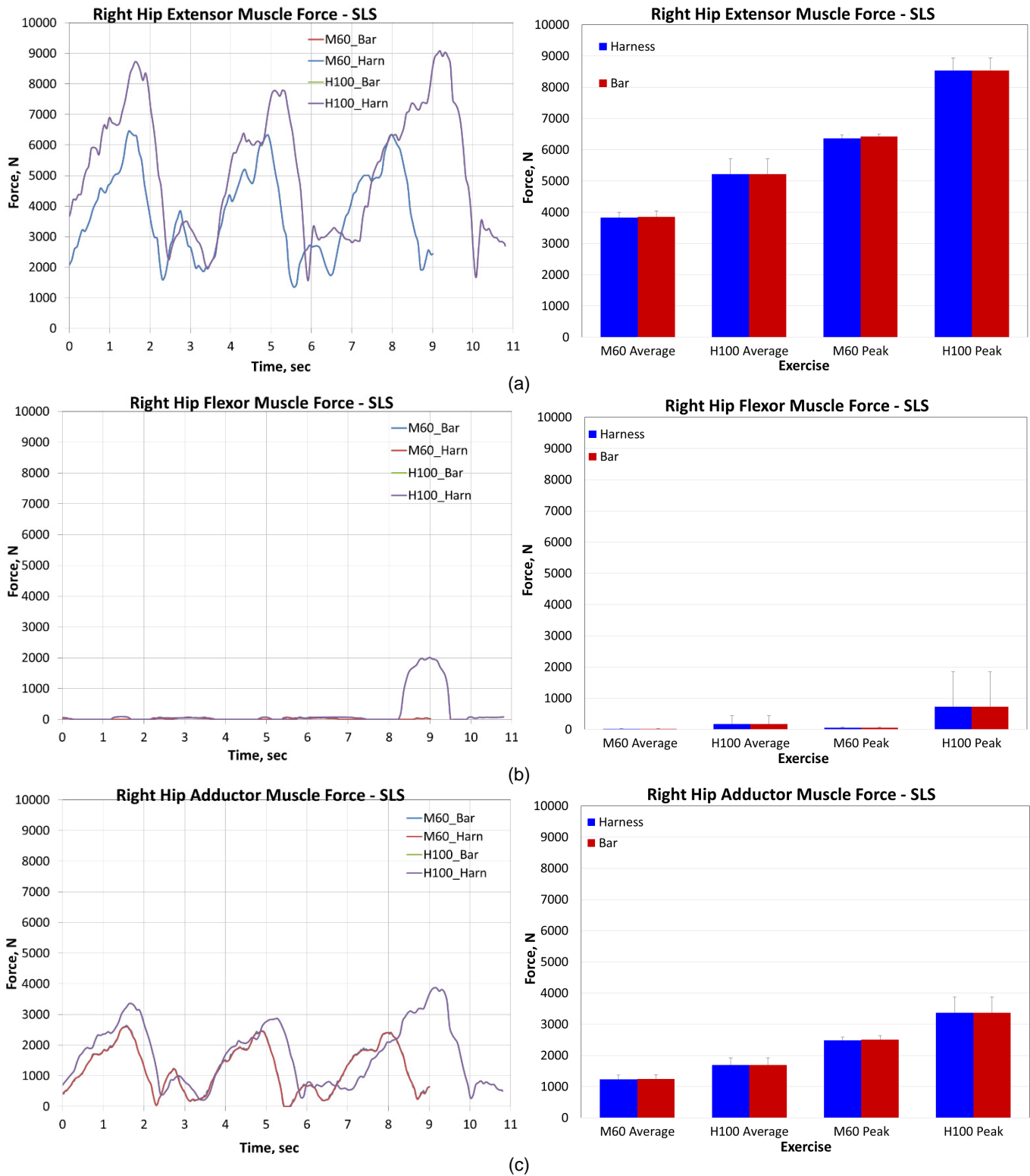


Figure 20.—Average and peak muscle forces in Newtons by muscle group for single-leg squat under all loading conditions for the following groups: (a) hip extensors, (b) hip flexors, (c) hip adductors, (d) hip abductors, (e) hip internal rotators, (f) hip external rotators, (g) knee extensors, (h) knee flexors, (i) dorsiflexors, (j) plantar flexors, (k) subtalar inverters, (l) subtalar everters, and (m) lumbar extensors.



Figure 20.—Continued. Average and peak muscle forces in Newtons by muscle group for single-leg squat under all loading conditions for the following groups: (a) hip extensors, (b) hip flexors, (c) hip adductors, (d) hip abductors, (e) hip internal rotators, (f) hip external rotators, (g) knee extensors, (h) knee flexors, (i) dorsiflexors, (j) plantar flexors, (k) subtalar inverters, (l) subtalar everters, and (m) lumbar extensors.

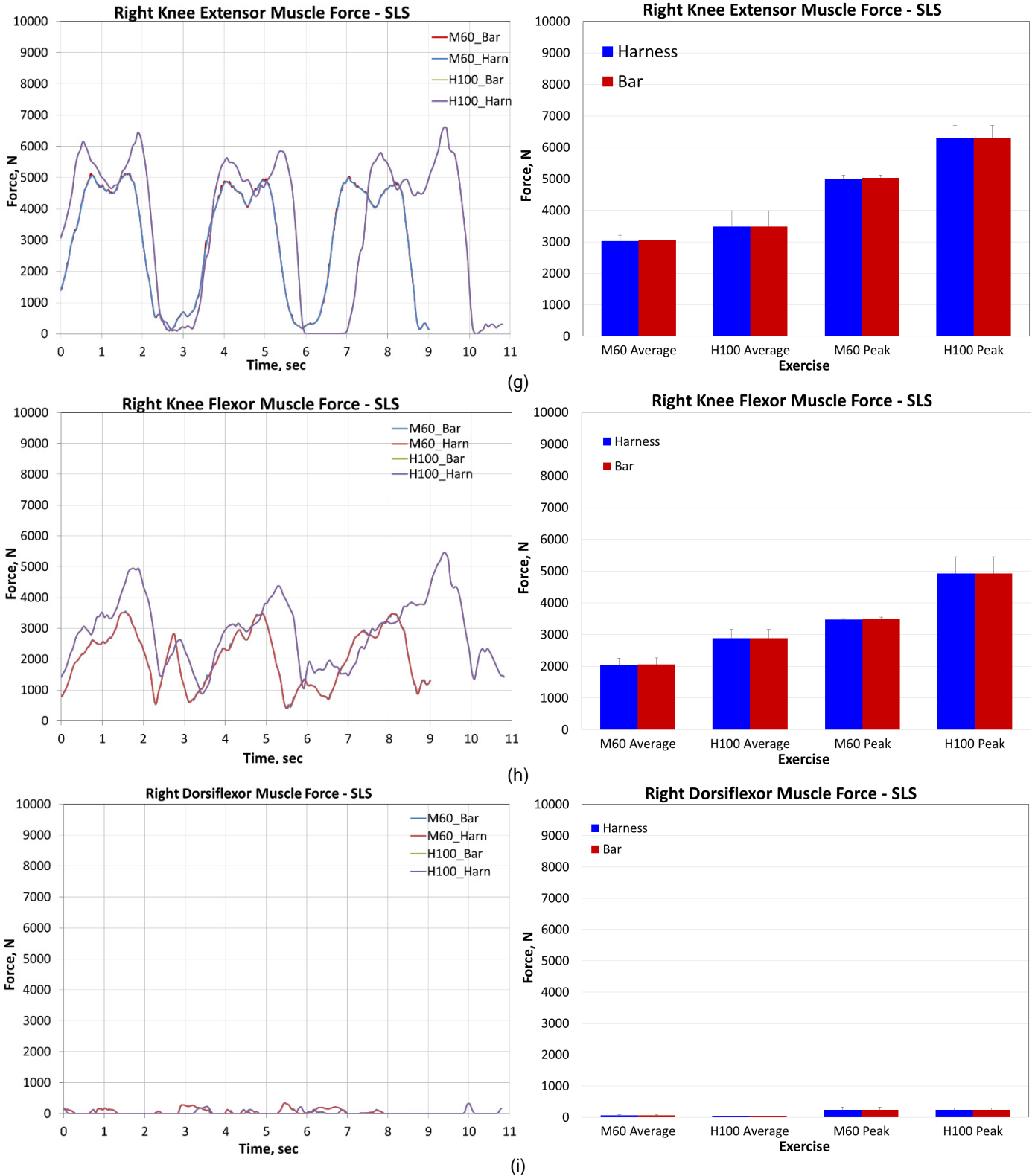


Figure 20.—Continued. Average and peak muscle forces in Newtons by muscle group for single-leg squat under all loading conditions for the following groups: (a) hip extensors, (b) hip flexors, (c) hip adductors, (d) hip abductors, (e) hip internal rotators, (f) hip external rotators, (g) knee extensors, (h) knee flexors, (i) dorsiflexors, (j) plantar flexors, (k) subtalar inverters, (l) subtalar everters, and (m) lumbar extensors.

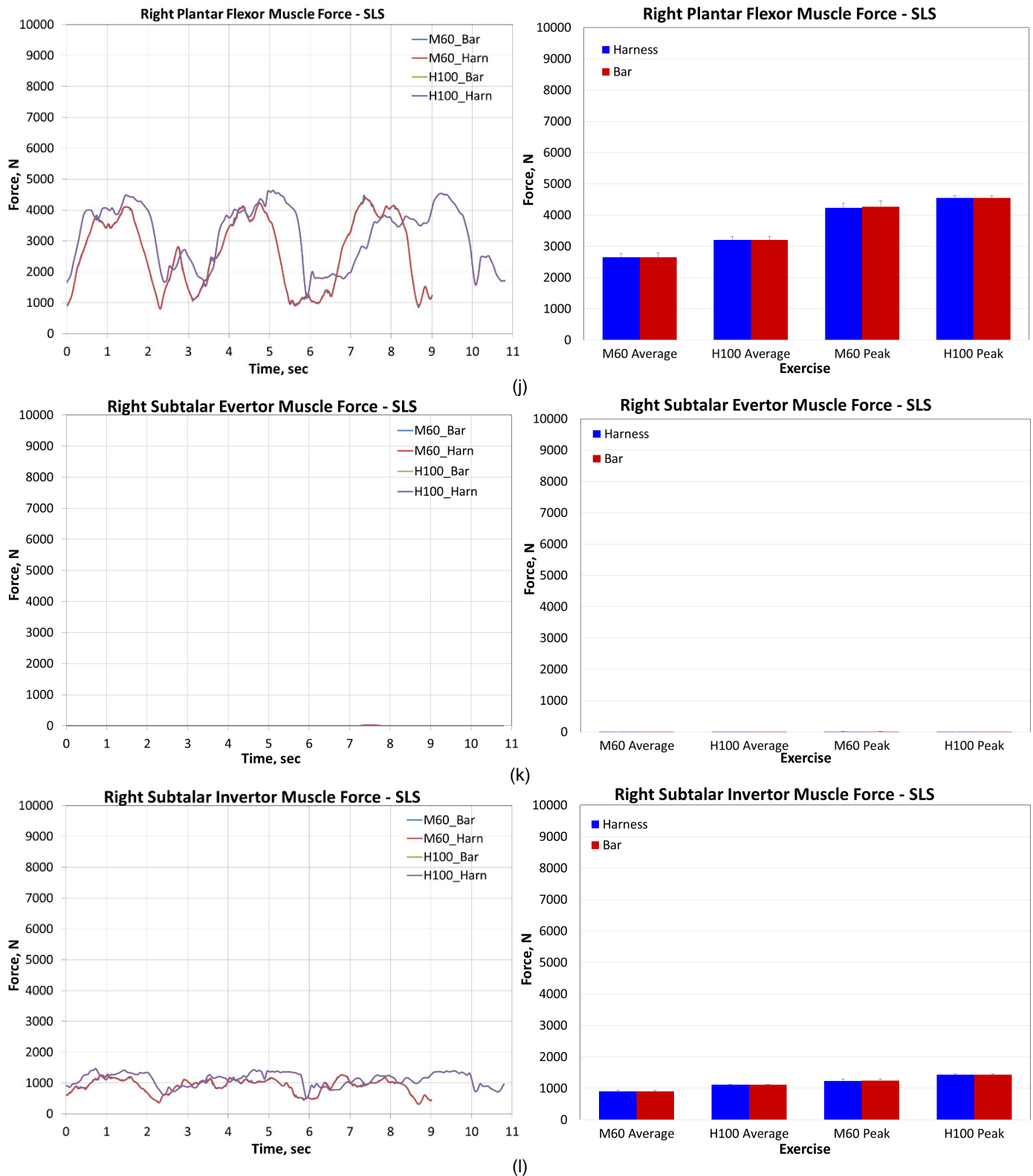


Figure 20.—Continued. Average and peak muscle forces in Newtons by muscle group for single-leg squat under all loading conditions for the following groups: (a) hip extensors, (b) hip flexors, (c) hip adductors, (d) hip abductors, (e) hip internal rotators, (f) hip external rotators, (g) knee extensors, (h) knee flexors, (i) dorsiflexors, (j) plantar flexors, (k) subtalar inverters, (l) subtalar everters, and (m) lumbar extensors.

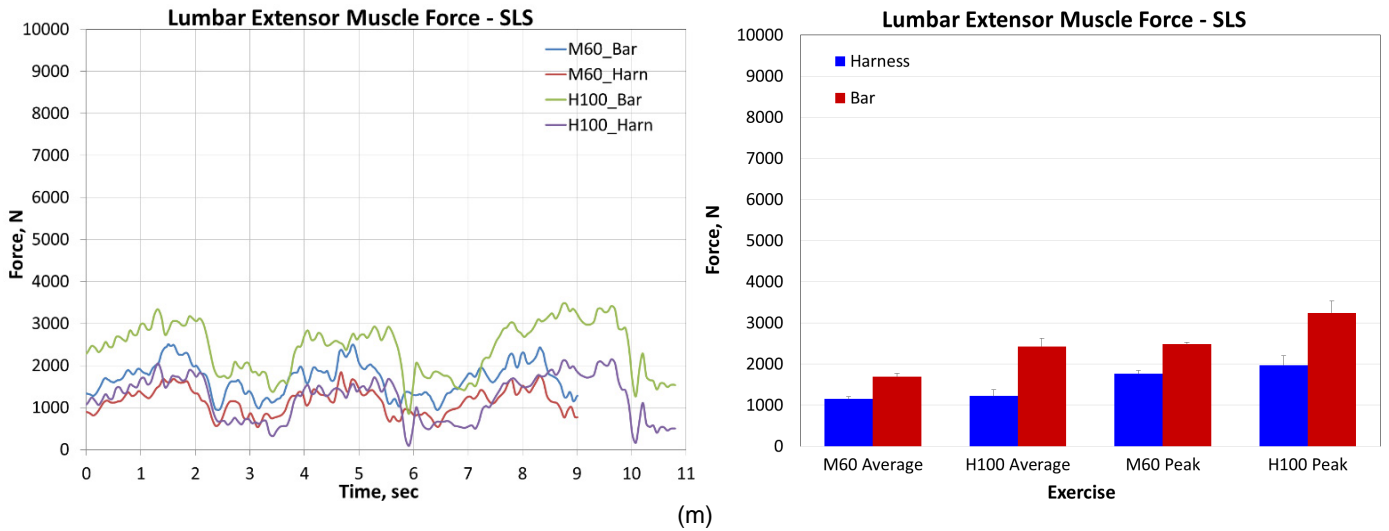


Figure 20.—Concluded. Average and peak muscle forces in Newtons by muscle group for single-leg squat under all loading conditions for the following groups: (a) hip extensors, (b) hip flexors, (c) hip adductors, (d) hip abductors, (e) hip internal rotators, (f) hip external rotators, (g) knee extensors, (h) knee flexors, (i) dorsiflexors, (j) plantar flexors, (k) subtalar inverters, (l) subtalar everters, and (m) lumbar extensors.

Residual Forces and Moments for the Single-Leg Squat

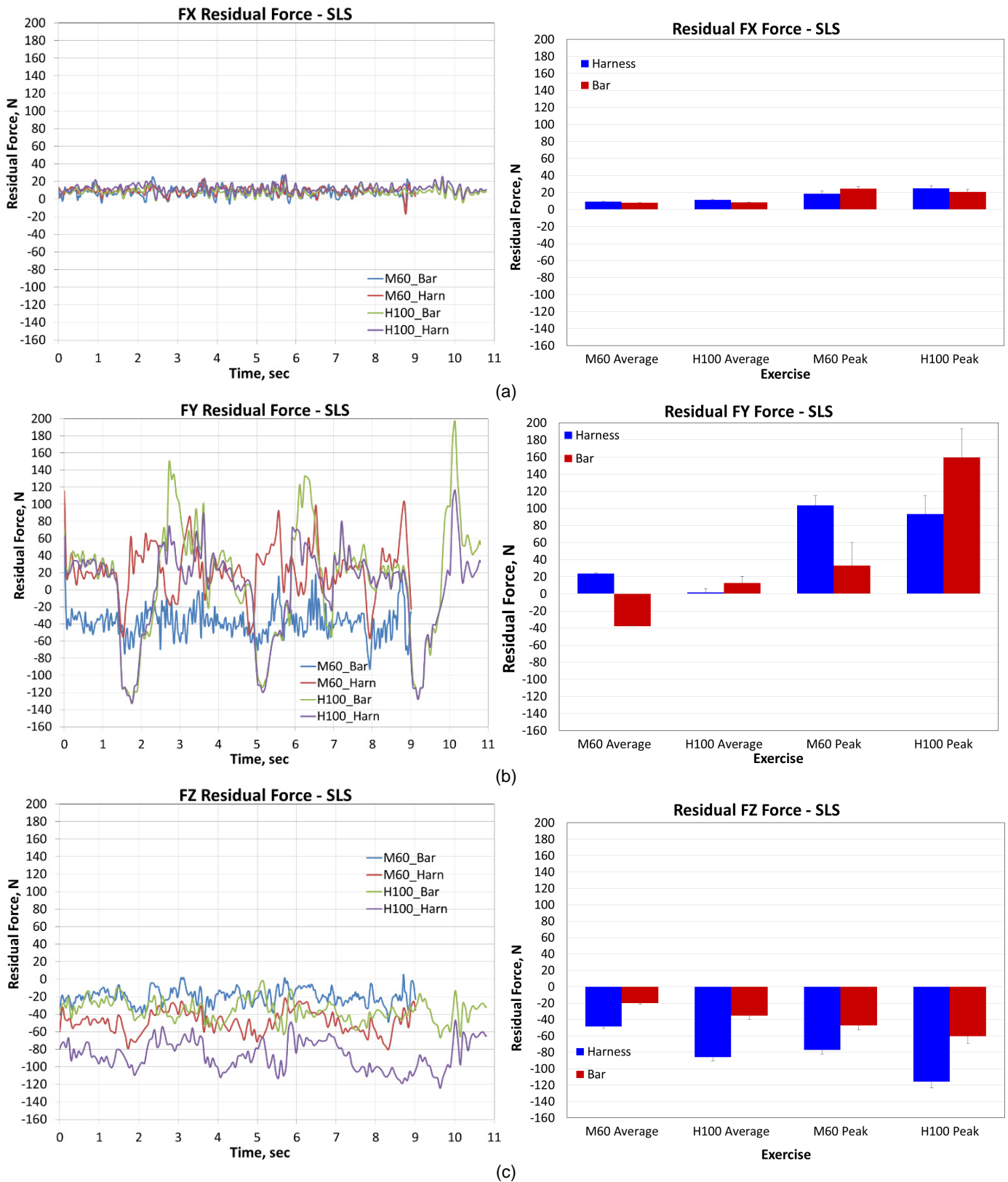


Figure 21.—Average and peak residual forces in Newtons and moments in Newton-meters for single-leg squat under all loading conditions for the following residual forces: (a) FX, (b) FY, (c) FZ; and residual moments: (d) MX, (e), MY, (f) MZ

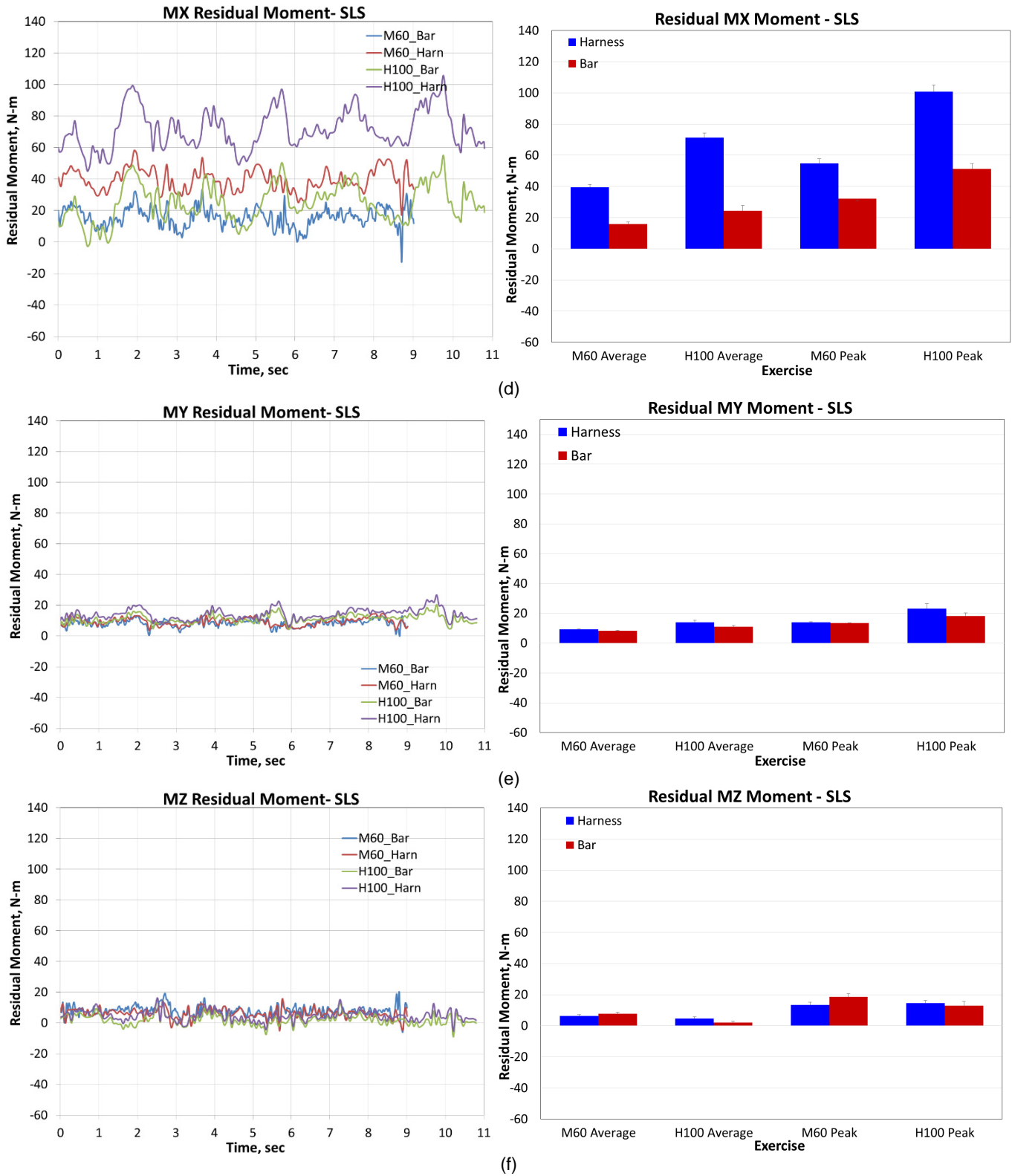
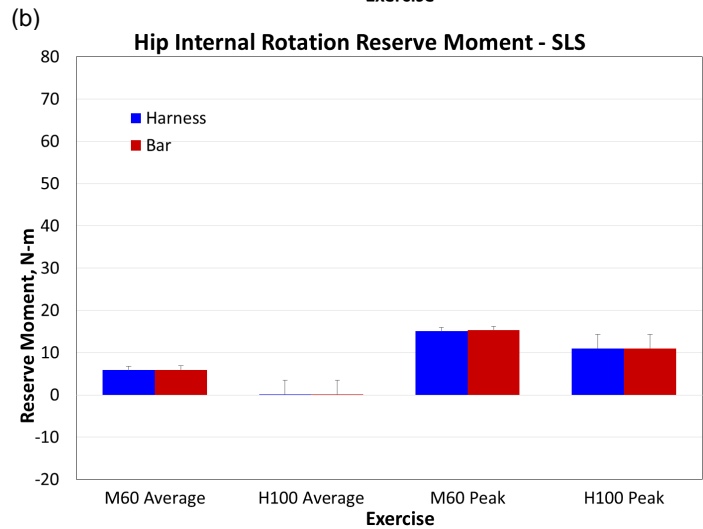
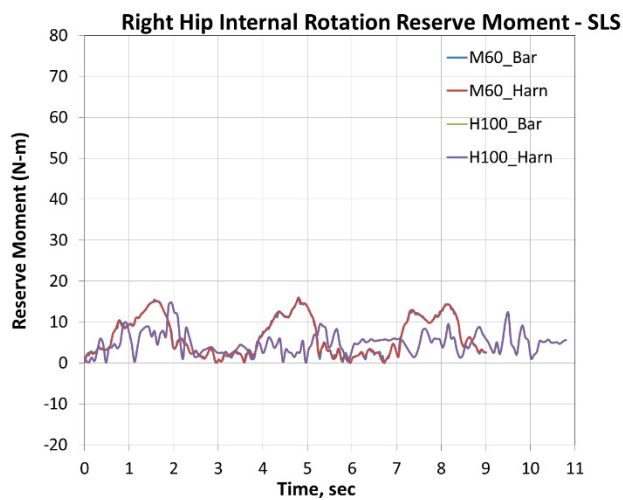
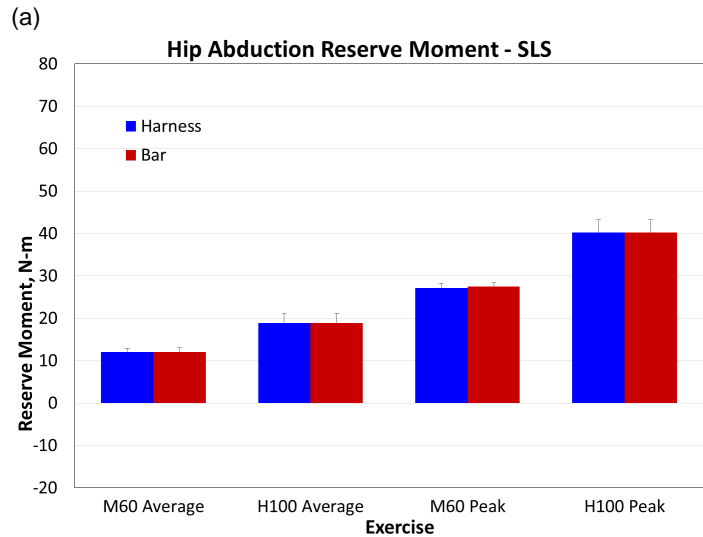
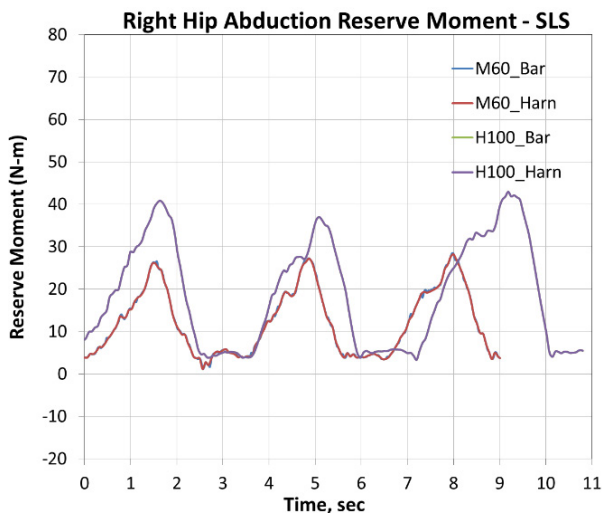
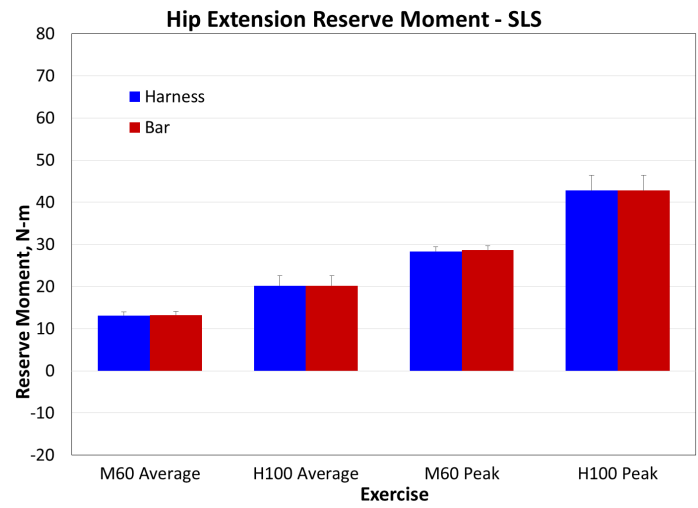
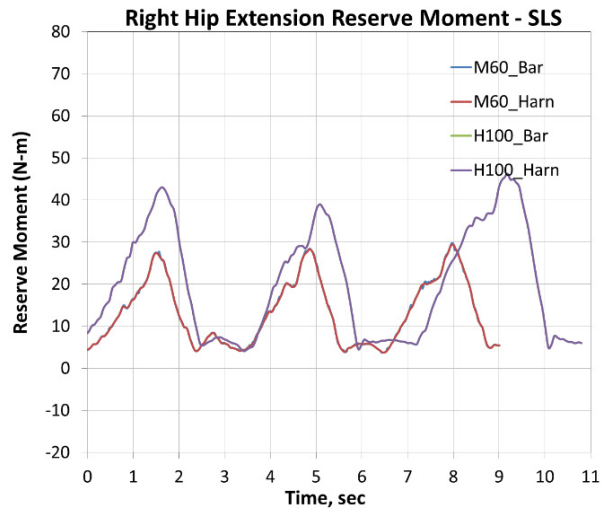


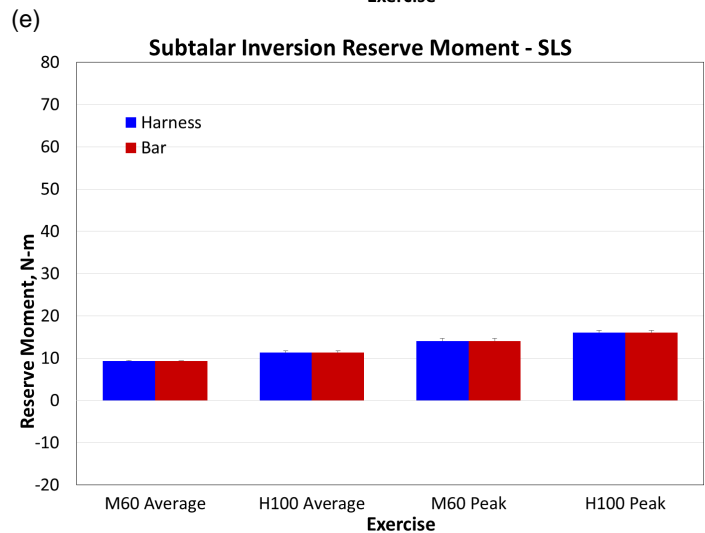
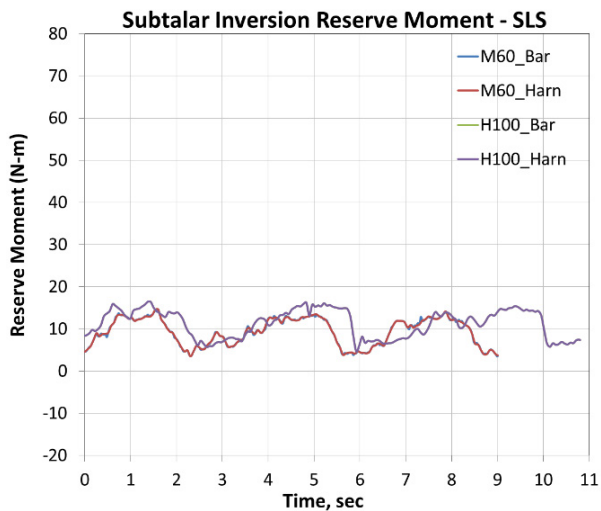
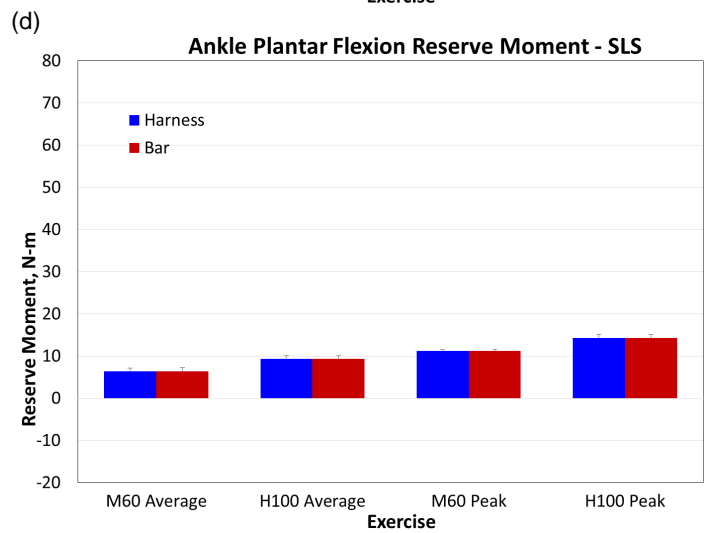
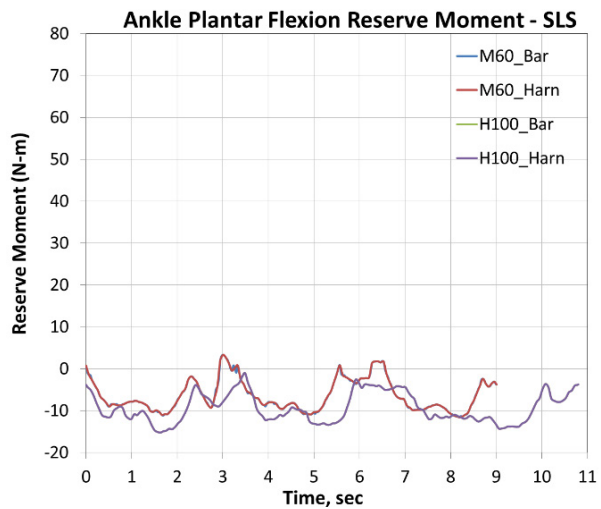
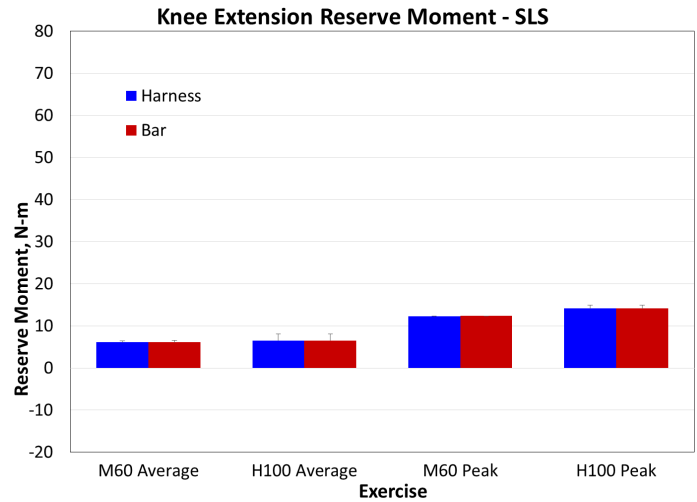
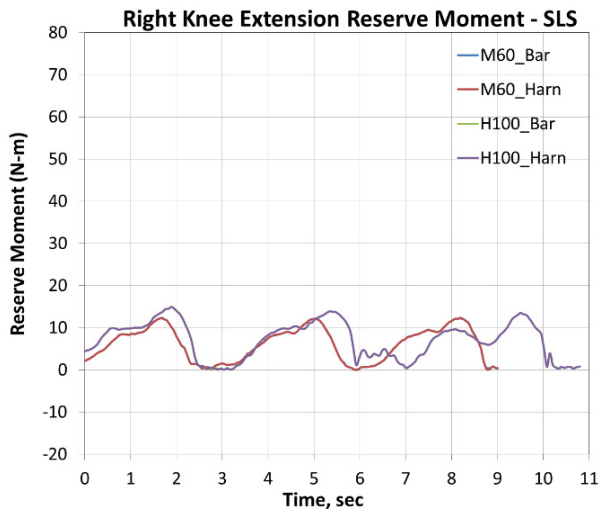
Figure 21.—Concluded. Average and peak residual forces in Newtons and moments in Newton-meters for single-leg squat under all loading conditions for the following residual forces: (a) FX, (b) FY, (c) FZ; and residual moments: (d) MX, (e), MY, (f) MZ

Reserve Moments for the Single-Leg Squat



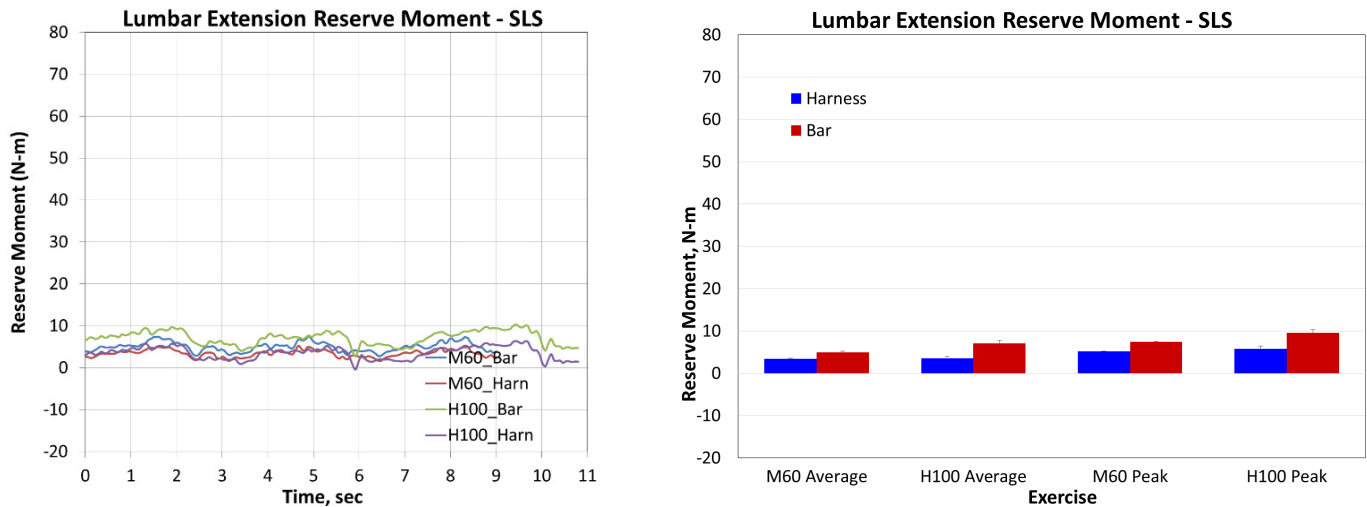
(c)

Figure 22.—Average and peak reserve actuator moments for single-leg squat under all loading conditions for the following joint articulations: (a) hip flexion, (b) hip adduction, (c) hip rotation, (d) knee flexion, (e) ankle dorsiflexion, (f) subtalar inversion (g) lumbar extension.



(f)

Figure 22.—Continued. Average and peak reserve actuator moments for single-leg squat under all loading conditions for the following joint articulations: (a) hip flexion, (b) hip adduction, (c) hip rotation, (d) knee flexion, (e) ankle dorsiflexion, (f) subtalar inversion (g) lumbar extension.



(g)

Figure 22.—Concluded. Average and peak reserve actuator moments for single-leg squat under all loading conditions for the following joint articulations: (a) hip flexion, (b) hip adduction, (c) hip rotation, (d) knee flexion, (e) ankle dorsiflexion, (f) subtalar inversion and (g) lumbar extension.

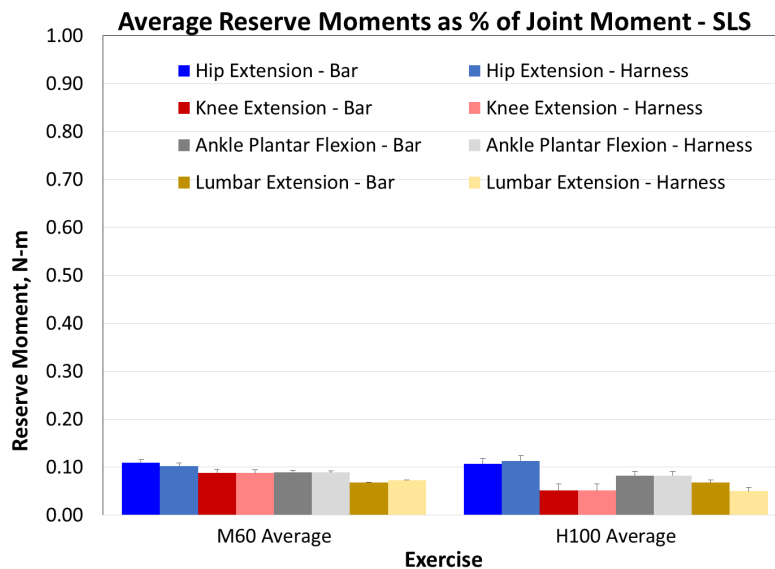


Figure 23.—Average reserve moments as a percentage of total joint moment for single-leg squat.

Heel Raise Exercise

Joint Kinematics for Heel Raise

Table 6 summarizes the joint angle ranges for the major lower body joints during the heel raise for the right leg. Left leg results are omitted, but are generally similar to the right leg. The subject is right-leg dominant. Because the heel raise is an isolation movement that targets the lower limb musculature, results for the hip and knee are not shown.

Figure 24 describes the joint kinematics trajectories for the heel raise. Figure 25 to Figure 27 describe the kinetics of the model, i.e., joint moments, resultant joint forces and muscle tension forces, respectively. Figure 28 describes the model's residual forces and moments during the heel raise movement. Figure 29 describes the model's reserve actuator moments during the heel raise movement. Figure 30 shows the reserve joint moments expressed as a percentage of the total joint moments as determined from ID.

TABLE 6.—KINEMATIC JOINT ANGLE RANGES IN DEGREES FOR HEEL RAISE

Joint articulation during heel raise	Angle at top of movement, °	Angle at bottom of movement, °
Hip flexion	12	27
Knee flexion	8	21
Ankle dorsiflexion	-33	18
Subtalar inversion	20	-13
MTP flexion	-41	11

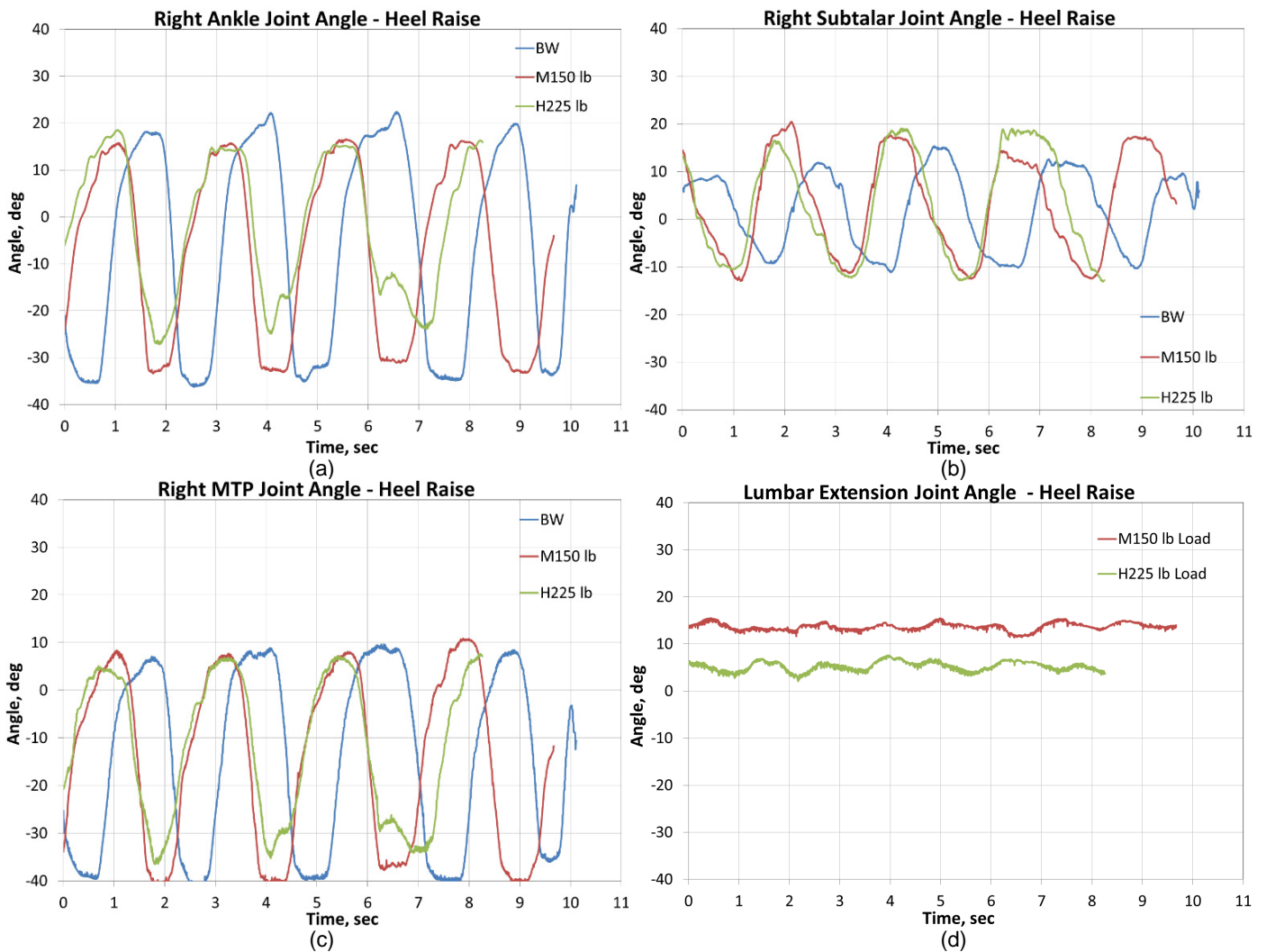


Figure 24.—Joint kinematics trajectories for heel raise: (a) ankle dorsiflexion, (b) subtalar inversion, (c) MTP flexion and (d) lumbar extension.

Joint Moments for Heel Raise

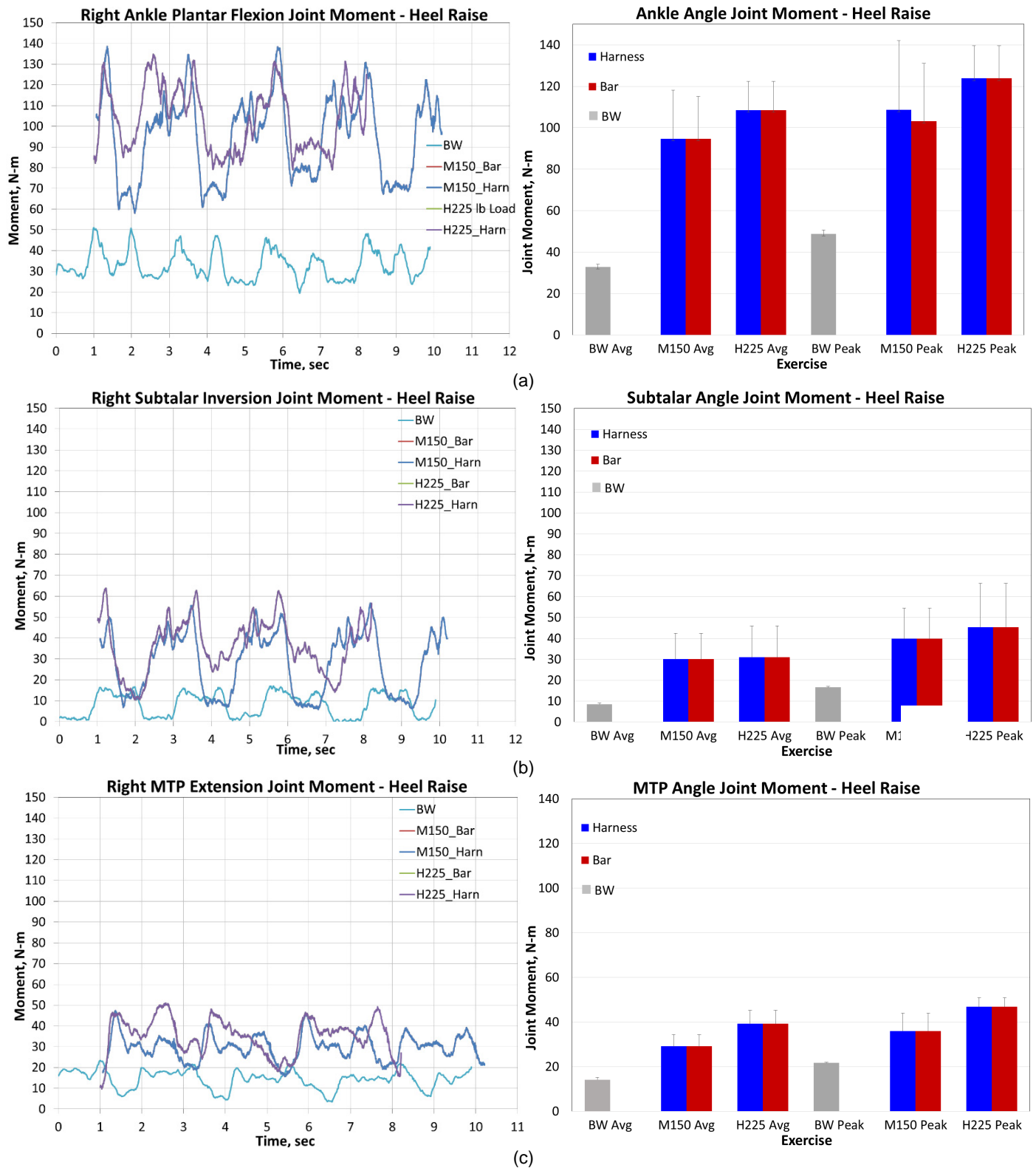


Figure 25.—Peak and average joint moments in Newton-meters for heel raise under all loading conditions for the following joint articulations: (a) ankle angle, (b) subtalar angle, (c) MTP angle and (d) lumbar extension.

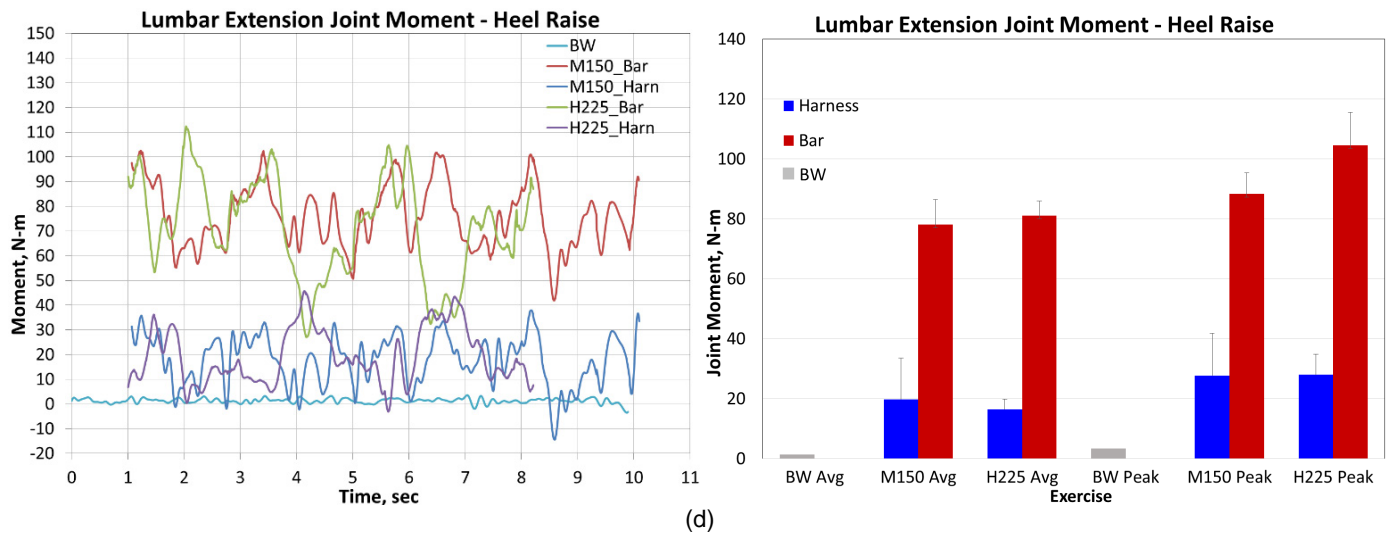


Figure 25.—Peak and average joint moments in Newton-meters for heel raise under all loading conditions for the following joints: (a) ankle angle, (b) subtalar angle, (c) MTP angle and (d) lumbar extension.

Resultant Joint Forces for Heel Raise

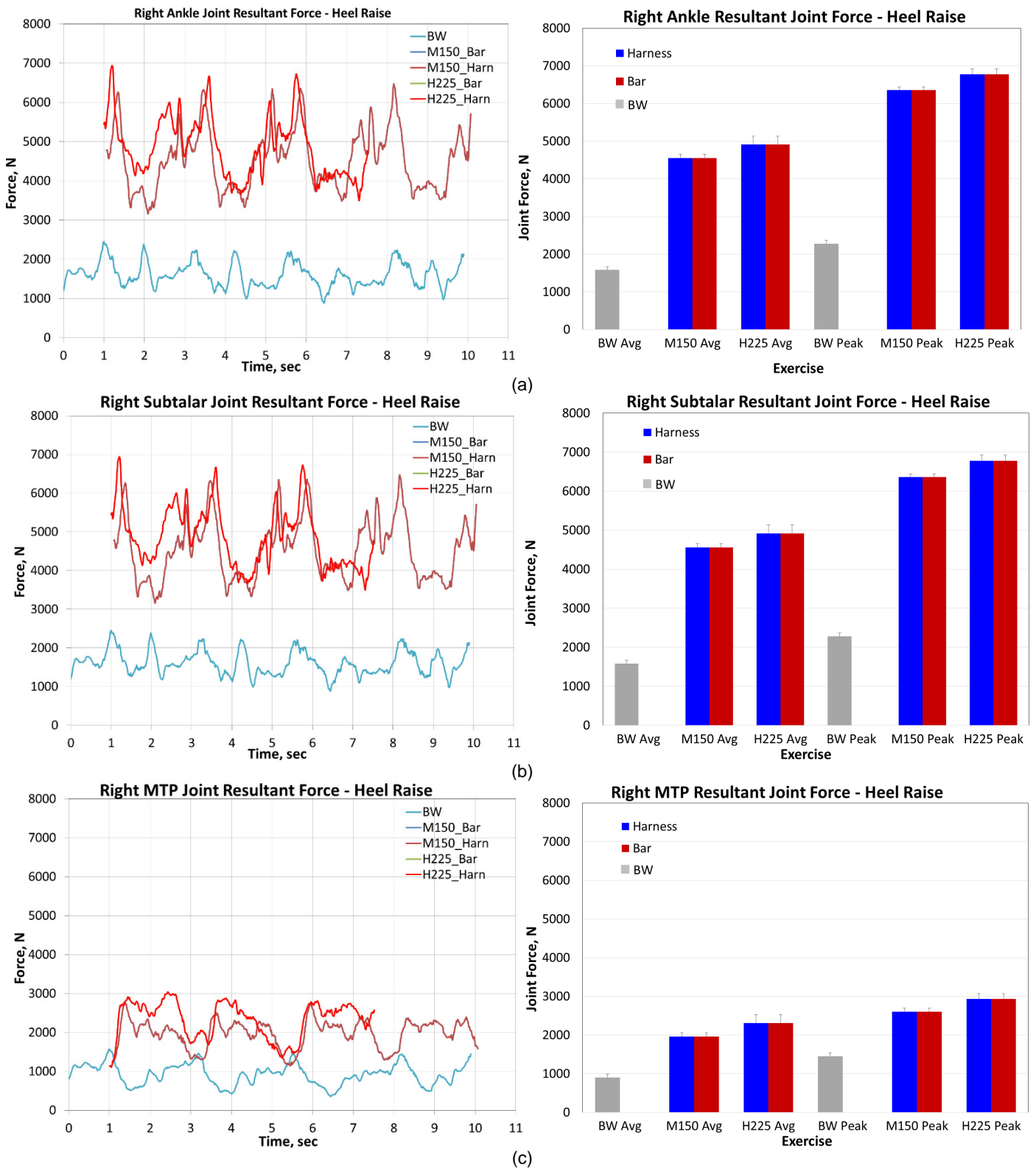


Figure 26.—Resultant joint forces in Newtons for heel raise under all loading conditions for the following joints: (a) ankle, (b) subtalar, (c) MTP and (d) lumbar.

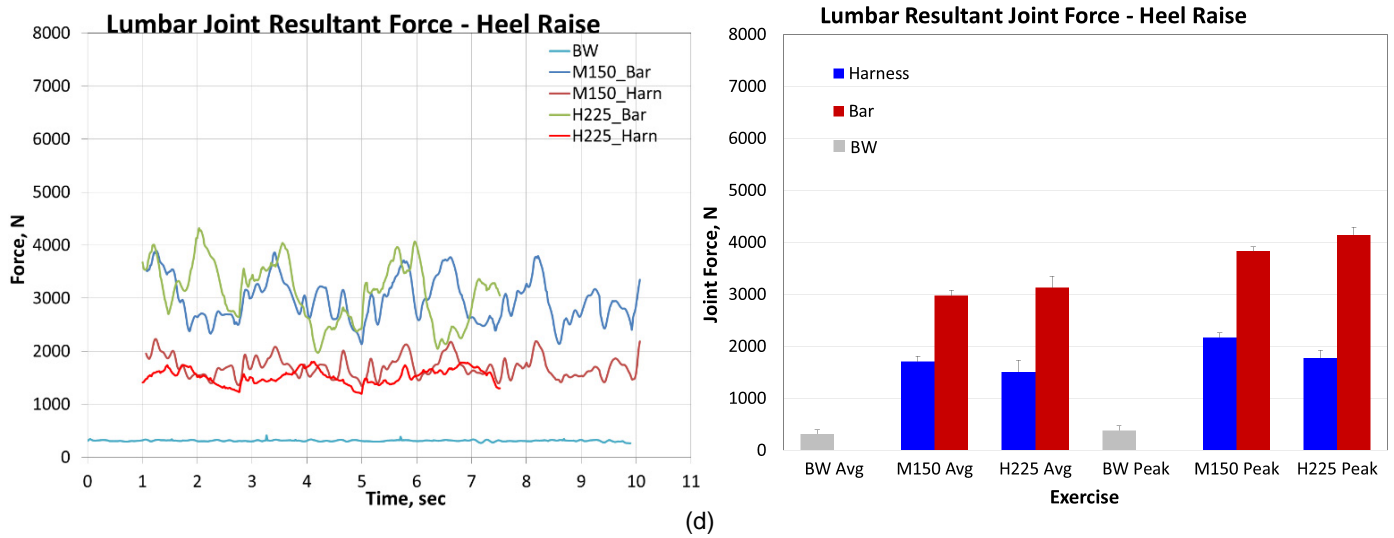


Figure 26.—Resultant joint forces in Newtons for heel raise under all loading conditions for the following joints: (a) ankle, (b) subtalar, (c) MTP and (d) lumbar.

Muscle Group Forces for Heel Raise

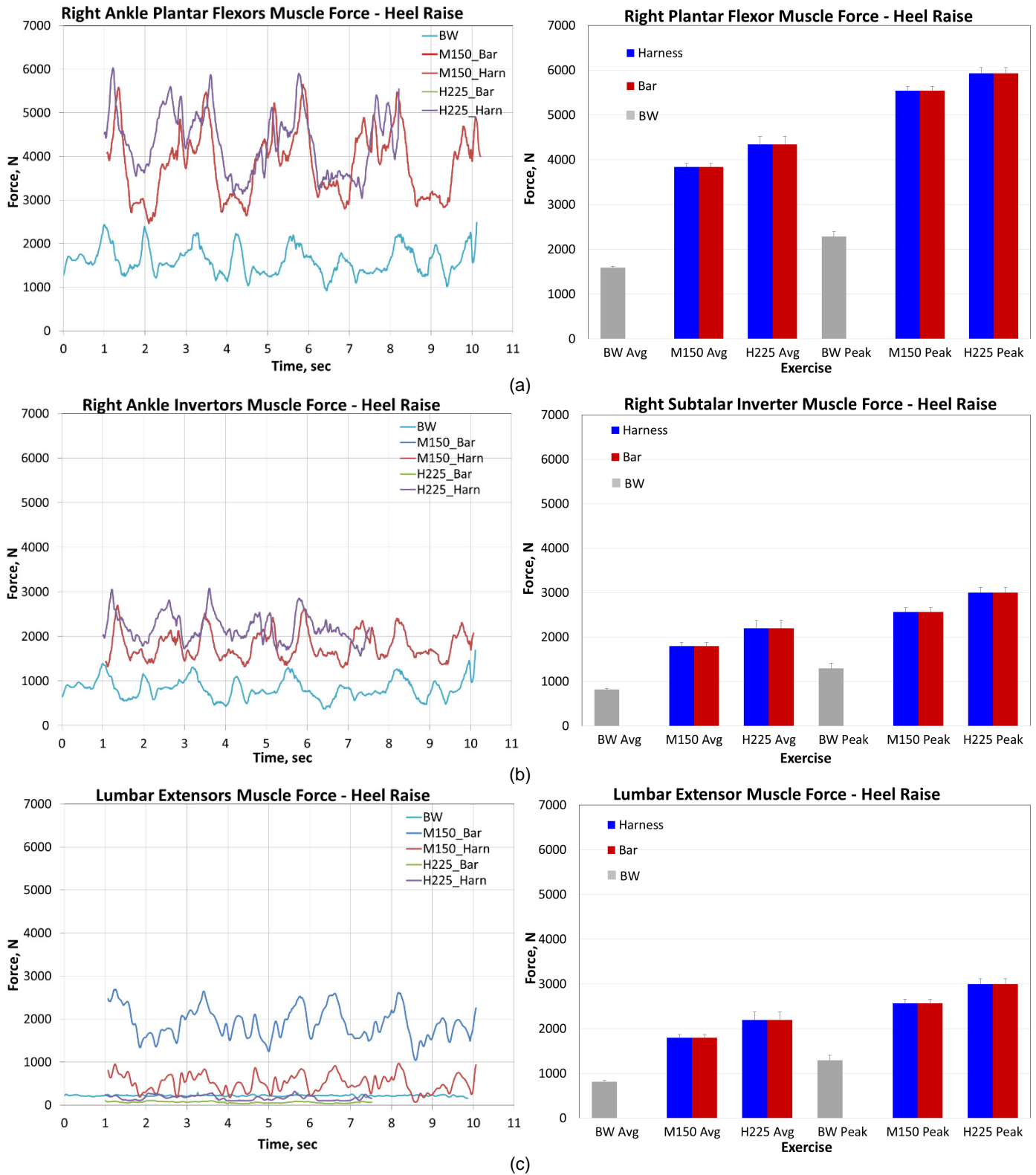


Figure 27.—Average and peak muscle forces by muscle group for heel raise under all loading conditions for the following groups: (a) plantar flexors, (b) subtalar invertors, and (c) lumbar extensors.

Residual Forces and Moments for Heel Raise

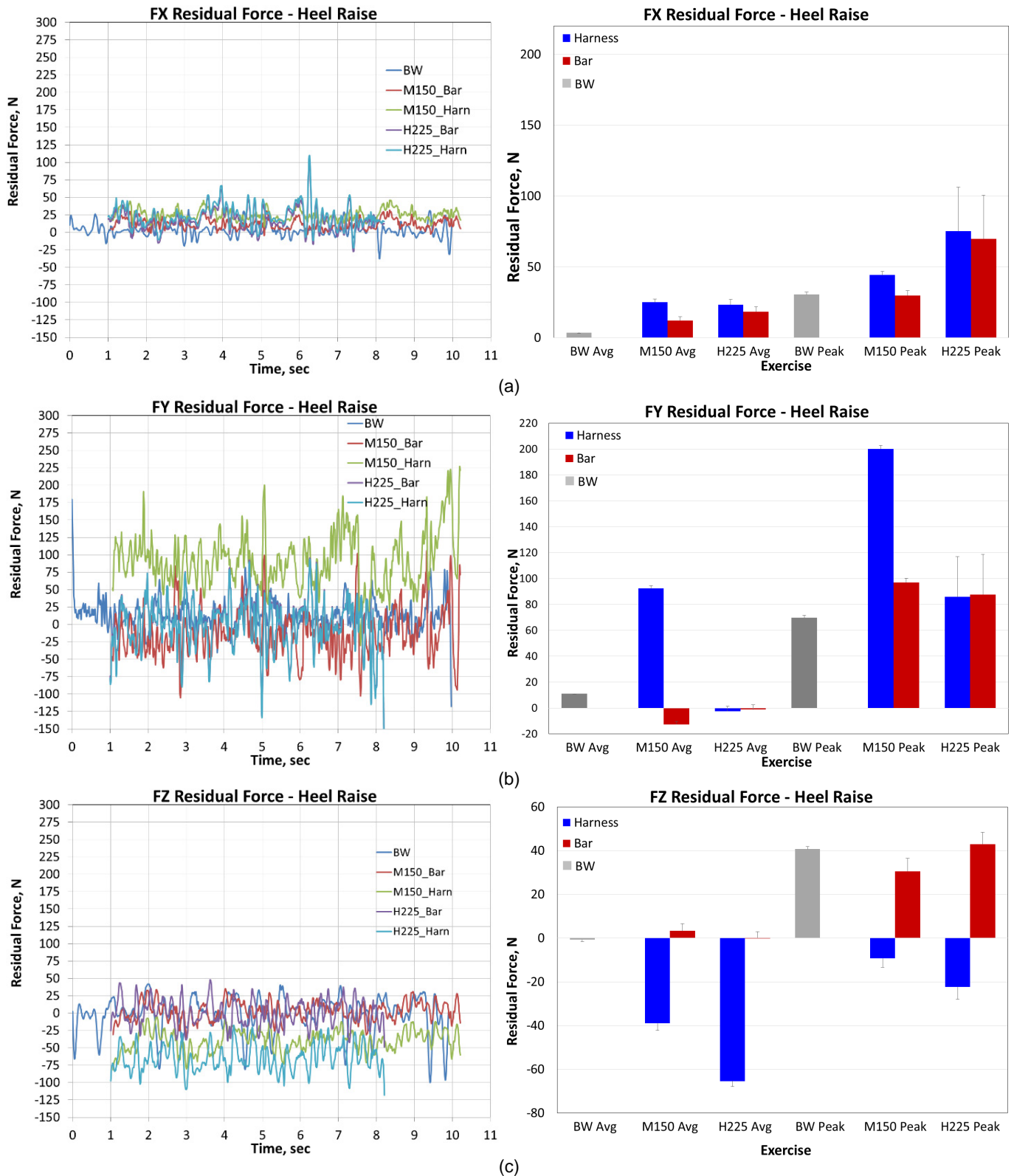
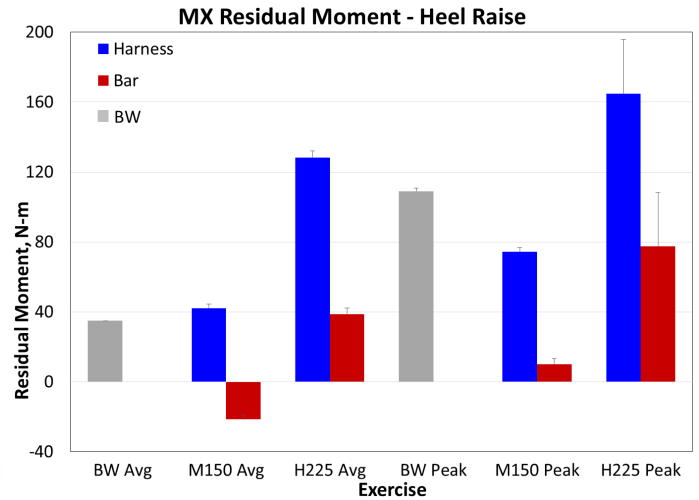
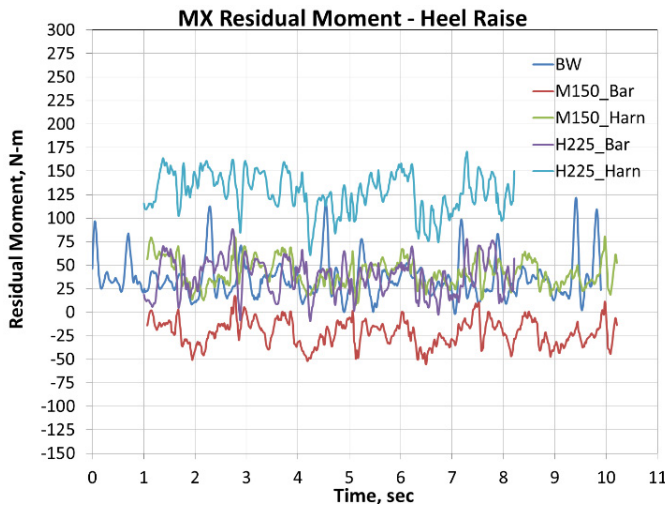
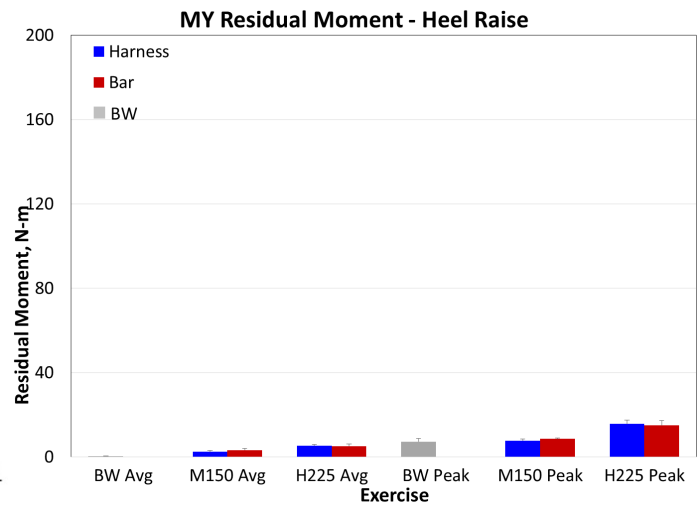
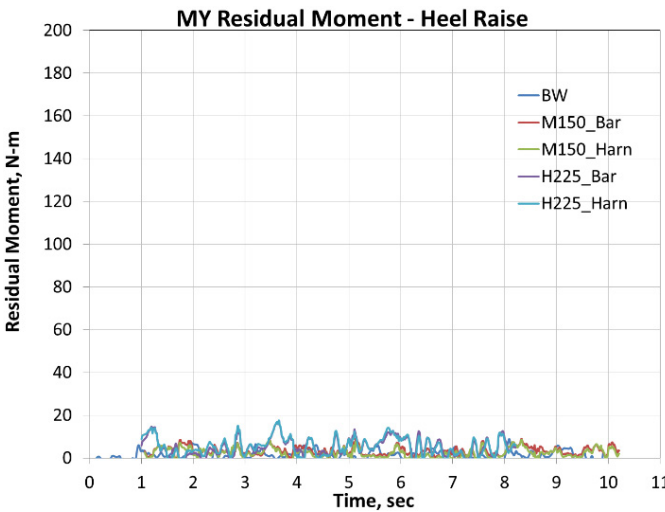


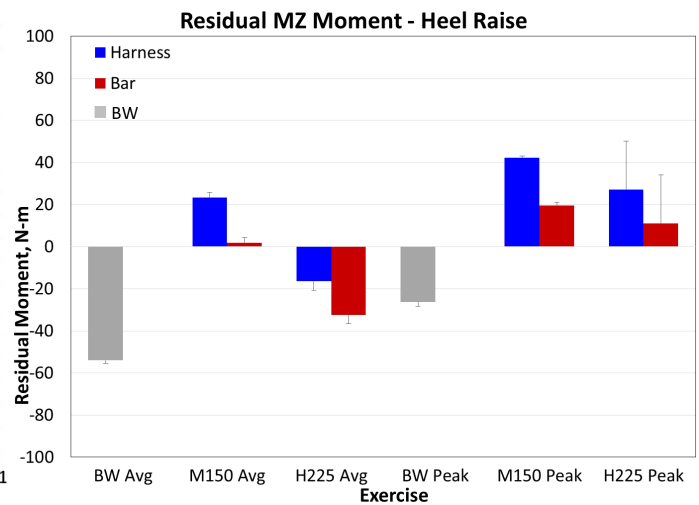
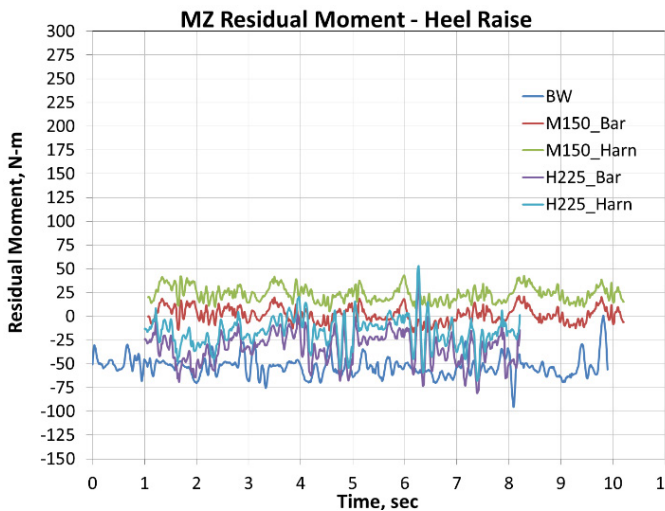
Figure 28.—Average and peak residual forces in Newton and moments in Newton-meters for heel raise under all loading conditions for the following residual forces: (a) FX, (b) FY, (c) FZ, and residual moments: (d) MX, (e) MY, (f) MZ.



(d)



(e)



(f)

Figure 28.—Concluded. Average and peak residual forces in Newton and moments in Newton-meters for heel raise under all loading conditions for the following residual forces: (a) FX, (b) FY, (c) FZ, and residual moments: (d) MX, (e) MY, (f) MZ.

Reserve Moments for Heel Raise

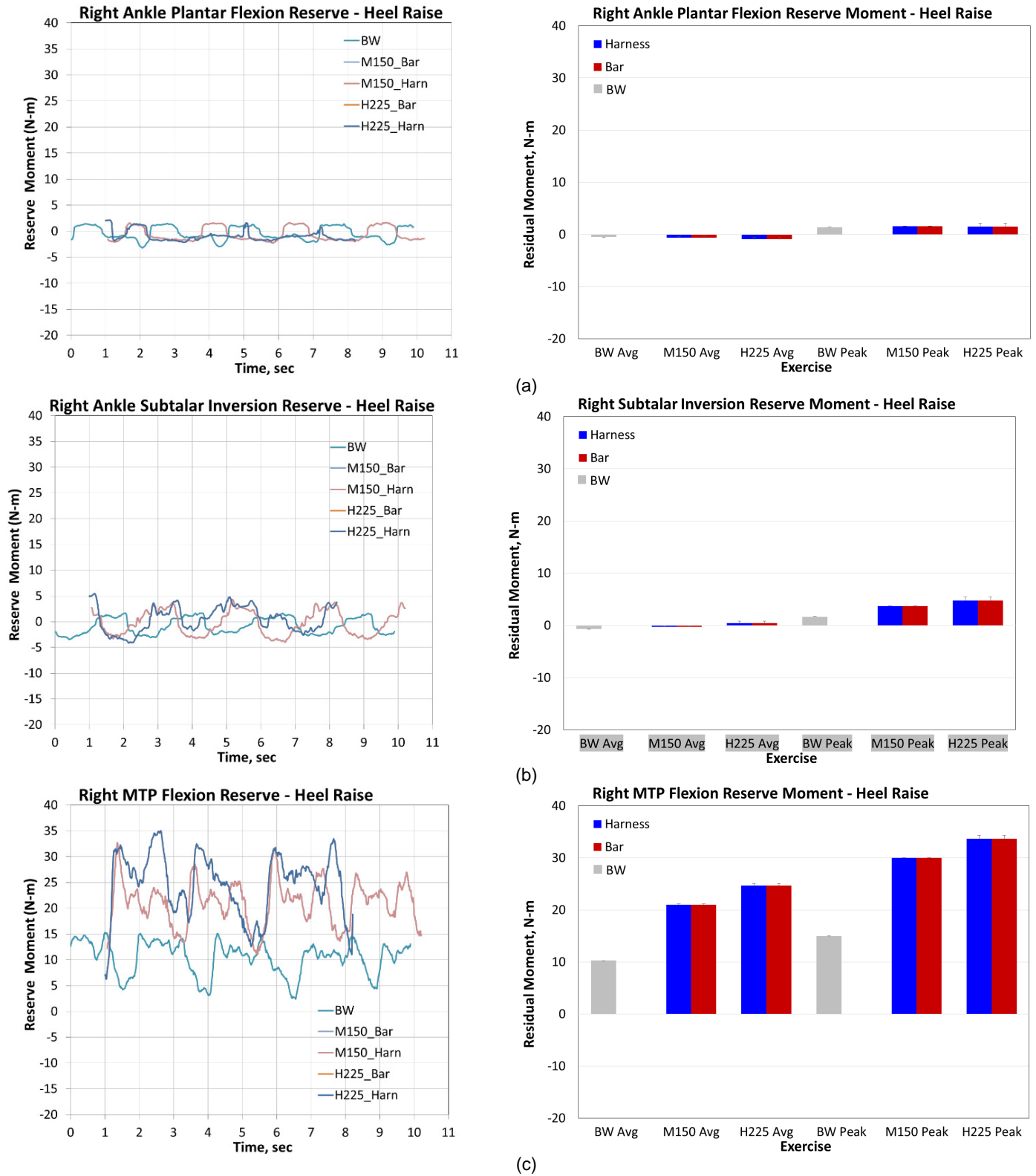
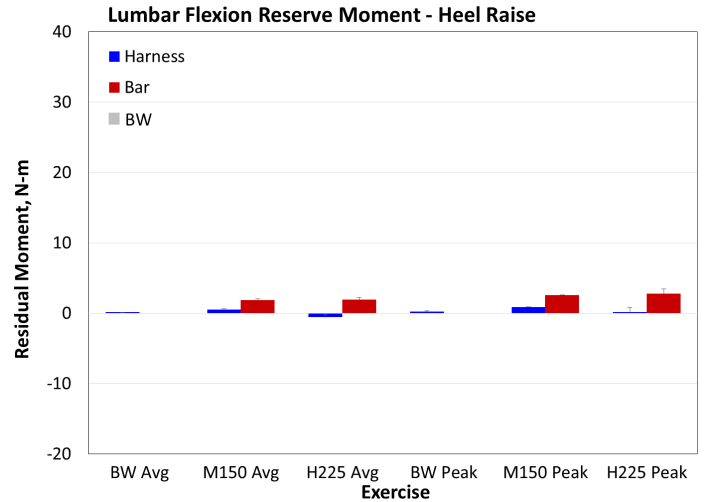
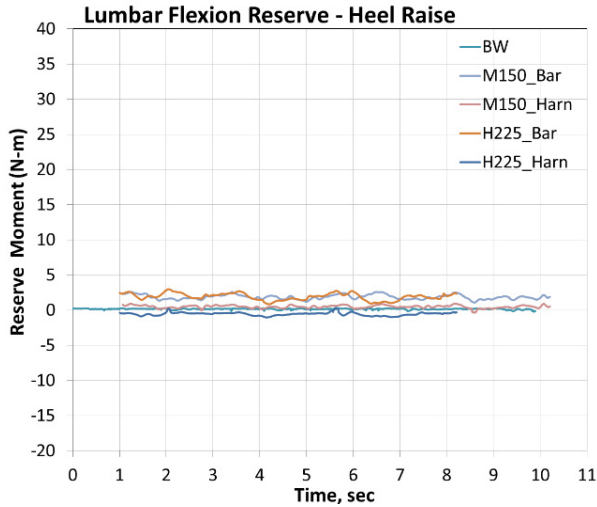


Figure 29.—Average and peak reserve actuator moments for heel raise under all loading conditions for the following joint articulations: (a) ankle plantar flexion, (b) subtalar inversion, (c) MTP extension, and (d) lumbar extension.



(d)

Figure 29.—Concluded. Average and peak reserve actuator moments for heel raise under all loading conditions for the following joint articulations: (a) ankle plantar flexion, (b) subtalar inversion, (c) MTP extension, and (d) lumbar extension.

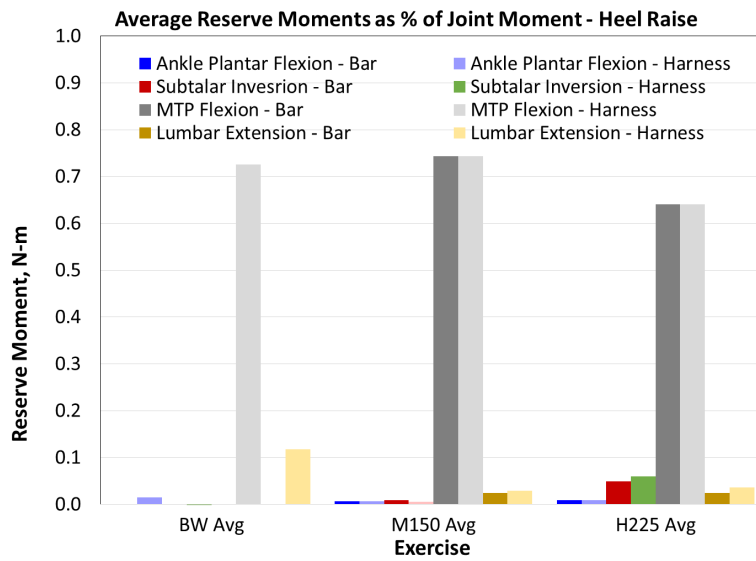


Figure 30.—Average reserve moments as a percentage of total joint moment for heel raise.

Summary of All Exercises

Peak resultant joint forces, joint moments, and muscle group forces increase with applied load. Table 7 summarizes these quantities as multiples of BW for forces, and BW-m for moments.

TABLE 7.—(a) PEAK RESULTANT JOINT FORCES EXPRESSED AS A MULTIPLE OF BW, (b) JOINT MOMENT EXPRESSED AS A MULTIPLE OF BW-m, (c) MUSCLE FORCES EXPRESSED AS A MULTIPLE OF BW FOR KEY JOINTS FOR ALL EXERCISES UNDER ALL LOADING CONDITIONS

(a)

Resultant Joint Forces (xBW)	Parallel Squat				Deep Squat			Single-Leg Squat		Heel Raise		
	BW	L125	M155	H185	L125	M155	H185	M60	H100	BW	M150	H225
Hip, average, bar/harness	4.0	7.0	7.9	8.5	6.7	7.9	8.3	5.5	7.5	2.8	2.6	3.6
Knee patellofemoral, average, bar/harness	3.8	6.6	7.8	7.4	6.9	7.4	8.3	4.1	4.7	1.7	2.8	3.5
Knee tibiofemoral, average, bar/harness	0.6	1.0	1.1	1.2	1.0	1.1	1.2	4.9	6.5	0.2	0.3	0.2
Ankle, average, bar/harness	5.7	9.3	10.5	12.0	9.9	11.1	12.0	4.6	5.4	2.1	6.1	6.6
Lumbar, average	2.0	5.7	7.5	8.4	6.3	7.5	8.6	3.1	4.4	0.4	4.0	4.2
Lumbar, average, harness	2.0	3.2	4.1	4.5	3.7	4.2	4.6	2.4	2.7	0.4	2.3	2.0
Hip, peak, bar/harness	5.7	10.7	11.9	12.7	10.8	12.9	12.4	8.1	11.3	4.5	3.3	5.1
Knee patellofemoral, peak, bar/harness	7.6	12.8	14.0	14.2	11.7	12.8	13.9	6.7	8.4	2.6	3.7	4.4
Knee tibiofemoral, peak, bar/harness	0.8	1.3	1.4	1.5	1.3	1.3	1.5	7.5	9.5	0.5	0.4	0.5
Ankle, peak, bar/harness	7.5	11.5	12.8	14.8	13.8	15.0	15.9	6.5	7.1	3.1	8.5	9.1
Lumbar, peak, bar	3.5	9.3	11.7	14.1	10.3	12.4	13.6	4.4	5.4	0.5	5.1	5.6
Lumbar, peak, harness	3.5	5.9	7.2	8.7	6.4	7.7	8.3	3.3	3.7	0.5	2.9	2.4

(b)

Joint Moments (xBW-m)	Parallel Squat				Deep Squat			Single-Leg Squat		Heel Raise		
	BW	L125	M155	H185	L125	M155	H185	M60	H100	BW	M150	H225
Hip extension, average, bar/harness	0.03	0.09	0.11	0.13	0.09	0.11	0.11	0.16	0.21	0.04	0.02	0.06
Hip adduction, average, bar/harness	0.08	0.11	0.10	0.12	0.06	0.07	0.08	0.02	0.02	0.03	0.00	0.00
Knee extension, average, bar/harness	0.15	0.25	0.29	0.28	0.30	0.34	0.38	0.08	0.09	0.04	0.03	0.07
Ankle, Plantar flexion, average, bar/harness	0.08	0.12	0.15	0.14	0.18	0.21	0.21	0.09	0.13	0.04	0.13	0.15
Lumbar extension, average	0.07	0.19	0.25	0.27	0.20	0.25	0.28	0.10	0.13	0.00	0.10	0.11
Lumbar extension, average, harness	0.07	0.09	0.12	0.12	0.10	0.12	0.12	0.06	0.07	0.00	0.03	0.02
Hip extension, peak, bar/harness	0.06	0.17	0.22	0.24	0.19	0.23	0.26	0.26	0.33	0.13	0.04	0.09
Hip adduction, peak, bar/harness	0.14	0.21	0.25	0.26	0.31	0.22	0.24	0.07	0.09	0.06	0.02	0.03
Knee extension, peak, bar/harness	0.26	0.43	0.49	0.50	0.53	0.57	0.60	0.17	0.19	0.08	0.04	0.09
Ankle, Plantar flexion, peak, bar/harness	0.12	0.18	0.22	0.23	0.28	0.30	0.32	0.15	0.18	0.07	0.15	0.17
Lumbar extension, peak	0.12	0.33	0.42	0.47	0.36	0.45	0.45	0.14	0.18	0.00	0.12	0.14
Lumbar extension, peak, harness	0.12	0.19	0.24	0.28	0.21	0.26	0.25	0.09	0.11	0.00	0.04	0.04

(c)

Muscle Group Forces (xBW)	Parallel Squat				Deep Squat			Single-Leg Squat		Heel Raise	
	BW	L125	M155	H185	L125	M155	H185	M60	H100	M150	H225
Hip extensors, average, bar/harness	3.2	5.7	6.7	7.2	5.7	6.9	7.2	5.2	7.0		
Hip flexors, average, bar/harness	0.6	0.7	0.8	0.9	0.9	0.9	1.0	0.0	0.2		
Hip adductors, average, bar/harness	0.0	0.0	0.0	0.0	0.0	0.1	0.2	1.7	2.3		
Hip abductors, average, bar/harness	3.2	5.4	6.2	6.6	5.3	6.3	6.5	2.4	3.2		
Knee extensors, average, bar/harness	3.8	6.6	7.8	7.4	7.0	7.4	8.3	4.1	4.7	0.3	0.2
Knee flexors, average, bar/harness	0.1	0.0	0.1	0.1	0.2	0.2	0.3	2.8	3.9	1.9	2.8
Ankle, Plantar flexors, average, bar/harness	3.6	6.0	6.7	8.1	6.2	7.1	7.9	3.6	4.3	5.2	5.8
Hip extensors, peak, bar/harness	5.2	9.8	11.3	13.1	10.7	13.5	13.4	8.6	11.5	0.0	0.0
Hip flexors, peak, bar/harness	1.3	1.7	2.5	1.9	2.3	1.8	2.1	0.1	1.0		
Hip adductors, peak, bar/harness	0.0	0.0	0.1	0.9	0.6	0.6	1.4	3.4	4.5		
Hip abductors, peak, bar/harness	4.7	8.5	9.4	10.2	8.4	9.8	9.3	3.2	4.4		
Knee extensors, peak, bar/harness	7.6	12.9	14.1	14.3	11.7	12.9	13.9	6.8	8.5	0.4	0.5
Knee flexors, peak, bar/harness	0.1	0.2	0.3	0.6	0.9	0.9	1.1	4.7	6.6	2.7	3.8
Ankle, Plantar flexors, peak, bar/harness	6.1	9.7	10.4	13.1	7.9	8.7	9.5	5.7	6.1	7.4	8.0

Discussion

Significance of Results

These models represent a significant extension of the application of the OpenSim modeling software to high-intensity resistance training exercise. The high degree of external loading on the subject combined with the very large ranges of motion for the joints, especially the knee and hip, challenge the ability of the models to estimate the desired outcomes of joint torque, resultant joint force and muscle group force in a physiologically relevant manner. Our modifications to the Arnold lower limb model have extended its useful operating ranges for hip and knee flexion as seen during deep squats and single-leg squats. The models provide important information and insight about the exercises themselves and about the HULK exercise device as a means for performing them.

The models generally show forces and torques that scale with applied external load and reach the local maximum value with maximal squatting depth or maxima heel raise height.

Another interesting finding is that the peak knee and hip resultant joint loads trend lower or are statistically equal for deep squat vs. parallel squat ($p > 0.05$). This is counterintuitive, but is consistent with the position of advocates of the deep squat who report similar knee stresses during deep squats vs. parallel squats (Ref. 24, 25, and 26). Replicating this finding boosts confidence in the ability of the squat model to estimate relative differences in joint force due to an altered range of motion as well as in the ability of subjects to exercise safely over a wide range of motion, as long as proper form is strictly maintained.

Validation of Results With Previous Exercise Studies

A frequent problem encountered when comparing exercise studies is the high variability in outcomes due to differences in exercise form, range of motion, subjects, cadence, loading and stance. Validating our models is, therefore, a matter of matching trends and relative values of outcomes across studies, rather than duplicating absolute values of outcomes.

Squat

Our subject's body weight translates to a 745 N load, and the applied squat loads of 125, 155 and 185 lb translate to applied loads of 557, 690, and 824 N, respectively, and a range spanning from 75 to 110 percent of BW.

Joint forces: The squat simulation results showed lumbar spine compressive force increasing proportionately with applied load during the squat exercise, which is consistent with previous exercise studies (Refs. 27 and 28). Additionally, when differences in squat depth and cadence are accounted for, our peak lumbar resultant joint forces are consistent with these studies, both at body weight (2,600 vs. 2,100 N (Ref. 27)) and over our applied load range (5,000 to 10,400 N vs. 5,400 to 9,500 N (Ref. 28)). Our peak patellofemoral forces at BW of 5,600 N are consistent with a slower cadence BW squat to 90° (3,750 N) performed with an instrumented artificial knee joint (Ref. 29). Patellofemoral force increases with applied load, but is actually slightly lower for deep squats (8,700 to 10,300 N-m) than for parallel (9,600 to 10,600 N-m), a counterintuitive finding that is supported by previous studies (Refs. 24, 25, and 26), as well as the trends in the measured external loading data (Appendix C, which are slightly higher (0 to 5 percent) for the parallel case than the deep case at similar loads ($p > 0.05$)).

Joint Torques: The models are also consistent with other studies that show hip and knee torque increasing with hip flexion and external load (Refs. 30, 31, and 32) and greater hip torque being generated for deep squats than for parallel squats (Refs. 31 and 32). However, peak hip torques for deep and parallel squats (130 to 190 N-m) are lower than similar studies using barbell squats heavier loads (200 to 300 N-m (Refs. 31 and 32)), even after accounting for loading differences, while peak knee torques in our models (300 to 450 N-m) exceed the knee torques (100 to 200 N-m) of those same studies. This finding warrants further investigation to determine if this is caused by the loading profile of the HULK device, the technique of the subject or an inconsistency between the model and the subject's true

anatomy and physiology. As with results reported elsewhere, knee torque does increase with knee flexion and load (Refs. 33 and 34), and greater knee torque is generated for deep squats than for parallel squats (Ref. 31).

Muscle forces: Despite our study's lack of EMG data, which can resolve the contributions of individual muscles within groups, the models can provide useful comparisons of relative muscle group force contributions versus both load and squatting depth with results in the literature. As reported elsewhere (Refs. 31, 35, 14, and 36) hip extensor and adductor activity increases with external load and squat depth in our models. Quadriceps, hamstrings and gastrocnemius activity all increase as knee flexion increases during the execution of the squat, as previously reported in (Ref. 3). There were no significant differences ($p > 0.05$) found in quadriceps activity between deep and parallel squats, as in (Refs. 31, 32, and 36), but the parallel squat trended higher than the deep squat for all loading cases, consistent with the findings noted above. Hamstring activity remained constant both with load, as in (Ref. 14), and with squat depth, as in (Refs. 31 and 36), however our model underreports estimated hamstring activity relative to studies, e.g., (Refs. 33 and 37). We attribute this to a lack of EMG data to properly guide activation levels, thereby transferring too much of the hip extension loading to the gluteal muscles, whose activity tends to be overestimated by our model. Ankle plantar flexor activity in our squat models increases with external load and increases slightly with squat depth, as in (Ref. 35). That study reports 70 percent of maximal voluntary contraction (MVC) for 90 percent of maximal squat loads in the plantar flexors, and our findings are generally consistent with that estimate.

Single-Leg Squat

The single-leg squat loads of 60 and 100 lb translate to applied loads of 267 and 445 N, respectively, and a range spanning from 35 to 60 percent BW.

Published results for the single-leg squat exercise are far less abundant than those for the squat. Therefore, not all outcomes of this study can be validated by the literature. The peak joint torques for hip (54 N-m), knee (126 N-m) and ankle (113 N-m) during a light load SLS in our study compared favorably to a previous study of body weight squats with the unloaded leg forward (Ref. 38). This same study found that patellar tendon force (roughly 70 percent of the sum of all knee extensor forces (Ref. 39)) peaks around 8.2 times body weight for 120° of knee flexion, and our model is consistent with this finding (8.4 times body weight) once differences in methods between the two studies are accounted for. This is less true for patellofemoral joint force where our results underreport the cited study (8.4 vs. 10.2 times body weight). We attribute these differences to the variation in cadence and exercise technique between the two studies, and the different methods employed to estimate patellofemoral joint force.

Heel Raise

The heel raise loads of 150 and 225 lb translate to applied loads of 668 and 1,000 N, respectively, and a range spanning from 90 to 135 percent BW.

Published results for the heel raise exercise are also far less abundant than those for the squat. Therefore, not all outcomes of this study can be validated by the literature. Furthermore, not all studies use blocks or other means that allow the full range of motion, as were used in this study. During unilateral body weight heel raises, with a 10° tilted wedge and a cadence of 0.65 sec, the average peak ankle joint torque was 2.6 N-m/kg (Ref. 7), which compares favorably with this present study when cadence and bilateral stance are accounted for. During double-leg heel raise exercises, performed without blocks, the average peak ankle plantar-flexion net joint moment was 0.85 N-m/kg for body weight exercises, 0.9 N-m/kg with an additional 5 percent of body weight and 0.95 N-m/kg with an additional 10 percent of body weight (Ref. 8). After noting differences in the test setup and cadence, our model roughly correlates with this trending.

Achilles tendon forces, which approximate the aggregate sum of the plantar flexor muscles, approach 5,000 N during unilateral BW heel raises (Ref. 40), and our model agrees with these findings for bilateral heel raises with an applied load close to the subject's body weight.

Harness Loading Versus Bar Loading

The outcomes for the simulated harness loading versus bar loading are generally identical (well within 1 percent) for all joints and muscle groups, with the exception of the lumbar joint, the six torso muscles, the residuals and the reserve actuators, for which some statistically significant differences do occur. For this reason, only the lumbar joint is reported separately for the bar case vs. the harness case in Table 7. This indicates that the model has reached a solution whereby the lumbar joint muscles, the residuals and the reserves experience the bulk of the changes in response due to the changes in loading configuration.

Given this, the result of the bar loading vs. harness loading analysis was a decrease in the resultant lumbar joint force in all exercises with the harness. A peak resultant lumbar joint force of approximately 10 kN was predicted for the deep and parallel squats performed at high external load when using the bar loading configuration. The predicted peak resultant lumbar joint force for deep and parallel squats performed at high external load when using the harness configuration was about 40 percent lower (~6 kN). This reduction is due to the redistribution of load to 70 percent applied to the upper back and 30 percent applied to the lower back. The resultant lumbar joint forces in the single-leg squat and the heel raise exercises were only approximately 4,000 N for each exercise during bar loading, and harness loading reduced this by between one-third and one-half. If maintenance of bone mineral density at the lumbar spine is dependent on stimulating forces greater than those provided by the single-leg squat and heel raise exercises, then, based on these preliminary findings, the harness loading configuration may be less effective in maintaining lumbar spine bone mineral density than the bar loading.

Similarly, a decrease in the peak lumbar extension joint moment was predicted in harness loading (~200 N-m) vs. bar loading (~350 N-m) for the high-intensity squat exercises. The peak lumbar extension joint moment was predicted to be lower in the single-leg squat exercise performed with medium external weight and higher when high external weight was used. However, the peak lumbar extension joint moments only ranged from 100 to 135 N-m in the single-leg exercise. For the heel raise, the lumbar joint moments were not statistically different between medium and high loads, and the harness reduced these moments by one-half.

In these analyses, the joint moments, resultant joint forces and muscle forces all remained nearly constant for all joints and muscles below the lumbar spine for all of the exercises. More investigation is needed to determine whether this is physiologically relevant or simply an artifact of our assumption of identical kinematics between the two cases. Laboratory testing of both cases with full motion capture and load data capture is needed to determine the veracity of our assumption. Testing is currently scheduled for spring 2015, after which another assessment of bar loading vs. harness loading will be made.

Comparison with ARED Squat Integrated Muscle Model (ASM-im)

In 2012 the Digital Astronaut Project released reports similar to that of the current study for the squat (Ref. 41) and deadlift (Ref. 42) exercises on the Advanced Resistive Exercise Device (ARED). Our previous ARED studies used LifeMOD (Life Modeler) as the modeling platform, and it is informative to compare the results of both studies.

The following differences should be noted when interpreting the comparative results:

1. The HULK and ARED devices are based on inherently different mechanisms and have different loading profiles vs. bar displacement for the same nominal load (Ref. 43). As such, one could expect different results for the same exercise on different devices.
2. The LifeMOD and OpenSim modeling software packages employ different methods for solving for the outcomes of this study. LifeMOD results were produced from forward dynamic analyses with an active controller minimizing the error relative to the known kinematics (Ref. 44), whereas OpenSim results were produced from inverse dynamics and static optimization without an active controller. Although they are estimating the same outcomes, the two packages are solving different mathematical problems.

3. The LifeMOD and OpenSim models differ in an anatomical sense. Each model uses 45 muscle actuators in the lower limb, however, differences exist in which small muscles are included. The LifeMOD model does not include wrapping surfaces at the knees as the OpenSim model does. Additionally, the LifeMOD model includes a 4-joint spine, but no torso muscles, only torque actuators; whereas, the OpenSim model includes a single a spine joint (lumbar) with 6 torso muscles representing the spinal erectors, abdominals, and obliques.
4. The kinematics differ somewhat between the exercises performed in the two models, particularly squat depth. Motion capture techniques employed a different marker set in the ARED study (Ref. 41) vs. the current study (Appendix D), with the former study having known deficiencies that were later corrected in this study.

With these differences in mind, Table 8 compares some of the key outcomes between the ARED and HULK squat models.

It is interesting to note the similarity in hip forces and the dissimilarity in the lower limb forces. The HULK model joint and muscle group forces for the knee and ankle are between 3x-4x those of the ARED model. Further investigation is required to determine the underlying causes of these discrepancies, e.g., device differences, motion capture differences or modeling approach differences.

Also noteworthy is the higher degree of ankle dorsiflexion (>50 percent) and hip flexion (10 percent) required to squat to parallel on the HULK device vs. the ARED. ARED loads the subject with a bar connected via pivot joint to a lever arm, whereas HULK uses tethering cables. This may result in a different foot placement to maintain comfort on the HULK, which may explain the differences in kinematics.

Comparison of Squat Versus Single-Leg Squat

For single-leg squat, our model estimates aggregate peak knee extensor forces (5,200 N) that are just over one-half of the hip extensors (9,800 N) for the single-leg squat with a 100 lb (45 kg) external load. Similar proportions are exhibited by the joint moments in the knee (143 N-m) and hip (244 N-m) joints. Ground reaction force data from these trials suggests that nearly three-quarters (73 percent) of the load is borne by the target right leg.

TABLE 8.—COMPARISON OF PEAK VALUES OF KEY OUTCOMES (JOINT ANGLES, JOINT TORQUES, RESULTANT JOINT FORCES AND MUSCLE GROUP FORCES) BETWEEN THE ARED SQUAT MODEL, ASM-im, AND THE HULK SQUAT MODEL

Load = 185 lb		Peak	
		HULK	ARED
Kinematic angles, °	Hip_Flexion_Angle	115	105
	Knee_Flexion_Angle	124	121
	Ankle_Dorsiflexion_Angle	36	23
Joint torques, N-m	Hip_Extension_Torque	182	230
	Knee_Extension_Torque	374	100
	Ankle_Joint_Torque	174	52
Resultant joint forces, KN	Hip_Joint_Force	10.0	11.1
	Knee_Joint_Force	10.4	4.3
	Ankle_Joint_Force	11.0	4.3
Muscle tension forces, KN	Hip_Extensors_Muscle_Force	11.2	5.6
	Knee_Extensors_Muscle_Force	10.4	5.3
	Plantar_Flexors_Muscle_Force	7.5	3.3

In contrast, the traditional parallel squat model estimates that peak knee extensor forces (9,600 N) exceed hip extensor forces (7,300 N) with a 125 lb (57 kg) external load. A greater difference occurs in the joint moments of the knee (320 N-m) and hip (125 N-m). In this case, due to the subject’s right-side dominance, 51 percent of the load is borne by the right leg.

These results clearly support the consistent findings in the literature asserting that single-leg and two-leg squats are not interchangeable exercises, even at similar intensities. This is because the single-leg version shifts the loading more heavily toward extending the hip, at the expense of extending the knee (Refs. 38, 39, 5, and 45). This behavior becomes even more pronounced with a greater degree of lumbar flexion (Ref. 45), but this factor was not investigated in our study.

Verification and Validation of the Models

In accordance with the Human Research Program’s (HRP) Unique Processes, Criteria, and Guidelines (HRP-47069), all DAP models are vetted in accordance with NASA Standard for Models and Simulations (NASA-STD-7009) (Ref. 46). This standard consists of a comprehensive set of requirements and processes for developing and applying models and simulations (M&S), while ensuring appropriate verification, validation and credibility of the M&S results. It was established as a result of the recommendations from the Columbia accident report to ensure that all M&S implemented by NASA that can potentially impact the crew or mission must be:

- Sufficiently vetted for the problem under consideration
- Well documented to capture the limitations and caveats
- Developed and implemented by personnel that are well qualified to address the problem under consideration
- Developed and implemented using processes that are appropriate for the problem under consideration

The credibility assessment for the HULK biomechanical models essentially mirrors the credibility assessment for the ARED Squat model with muscles (ASM-i) described previously (Ref. 41). The credibility score is a 2.3, as summarized in Table 9.

TABLE 9.—CREDIBILITY ASSESSMENT FOR HULK BIOMECHANICAL MODELS USING METHODS OUTLINED IN NASA-STD-2009

	CAS score	Overall weight	Overall credibility	Thresholds	MAX
Verification	2	0.4	2.3	3	4
Validation	2	0.5		2	4
Input pedigree	3	0.3		3	4
Results uncertainty	1	0.1		2	4
Results robustness	1	0.1		2	4
Use history	1	0.15		2	4
M&S management	2	0.1		3	4
People qualifications	3	0.6		3	4

Interpretation and Limitations

Readers should interpret results from these models with the following points in mind:

- One cannot verify the true accuracy of the outcomes estimated by the models in an absolute sense. The quantities cannot be measured directly, and validation with similar results in the literature is confounded by differences in subjects, exercise techniques, cadence, form and posture among studies. Estimating relative differences due to perturbations is likely to be more useful.
- The models are currently only valid for 1g estimations. Estimating results for microgravity requires knowledge of the kinematic changes that occur in space. Motion capture as done for this study is generally infeasible in space. While limited estimation of joint angles is possible from in-flight videos, a predictive model with an adaptive controller is required to make a more thorough and accurate estimation. The Digital Astronaut Project is currently developing such a controller, outside the scope of this study. Given accurate kinematics and measured loading profiles, these models will be useful for estimating the resulting kinetic outcomes.
- The muscle model used in these analyses was not a full representation of the Millard (Ref. 23) and Hill actuator model (Ref. 47) (i.e., they did not include active and passive force-length characteristics, force-velocity characteristics and activation dynamics). Instead, the muscle model was a simple force actuator with a given maximum isometric force and the rest of the muscle parameters turned off. This was done to simplify the static optimization methods.
- Prediction of the muscle activations and force levels during the exercises is a difficult problem because the static optimization used to calculate these values is an under-constrained problem. Comparison of the muscle activations to EMG data is a method that can be used for validation, but was not performed in these analyses due to the lack of EMG data. Alternatively, EMG data can be used to help constrain the optimization problem during analysis. Future studies will include the collection of EMG data and their appropriate use in the analysis procedure will be determined.
- Residual and reserve actuator contributions remain somewhat high for both the squat and single-leg squat, both of which exceed OpenSim best practice guidelines for residual and reserve values (Ref. 22). While these guidelines were developed mostly with gait applications in mind, the value of some residual actuators remain significant compared with the contributions of the muscles in the model. Further refinement of these models could reduce the residuals to more acceptable values.
- The subjectively-determined estimation for harness loading (70-30 percent split) and the lack of control for cadence are potentially confounding variables.

Future Work

This work is preliminary, pending the results of the aforementioned harness testing and the subsequent modeling efforts. Many further refinements of the models are possible. The current work extends the current range of application of OpenSim models to high-intensity resistance training. Our work clearly indicates a need to extend the valid joint angle operating ranges for the Arnold lower body model. Specifically, the anatomical paths and wrapping surfaces of muscles in the model need to be further refined to allow knee angles up to 150° of flexion and hip angles up to 130° of flexion while minimizing any sign changes of muscle moment arms over the entire operating range of joint angles (i.e., agonist muscles should remain as agonists throughout the movements and vice versa for the antagonist muscles).

With regard to harness loading, the current work assumes that the kinematics do not change significantly between loading schemes. Yet, harness loading will likely alter the amounts of lumbar, hip and knee flexion, when compared with bar loading. The extent to which this occurs must be tested in 1g, and possibly in 0g as well if the opportunity

presents itself. Kinematic changes will ultimately result in changes to the kinetic outcomes as well. Our work will quantify these changes.

This study currently does not include electromyography (EMG) data. Because static optimization is a severely under-constrained problem with an infinite solution set, EMG data can be used to increase the optimization constraints, guiding the muscle activation predictions to a more physiologically relevant solution. Alternatively, the EMG data can be used to validate the optimization results. Improving the optimization methodologies used and adding the capability to validate the muscle activation predictions will result in two benefits: 1) the ability to estimate individual muscle forces rather than aggregate muscle forces by group, and 2) the ability to estimate resultant joint forces more accurately since the loads on specific bones depend on specific individual muscles and their relative spatial relationships. Future work will include acquiring EMG data for all trials and re-incorporating the more complex Millard muscle model into the analyses.

The DAP project has acquired a full set of motion capture and loading data for the deadlift exercise on HULK. Modeling efforts for the deadlift exercise will begin in Spring 2015 with the addition of a research fellow to the modeling team.

Finally, the data acquired to date have not fully explored all of the configurations in which subjects could perform the exercise. A rigorous set of testing combined with a thorough model sensitivity analysis would provide insight into the effects of cadence, stance, foot placement and the various parameters inherent in the models, e.g., muscle properties and analysis settings. The project will also explore these activities more fully in the coming year.

Conclusions

We have developed OpenSim models for three high-intensity lower-body resistance exercises (SQ, SLS and HR) on the HULK device in 1g based on motion capture and measured external loading data. These models operate over a fuller range of motion and loading intensities than previously reported similar models. The models describe the subject's kinematics during the movement, and they estimate average and peak values for joint torques, resultant joint forces, and muscle forces by muscle group (not by individual muscle). We have identified the useful applications for these models, validated their outcomes against similar exercise studies previously reported, and identified their inherent limitations.

Appendix A.—Acronyms

AEC	Advanced Exercise Concepts
ARED	Advanced Resistive Exercise Device
BW	body weight
COA	center of application (of applied external force)
COP	center of pressure (of GRF)
DAP	Digital Astronaut Project
EMG	electromyography
ExPC	Exercise Physiology and Countermeasures
GRC	NASA Glenn Research Center
GRF	ground reaction force
H	heavy
HHC	Human Health and Countermeasures (Element)
HR	heel raise
HRP	Human Research Program
HULK	Hybrid Ultimate Lifting Kit
ID	inverse dynamics
IK	inverse kinematics
ISS	International Space Station
JSC	NASA Johnson Space Center
L	light
M	medium
mocap	motion capture
MPCV	Multi-purpose Crew Vehicle
M&S	models and simulations
NASA	National Aeronautics and Space Administration
PF	plantar flexor or patellofemoral
x RM	x repetition maximum
RMS	root mean square
RMSD	root mean square difference
SE	standard error
SLS	single-leg squat
SO	static optimization
SQ	squat
SQD	(deep) squat
SQP	(parallel) squat
TF	tibiofemoral

Appendix B.—Model Parameters and Configurations

OpenSim Muscle Parameters										
Muscle name	OpenSim muscle name	Muscle type	Max isometric force, N		Optimal fiber length, m		Tendon slack length, m		Pennation angle, rad	
			Right	Left	Right	Left	Right	Left	Right	Left
Adductor Brevis	addbrev	Millard	455	456	0.115	0.115	0.033	0.033	0.106	0.106
Adductor Longus	addlong	Millard	600	600	0.085	0.085	0.115	0.115	0.124	0.124
Adductor Magnus Distal	addmagDist	Millard	486	486	0.187	0.187	0.095	0.095	0.241	0.241
Adductor Magnus Ischium	addmagIsch	Schutte	486	486	0.165	0.165	0.229	0.228	0.208	0.208
Adductor Magnus Middle	addmagMid	Millard	486	486	0.140	0.140	0.052	0.052	0.257	0.257
Adductor Magnus Proximal	addmagProx	Millard	486	486	0.105	0.105	0.047	0.047	0.387	0.387
Biceps Femoris Long Head	bflh	Millard	1058	1058	0.090	0.090	0.341	0.340	0.202	0.202
Biceps Femoris Short Head	bfsh	Millard	474	474	0.117	0.117	0.105	0.105	0.215	0.215
Extensor Digitorum Longus	edl	Millard	518	518	0.077	0.077	0.408	0.410	0.188	0.188
Extensor Hallucis Longus	ehl	Millard	248	248	0.082	0.083	0.365	0.367	0.164	0.164
Flexor Digitorum Longus	fdl	Millard	412	412	0.049	0.049	0.412	0.413	0.237	0.237
Flexor Hallucis Longus	fhl	Millard	655	655	0.057	0.057	0.385	0.386	0.295	0.295
Gastrocnemius Lateral	gaslat	Millard	910	910	0.060	0.060	0.444	0.447	0.209	0.209
Gastrocnemius Medial	gasmed	Millard	1962	1962	0.100	0.100	0.435	0.435	0.173	0.173
Gemellus	gem	Millard	164	164	0.027	0.027	0.044	0.044	0.000	0.000
Gluteus Maximus 1	glmax1	Millard	819	819	0.170	0.170	0.051	0.051	0.382	0.382
Gluteus Maximus 2	glmax2	Millard	1171	1171	0.180	0.180	0.075	0.075	0.382	0.382
Gluteus Maximus 3	glmax3	Millard	789	789	0.200	0.200	0.074	0.074	0.382	0.382
Gluteus Medius 1	glmed1	Millard	1322	1322	0.085	0.085	0.057	0.057	0.358	0.358
Gluteus Medius 2	glmed2	Millard	925	925	0.090	0.090	0.069	0.069	0.358	0.358
Gluteus Medius 3	glmed3	Millard	1053	1053	0.130	0.130	0.060	0.049	0.358	0.358
Gluteus Minimus 1	glmin1	Millard	270	270	0.090	0.090	0.016	0.017	0.175	0.175
Gluteus Minimus 2	glmin2	Millard	285	285	0.070	0.070	0.027	0.027	0.000	0.000
Gluteus Minimus 3	glmin3	Millard	323	323	0.060	0.060	0.054	0.054	0.017	0.017
Gracilis	grac	Millard	206	206	0.244	0.244	0.178	0.178	0.143	0.143
Iliacus	iliacus	Millard	933	933	0.109	0.109	0.080	0.080	0.250	0.250
Patellar Ligament	patlig	Schutte	2	2	0.057	0.058	0.006	0.006	0.000	0.000
Pectineus	pect	Millard	266	266	0.105	0.105	0.001	0.011	0.000	0.000
Peroneus Brevis	perbrev	Millard	459	459	0.052	0.052	0.169	0.170	0.201	0.201
Peroneus Longus	perlong	Millard	980	980	0.057	0.057	0.374	0.376	0.246	0.246
Peroneus Tertius	pertert	Millard	135	135	0.090	0.090	0.113	0.114	0.227	0.227
Piriformis	piri	Millard	444	444	0.050	0.050	0.124	0.124	0.175	0.175
Psoas	psoas	Millard	720	720	0.119	0.119	0.099	0.099	0.187	0.187
Quadratus Femoris	quadfem	Millard	381	381	0.061	0.061	0.027	0.027	0.000	0.000
Rectus Femoris	recfem	Millard	1273	1273	0.060	0.060	0.345	0.345	0.243	0.243
Sartorius	sart	Millard	170	170	0.400	0.400	0.117	0.117	0.023	0.023
Semimembranosus	semimem	Millard	1744	1744	0.060	0.060	0.360	0.330	0.264	0.264

OpenSim Muscle Parameters										
Muscle name	OpenSim muscle name	Muscle type	Max isometric force, N		Optimal fiber length, m		Tendon slack length, m		Pennation angle, rad	
			Right	Left	Right	Left	Right	Left	Right	Left
Semitendinosus	semiten	Millard	453	453	0.207	0.207	0.262	0.263	0.225	0.225
Soleus	soleus	Millard	5379	5379	0.060	0.060	0.375	0.375	0.494	0.494
Tensor Fasciae Latae	tfl	Millard	233	233	0.092	0.092	0.453	0.469	0.052	0.052
Tibialis Anterior	tibant	Millard	1011	1011	0.078	0.079	0.275	0.277	0.168	0.168
Tibialis Posterior	tibpost	Millard	1358	1358	0.043	0.044	0.323	0.325	0.239	0.239
Vastus Intermedius	vasint	Millard	1536	1536	0.140	0.140	0.112	0.111	0.079	0.079
Vastus Lateralis	vaslat	Millard	3383	3383	0.140	0.140	0.137	0.137	0.321	0.321
Vastus Medialis	vasmed	Millard	2166	2166	0.140	0.140	0.118	0.118	0.517	0.517
Erector Spinae	ercspn	^a Thelen	2500	2500	0.141	0.141	0.035	0.035	0.000	0.000
Abdominal Internal Oblique	intobl	^a Thelen	900	900	0.116	0.116	0.116	0.116	0.000	0.000
Abdominal External Oblique	extobl	^a Thelen	900	900	0.138	0.138	0.161	0.161	0.000	0.000

^aReference 48

Appendix C.—Measured External Force Data

C.1 Squat Exercise



Figure 31.—External force data as measured during deep and parallel squats. Average and peak (a) ground reaction forces in the normal (Y) direction, (b) resultant ground reaction forces in the shear direction, and (c) cable tension forces on the bar reported by the HULK device.

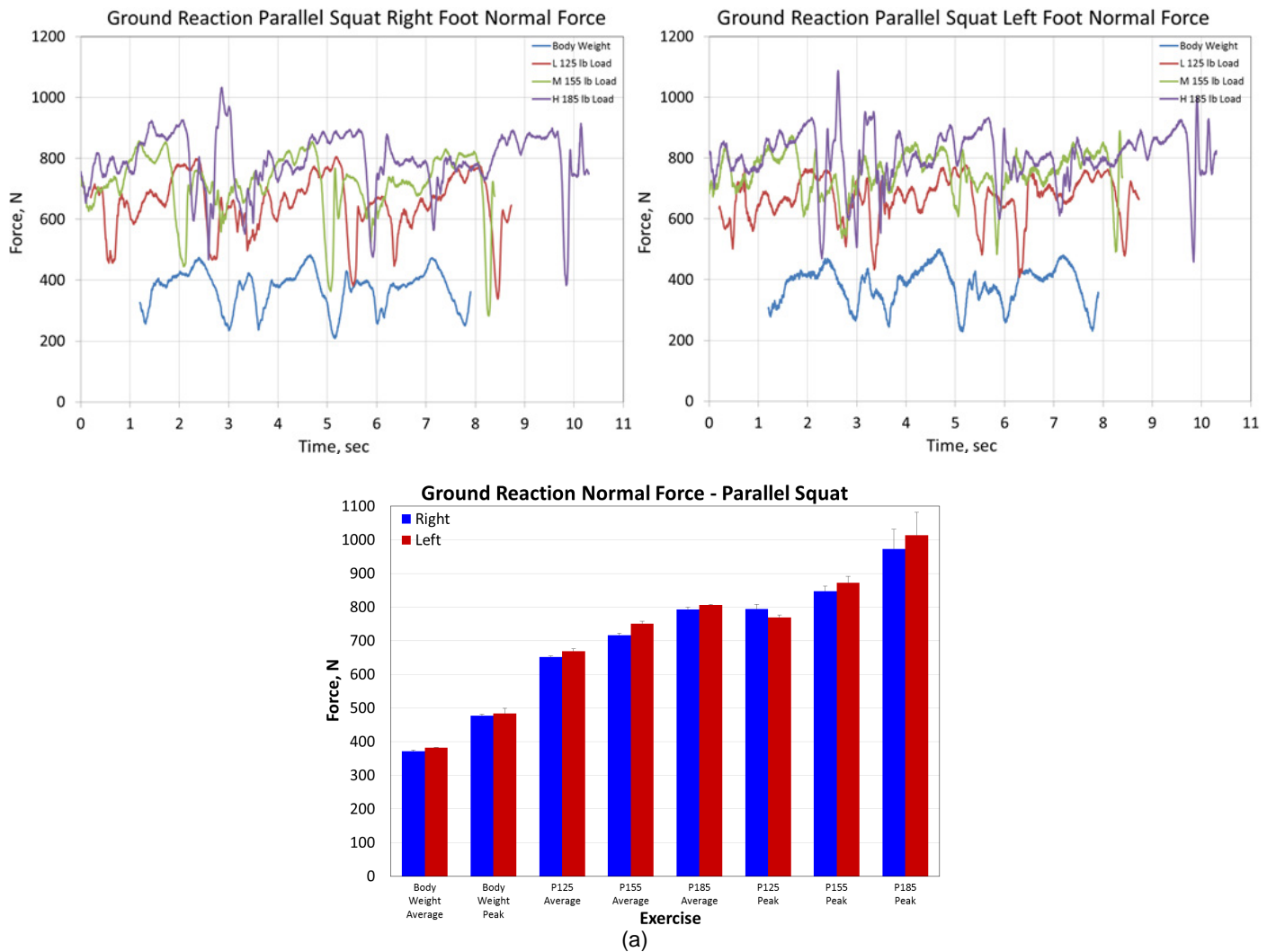


Figure 31.—Continued. External force data as measured during deep and parallel squats. Average and peak (a) ground reaction forces in the normal (Y) direction, (b) resultant ground reaction forces in the shear direction, and (c) cable tension forces on the bar reported by the HULK device.

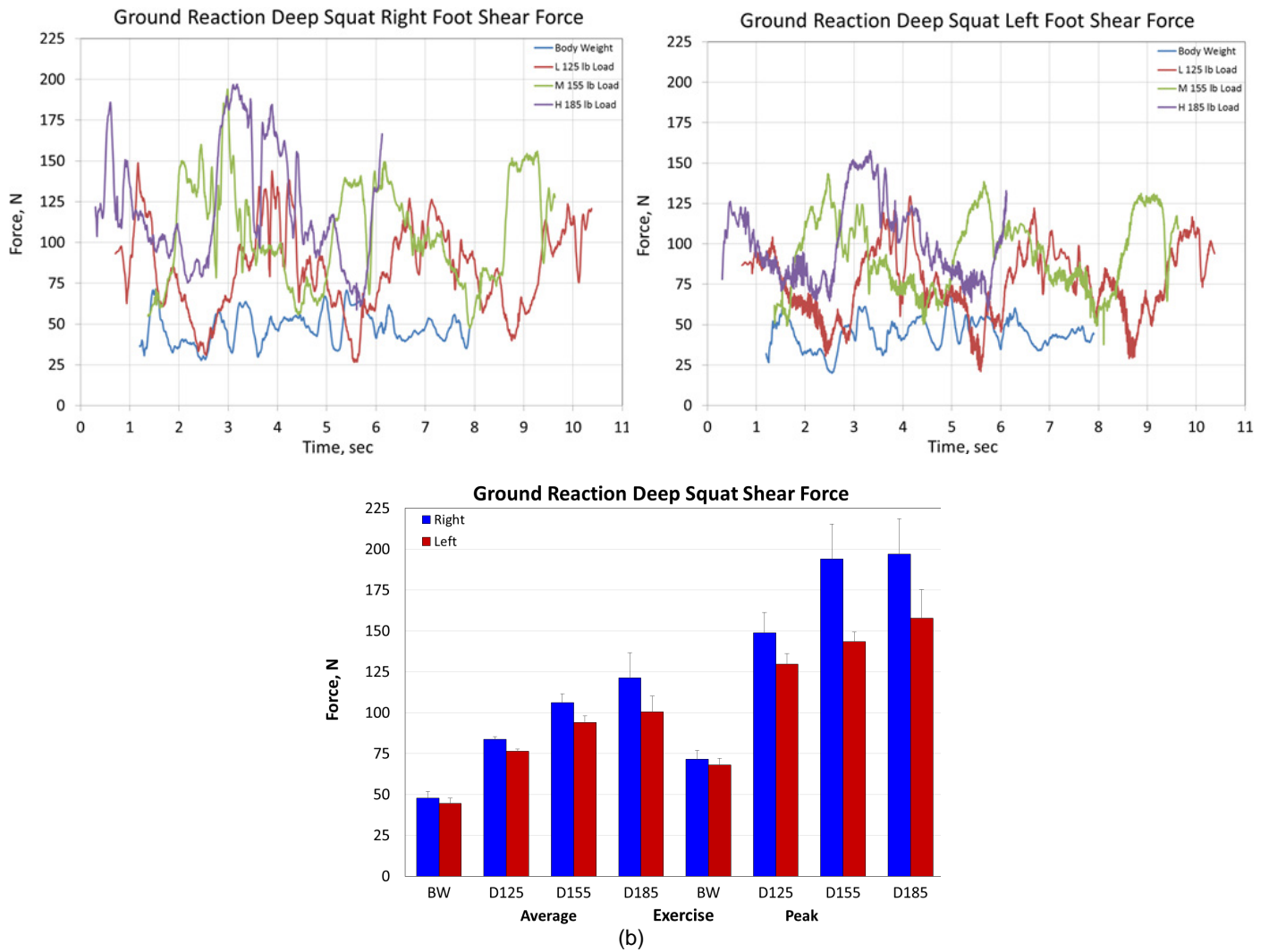


Figure 31.—Continued. External force data as measured during deep and parallel squats. Average and peak (a) ground reaction forces in the normal (Y) direction, (b) resultant ground reaction forces in the shear direction, and (c) cable tension forces on the bar reported by the HULK device.

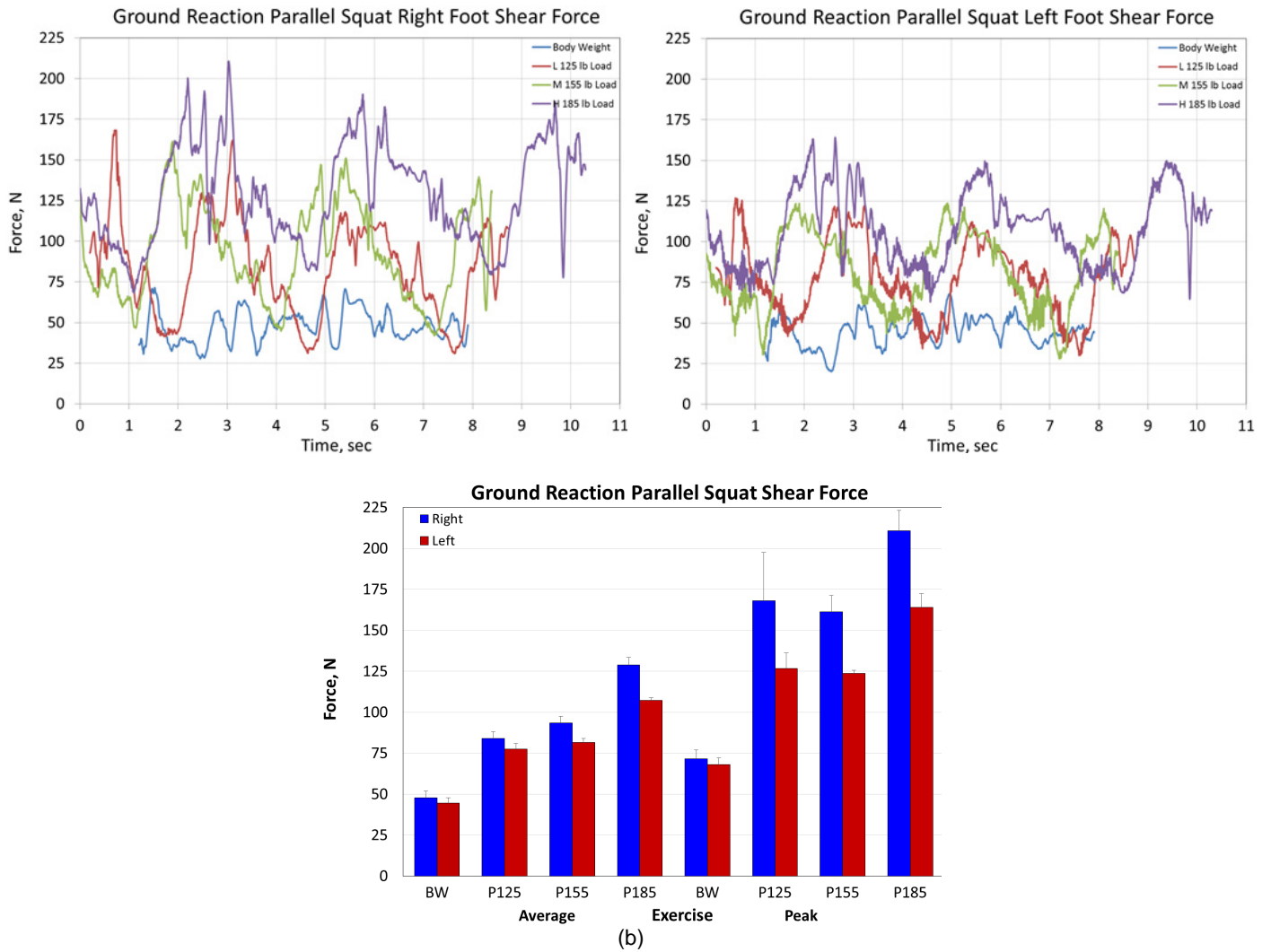


Figure 31.—Continued. External force data as measured during deep and parallel squats. Average and peak (a) ground reaction forces in the normal (Y) direction, (b) resultant ground reaction forces in the shear direction, and (c) cable tension forces on the bar reported by the HULK device.

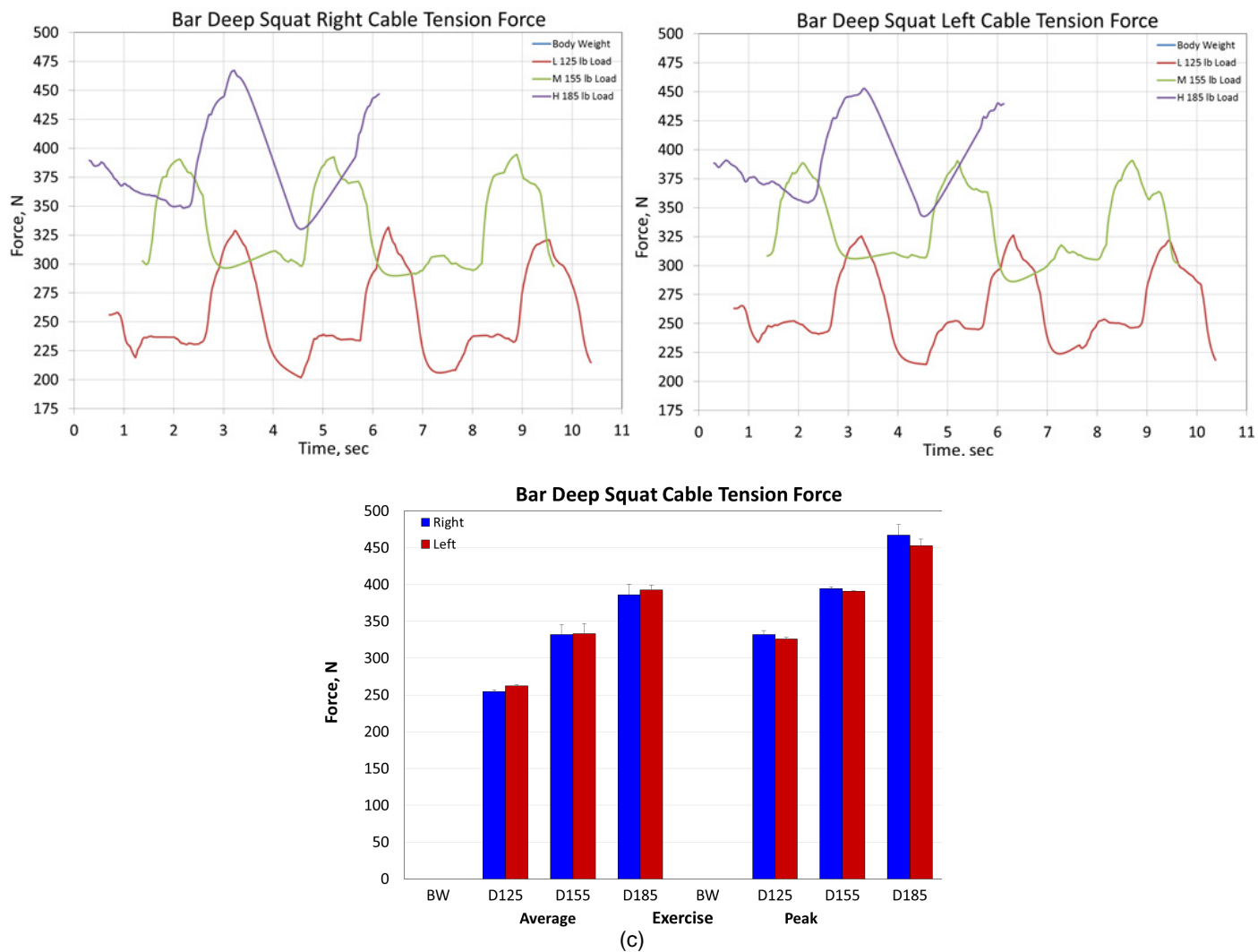


Figure 31.—Continued. External force data as measured during deep and parallel squats. Average and peak (a) ground reaction forces in the normal (Y) direction, (b) resultant ground reaction forces in the shear direction, and (c) cable tension forces on the bar reported by the HULK device.

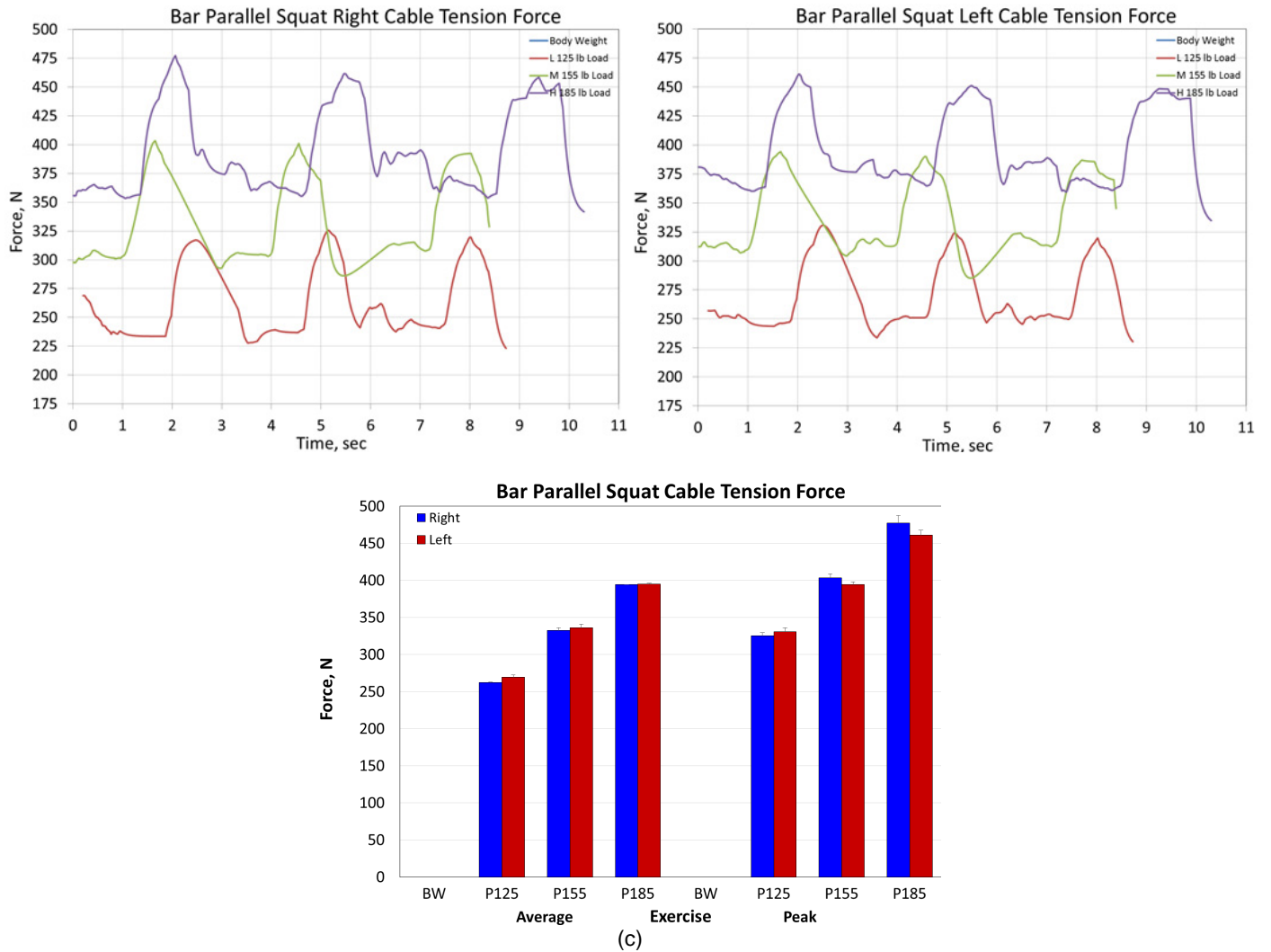


Figure 31.—Concluded. External force data as measured during deep and parallel squats. Average and peak (a) ground reaction forces in the normal (Y) direction, (b) resultant ground reaction forces in the shear direction, and (c) cable tension forces on the bar reported by the HULK device.

C.2 Single-Leg Squat Exercise

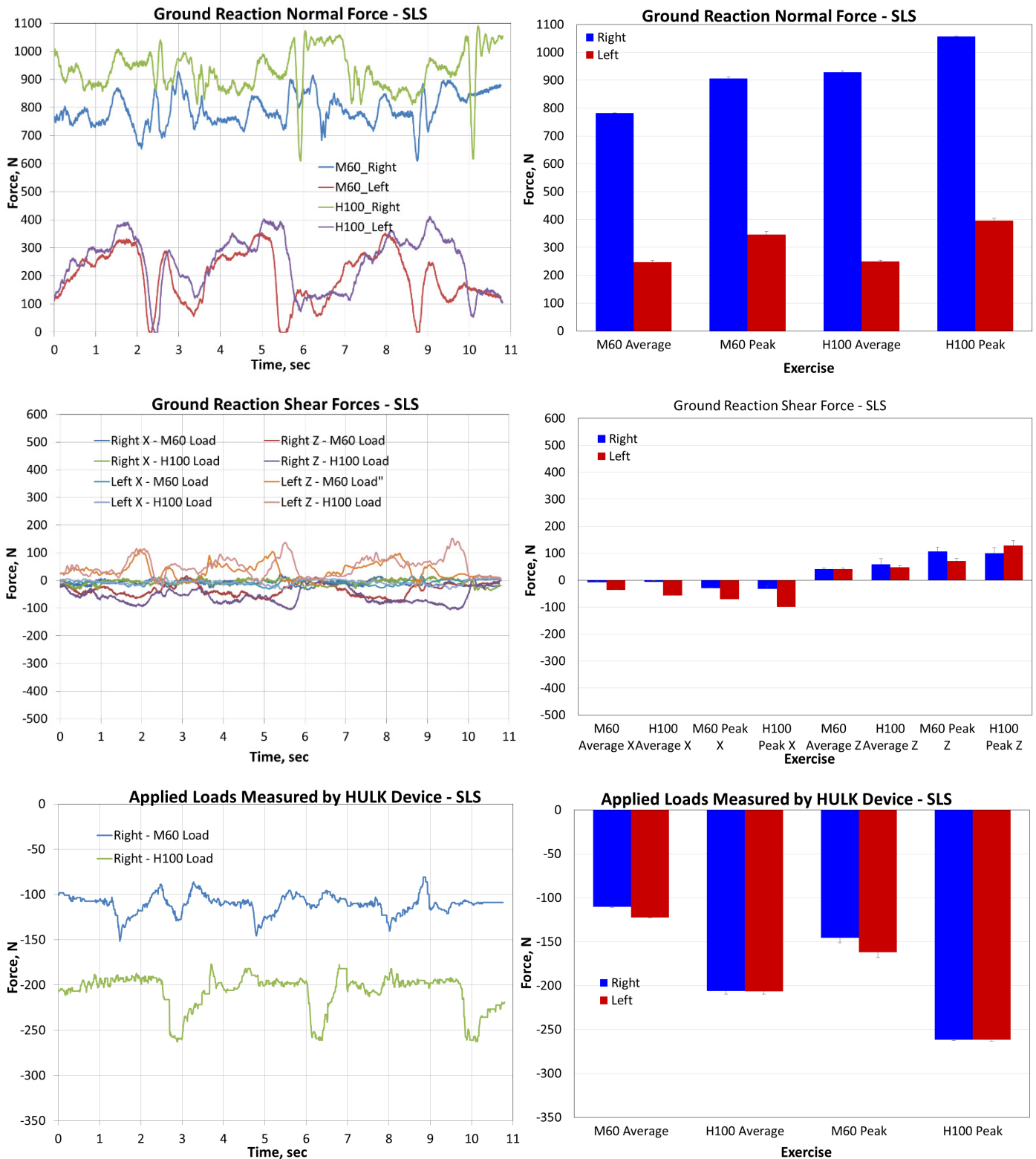


Figure 32.—External force data as measured during single-leg squats. Average and peak ground reaction forces in the normal (Y) and shear directions for the SLS and average and peak cable tension forces on the bar reported by the HULK device.

C.3 Heel Raise Exercise

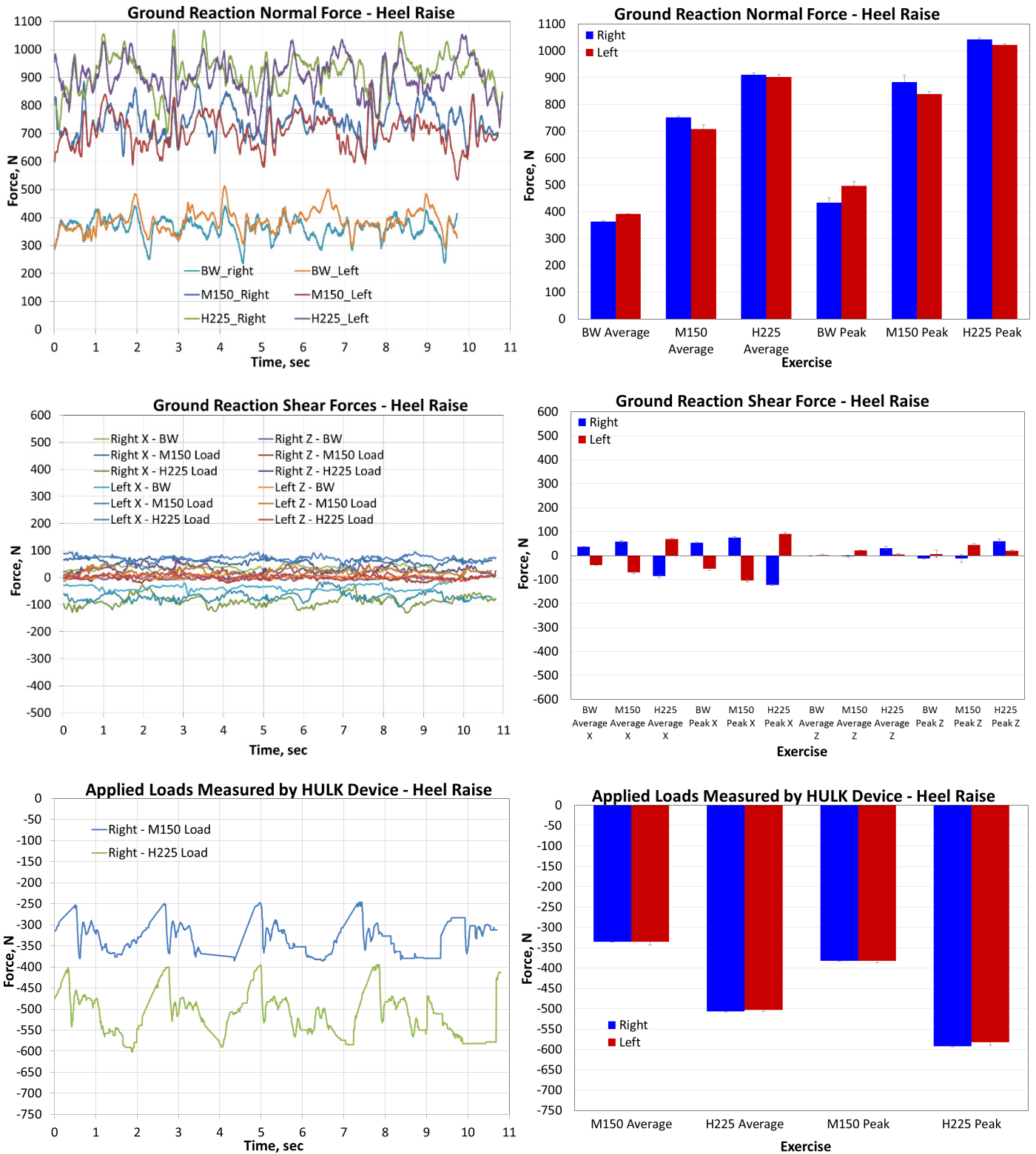


Figure 33.—External force data as measured during heel raises. Average and peak ground reaction forces in the normal (Y) and shear directions for the SLS and average and peak cable tension forces on the bar reported by the HULK device.

Appendix D.—Marker Set Used For Data Collection

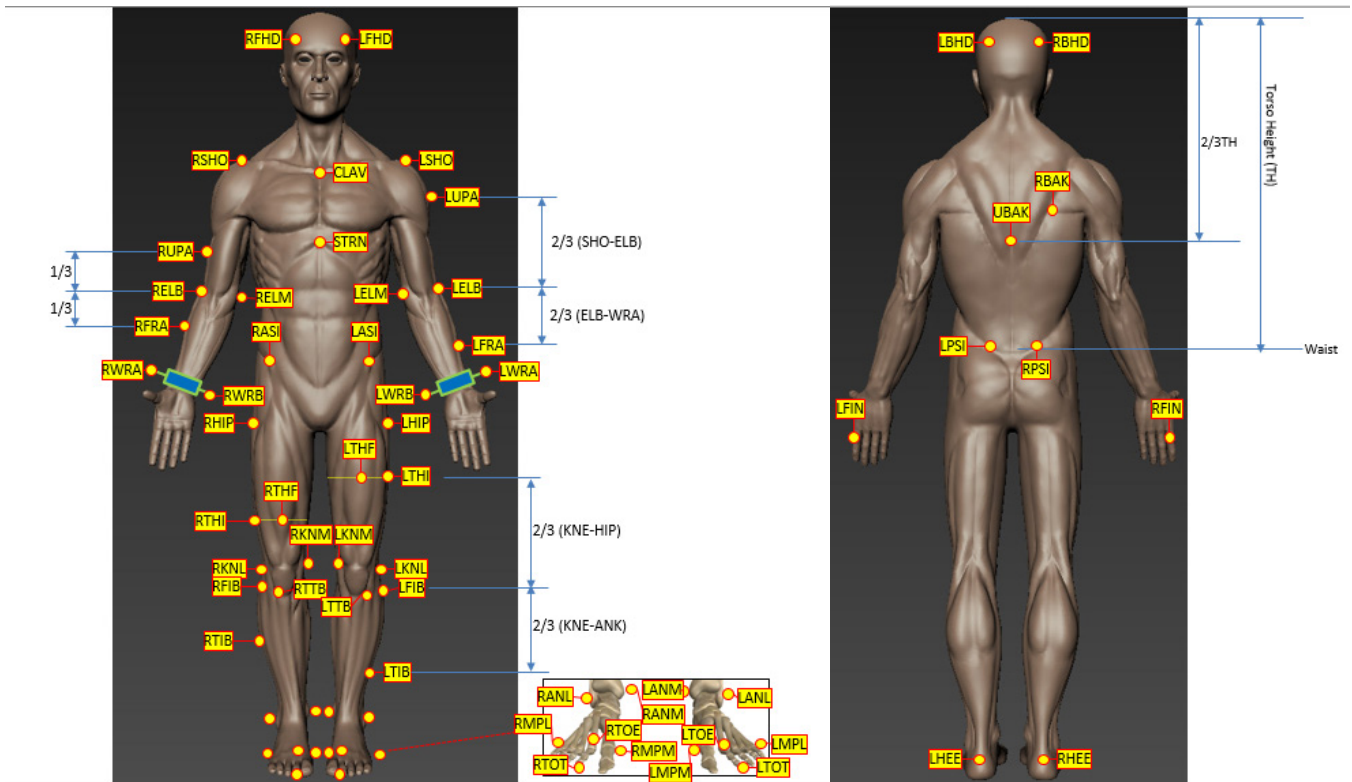


Figure 34.—Modified plug-in gait marker set used for motion capture data collection

Appendix E.—Procedure For Producing External Force Files From Device Load and Ground Reaction Force Data

How to make External loads files (*.MOT) by combining GRF and device load data

1. Determine the precise start and stop times and duration for each rep in the set from the TRC files. Plot the LBAR_Y and RBAR_Y marker positions and find the peaks and valleys of the bar displacement for each exercise to determine the start of each rep in the lift from the kinematic sense. You must do this for each load case individually! Record the data in a note or spreadsheet we can share.
2. Open the corresponding device load file in Matlab and select the Time, RForce, LForce and BarDisp columns and make them Matlab variables. Convert RForce and LForce from pounds to Newtons by multiplying them by 4.44822.

```
RForce = RForce .* 4.44822; LForce = LForce .* 4.44822;
```

3. Define a new Time_Resamp variable in Matlab that spans from the start time of the MOT file for GRF's (usually 0.000) and spans to the end time of the GRF MOT file in 0.004 sec increments, e.g.,

```
Time = 0.000 : 0.004 : 10.912;
```

4. Use the interp1 function to resample the device load and bar displacement data onto the new Time variable, e.g.,

```
RForce_Resamp = interp1(Time, RForce, TimeSamp);
```

```
LForce_Resamp = interp1(Time, LForce, TimeSamp);
```

```
BarDisp_Resamp = interp1(Time, BarDisp, TimeSamp);
```

Now find the corresponding start and end of each rep in the BarDisp_Resamp data. Determine the relative time offset in order to sync the bar displacement with the marker kinematics in step 1. Eliminate the time difference from the beginning of each Force variable so that the force data is synchronized with the kinematics data. Also trim the back end of the force variables so that the data length exactly matches that of the kinematics. Redefine the time variables so that they also exactly match the kinematics.

5. Look for the Bluetooth dropouts in the data. If data for one foot exists but not the other, copy the good data onto the other and assume they are equal over that time interval. At the end of this, you will have the force magnitudes for Left and Right on the bar, but you still need to define the center of application (COA) and the directional components of force.
6. Now open the corresponding *.TRC marker data file and select the X, Y and Z positions of RBAR, RPLT, LBAR, and LPLT as Matlab variables over the same time interval as you used for the GRF MOT files. That is 12 variables in total. Remember TRC files are in mm not meters, and so are the COP locations in the MOT file to be created.

7. Compute the COA positions of RBAR and LBAR. First convert the marker positions (in mm) to meters by dividing by 1000. Add the strap offset (0.03 m) to each X marker position to get the COA's and use the same Y and Z. Remember to subtract 0.03 m from LBAR_X, not add it.

```
RBar_Force_px = RBAR_X/1000 + 0.03;
```

```
RBar_Force_py = RBAR_Y/1000;
```

```
RBar_Force_pz = RBAR_Z/1000;
```

```
LBar_Force_px = LBAR_X/1000 - 0.03;
```

```
LBar_Force_py = LBAR_Y/1000;
```

```
LBar_Force_pz = LBAR_Z/1000;
```

8. Now compute the direction cosines for each axis based on the vectors defined by RBAR-RPLT and LBAR-LPLT.

```
RVec = [RPLT_X - RBAR_X RPLT_Y - RBAR_Y RPLT_Z - RBAR_Z];
```

```
LVec = [LPLT_X - LBAR_X LPLT_Y - LBAR_Y LPLT_Z - LBAR_Z];
```

```
MagRVec = sqrt(RVec(:, 1).^2 + RVec(:, 2).^2 + RVec(:, 3).^2);
```

```
MagLVec = sqrt(LVec(:, 1).^2 + LVec(:, 2).^2 + LVec(:, 3).^2);
```

```
DirCos_RVec = [RVec(:, 1) ./ MagRVec, RVec(:, 2) ./ MagRVec, RVec(:, 3) ./ MagRVec];
```

```
DirCos_LVec = [LVec(:, 1) ./ MagLVec, LVec(:, 2) ./ MagLVec, LVec(:, 3) ./ MagLVec];
```

9. Now, compute the directional components of the Force on the bar.

```
RBar_Force_vx = RForce_Resamp .* DirCos_RVec(:,1);
```

```
RBar_Force_vy = RForce_Resamp .* DirCos_RVec(:,2);
```

```
RBar_Force_vz = RForce_Resamp .* DirCos_RVec(:,3);
```

```
LBar_Force_vx = LForce_Resamp .* DirCos_LVec(:,1);
```

```
LBar_Force_vy = LForce_Resamp .* DirCos_LVec(:,2);
```

```
LBar_Force_vz = LForce_Resamp .* DirCos_LVec(:,3);
```

10. And finally, append 12 new columns into the *.MOT file for GRF and save it under a new name with the suffix "ExtFor" (e.g., HULK_S10_HR_M150_ExtFor.MOT). Remember to change the number of columns from 19 to 31!

```
RBar_Force_vx RBar_Force_vy RBar_Force_vz RBar_Force_px RBar_Force_py RBar_Force_pz  
LBar_Force_vx LBar_Force_vy LBar_Force_vz LBar_Force_px LBar_Force_py LBar_Force_pz
```

11. In the GRF Setup files for Inverse Dynamics, RRA and Static Optimization, you need to specify how these forces get applied to the model. Make sure you are using a model with the bar connected to the torso by a free

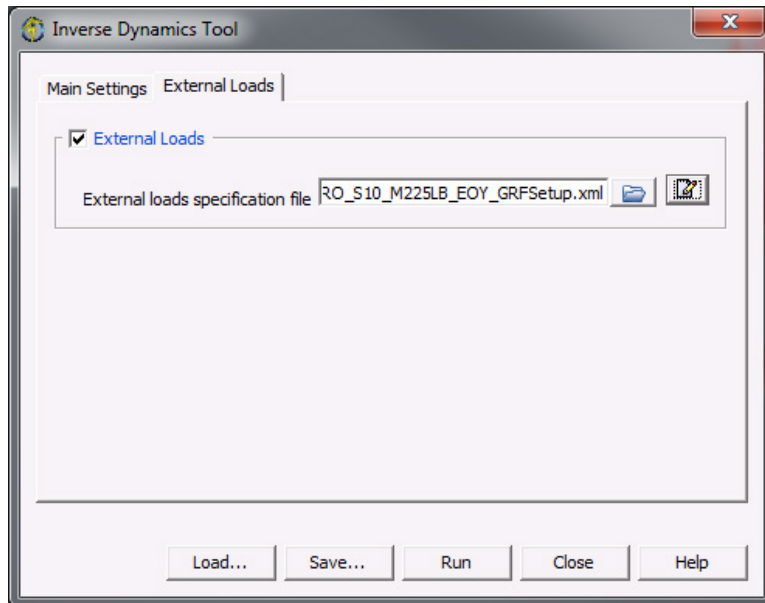
joint (6 DOF). Make sure the RBAR, RPLT, LBAR and LPLT markers are also in the model. Run IK to get the true position of the bar versus time. Our upper body model is low fidelity, so the bar will appear to impale the neck—go with it, don't try to fix it.

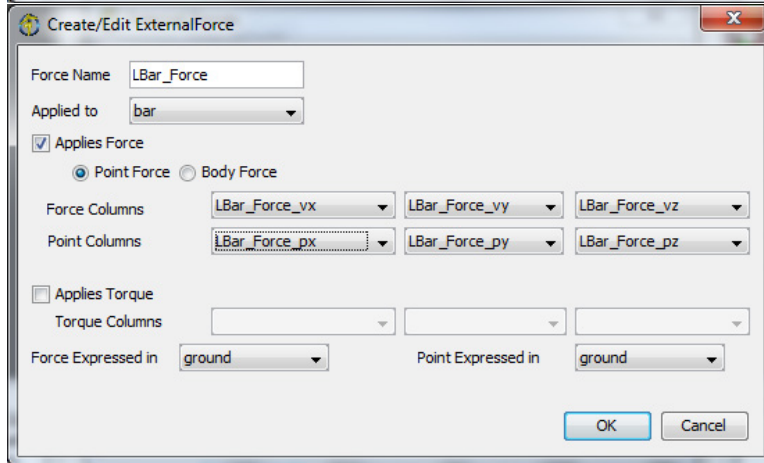
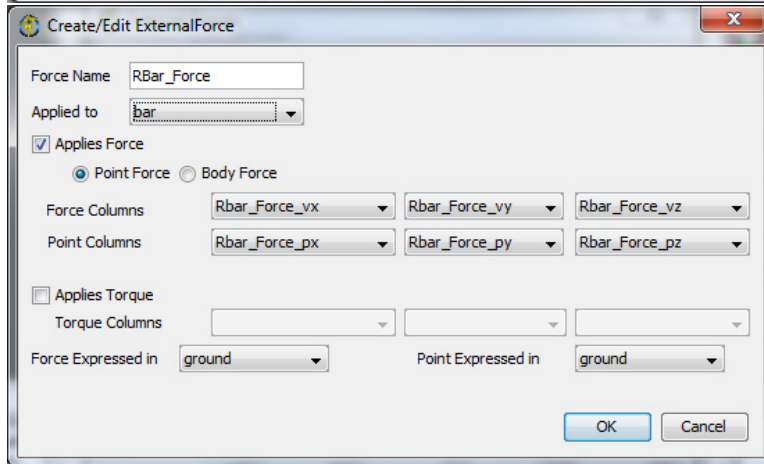
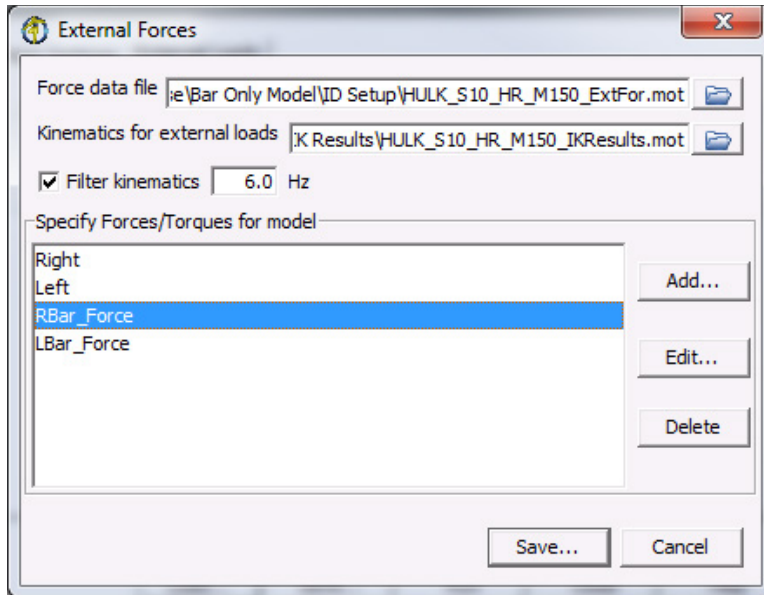
12. Compute the midpoint of the bar as the midpoint of the two markers in ground coordinates:

$$[x, y, z] = [(LBAR_X - RBAR_X)/2, (LBAR_Y - RBAR_Y)/2, (LBAR_Z - RBAR_Z)/2]$$

Place a new marker here in the OpenSim GUI referenced to ground. Now change the body reference of the new marker to Bar and save those coordinates. Then change the body reference of the marker to torso and save those coordinates.

13. Add a point constraint to the model between the bar (child) and torso (parent). Use the point coordinates saved above to define the location of the point constraint in each body. Rerun IK.
14. When you go to run ID and you make your GRF setup file, you need to specify the new forces on the ID setup dialog, External loads tab. Click on the edit icon to the far right. Add the new forces as show in the series of dialogs below, but use the filenames that are appropriate to your specific exercise.





Remember! When you save from the ID External Loads tab, you save the XML file for External Loads setup. When you save from the Main Settings tab, you save the XML file for ID Setup.

References

1. Delp, S.L., Loan, J.P., Hoy, M.G., Zajac, F.E., Topp E.L., Rosen, J.M., “An interactive graphics-based model of the lower extremity to study orthopaedic surgical procedures,” *IEEE Transactions on Biomedical Engineering*, Vol. 37, pp. 757-767, 1990.
2. Human Research Roadmap, website, <http://humanresearchroadmap.nasa.gov/>
3. Escamilla, R.F., “Knee biomechanics of the dynamic squat exercise,” *Med. Sci. Sports Exerc.*, vol. 33, pp. 127-141, 2001.
4. Nicogossian, A.E., Huntoon, C.L., Pool, S.L., *Space Physiology and Medicine*, 3rd Ed., Lea & Febiger, 1994.
5. McCurdy, K., O’Kelley, E., Kutz, M., Langford, G., Ernest, J., Torres, M., “Comparison of lower extremity EMG between the 2-leg squat and modified single-leg squat in female athletes,” *J Sport Rehabil.*, 2010 Feb; 19(1):57-70.
6. Arnsdorff, K., Limbaugh, K., and Riemann, B., “Analysis of heel raise exercise with three foot positions,” *Int J Exerc Sci*, vol. 4, no. 1, pp. 13-21, 2011.
7. Österberg, U., Svantesson, U., Takahashi, H., and Grimby, G., “Torque, work and EMG development in a heel-rise test,” *Clin. Biomech.*, vol. 13, pp. 344-350, 1998.
8. Flanagan, S.P., Song, J.E., Wang, M.Y., Greendale, G.A., Azen, S.P., and Salem, G.J., “Biomechanics of the heel raise exercise,” *J. Aging Phys. Act.*, vol. 13, pp. 160-171, 2005.
9. Riemann B.L., Limbaugh G.K., Eitner J.D., and LeFavi R.G., “Medial and lateral gastrocnemius activation differences during heel raise exercise with three different foot positions,” *J. Strength Cond. Res.*, vol. 25, pp. 634-639, 2011.
10. Ploutz-Snyder, L., personal communication, 2014.
11. Goel, R., Kaderka, J., and Newman, D., “Modeling the benefits of an artificial gravity countermeasure coupled with exercise and vibration,” *Acta Astronautica*, Feb; 70:43-51, 2012.
12. Shelburne, K.B., Decker M.J., Krong J., Torry M.R., Philippon M.J., “Muscle Forces at the Hip during Squatting Exercise,” *Transactions of the Annual Meeting-Orthopaedic Research Society*, CD-ROM Edition; 2010.
13. Kosterina, N., Wang, R., Eriksson, A., and Gutierrez-Farewik, E.M., “Force enhancement and force depression in a modified muscle model used for muscle activation prediction,” *J of Electromyography and Kinesiology*, 23 (2013) 759-765.
14. McCaw, S.T. and Melrose, D.R., “Stance width and bar load effects on leg muscle activity during the parallel squat,” *Med. Sci. Sports Exerc.*, vol. 31, pp. 428-436, 1999.
15. Escamilla, R.F., Fleisig, G.S., Lowry, T.M., Barrentine, S.W., and Andrews, J.R., “A three-dimensional biomechanical analysis of the squat during varying stance widths,” *Med. Sci. Sports Exerc.*, vol. 33, pp. 984-998, 2001.
16. Escamilla, R.F., Fleisig, G.S., Zheng, N., Lander, J.E., Barrentine, S.W., Andrews, J.R., Bergemann, B.W., and Moorman, C.T., “Effects of technique variations on knee biomechanics during the squat and leg press,” *Med. Sci. Sports Exerc.*, vol. 33, pp. 1552-1566, 2001.
17. Fry, A.C., Smith, J.C., and Schilling, B.K., “Effect of knee position on hip and knee torques during the barbell squat,” *J. Strength Cond. Res.*, vol. 17, pp. 629-633, 2003.
18. Gullett J. C., Tillman M. D., Gutierrez G. M., and Chow J. W.; “A biomechanical comparison of back and front squats in healthy trained individuals,” *J. Strength Cond. Res.*, vol. 23, pp. 284-292, 2009.
19. Lynn, S.K. and Noffal, G.J., “Lower Extremity Biomechanics During a Regular and Counterbalanced Squat,” *J. Strength Cond. Res.*, vol. 26, pp. 2417-2425, 2012.
20. Chiu, L.Z.F. and Salem, G.J., “Comparison of joint kinetics during free weight and flywheel resistance exercise,” *J. Strength Cond. Res.*, vol. 20, pp. 555-562, 2006.
21. Arnold, E.M., Ward, S.R., Lieber, R. L., and Delp, S.L., “A model of the lower limb for analysis of human movement,” *Annals Biomedical Engineering* 2010 Feb; 38(2):269-79. Epub 2009, Dec 3. 2010.
22. SimTK website, <https://simtk.org/xml/index.xml>.
23. Millard, M., Uchida, T., Seth, A., and Delp, S.L., “Flexing computational muscle: modeling and simulation of musculotendon dynamics,” *ASME Journal of Biomechanical Engineering*, 135(2):021005, 2013.

24. Schoenfeld, B.J., "Squatting kinematics and kinetics and their application to exercise performance," *J. Strength Cond. Res.*, 24(12): 3497-3506, 2010.
25. Fry, A.C., Smith, J.C., and Schilling, B.K., "Effect of hip position on hip and knee torques during the barbell squat," *J. Strength Cond. Res.*, 17(4): 629-633, 2003.
26. Orloff, H., Veil, G., and Askins, R., "Forces on the lumbar spine during the parallel squat," Conference Proceedings Archive, 15 International Symposium on Biomechanics in Sports, 1997.
27. Cappozzo A., Felici F., Figura F., and Gazzani F., "Lumbar spine loading during half-squat exercises," *Med. Sci. Sports Exerc.*, vol. 17, pp. 613-620, 1985.
28. Bazrgari, B., Shirazi-Adl, A., and Arjmand, N., "Analysis of squat and stoop dynamic liftings: Muscle forces and internal spinal loads," *Eur. Spine J.*, vol. 16, pp. 687-699, 2007.
29. Trepczynski, A., "Patellofemoral Joint Contact Forces during Activities with High Knee Flexion," *J Orthop Res* 30:408-415, 2012.
30. Biscarini A., Benvenuti P., Botti F., Mastrandrea F., and Zanuso S.; "Modeling the joint torques and loadings during squatting at the Smith machine.," *J. Sports Sci.*, vol. 29, pp. 457-469, 2011.
31. Wretenberg, P., Feng, Y., and Arborelius, U.P., "High- and low-bar squatting techniques during weight-training.," *Med. Sci. Sports Exerc.*, vol. 28, pp. 218-224, 1996.
32. Wretenberg, P., Feng, Y., Lindberg, F., and Arborelius, U.P., "Joint moments of force and quadriceps muscle activity during squatting exercise," *Scand. J. Med. Sci. Sports*, vol. 3, pp. 244-250, 1993.
33. Escamilla, R.F., Fleisig, G.S., Zheng N., Barrentine, S.W., Wilk K.E., and Andrews J.R., "Biomechanics of the knee during closed kinetic chain and open kinetic chain exercises," *Med. Sci. Sports Exerc.*, vol. 30, pp. 556-569, 1998.
34. Hattin, H.C., Pierrynowski, M.R., and Ball, K.A. ; "Effect of load, cadence, and fatigue on tibio-femoral joint force during a half squat.," *Med. Sci. Sports Exerc.*, vol. 21, pp. 613-618, 1989.
35. Bryanton, M.A., Kennedy, M.D., Carey, J.P., and Chiu, L.Z.F., "Effect of Squat Depth and Barbell Load on Relative Muscular Effort in Squatting," *J. Strength Cond. Res.*, vol. 26, pp. 2820-2828, 2012.
36. Caterisano, A., Moss, R.F., Pellingier, T.K., Woodruff, K., Lewis V.C., Booth W., and Khadra T., "The effect of back squat depth on the EMG activity of 4 superficial hip and thigh muscles," *J. Strength Cond. Res.*, vol. 16, pp. 428-432, 2002.
37. Gullett, J.C., Tillman, M.D., Gutierrez, G.M., and Chow, J.W., "A Biomechanical Comparison of Back and Front Squats in Healthy Trained Individuals," *J Strength Cond Res*, 23(1):284-292, 2008.
38. Zwerver, J., Bredeweg, S.W., Hof, A.L., "Biomechanical analysis of the single-leg decline squat", *Br J Sports Med* 41: 264-268, 2007.
39. Kobayashi, K., et al., "In Vivo Kinematics of the Extensor Mechanism of the Knee During Deep Flexion," *J Biomech Eng.*, Aug; 135(8):81002, 2013.
40. Sakuma, J., et al.; "Fascicle-tendon behavior of the gastrocnemius and soleus muscles during ankle bending exercise at different movement frequencies," *Eur J Appl Physiol*, 112:887-898, 2012.
41. Thompson W.K., et al., "ARED Squat Model - Integrated (ASM-i)," Report, NASA GRC 2012.
42. Newby N., Caldwell E., "ARED Deadlift Model Integrated (ADM-i)," Report, Wyle, 2012.
43. Humphreys, B.T., Thompson, W.K., Weaver, A., Perusek, G.P., and Mulugeta, L., "Toolbox for Simulating Advanced Exercise Concept Devices," HRP IWS 2014, Poster.
44. Website, www.LifeMODEler.com.
45. Farrokhi, S., Pollard, C.D., Souza, R.B., Chen, Y.J., Reisch S., and Powers, C.M., "Trunk position influences the kinematics, kinetics, and muscle activity of the lead lower extremity during the forward lunge exercise," *J Orthop Sports Phys Ther.* Jul; 38(7):403-9, 2008.
46. NASA Standard 7009 (NASA-STD-7009), "Standard for Models and Simulations," National Aeronautics and Space Administration, Washington, DC, 2008.
47. Hill, A.V. "The heat of shortening and the dynamic constants of muscle," *Proc. Roy. Soc.* 126B:136-195, 1938.
48. Thelen, D.G., "Adjustment of muscle mechanics model parameters to simulate dynamic contractions in older adults," *ASME J. of Biomechanical Engineering*, 125(1):70-77, 2003.

